Studies on PNP-Pincer Type Phosphaalkene Complexes Stabilized by a Fused-Ring Bulky Protection Group

Hiro-omi Taguchi

2018

Contents

General Introduction		1
Chapter 1	Catalytic Synthesis of an Unsymmetrical PNP-Pincer Type Phosphaalkene Ligand	19
Chapter 2	Unsymmetrical PNP-Pincer Type Phosphaalkene Ligands Protected by a Fused-Ring Bulky Eind Group: Synthesis and Applications to Rh(I) and Ir(I) Complexes	43
Chapter 3	Unsymmetrical PNP-Pincer Type Phosphaalkene Complexes of Group 9 Metals: Catalytic Application to Hydrosilylation of Carbon Dioxide	69
Chapter 4	A Square Planar Complex of Platinum(0)	83
Chapter 5	On Geometrical Stability of Square Planar Platinum(0) Complexes Bearing a PNP-Pincer Type Phosphaalkene Ligand ($Eind_2$-BPEP)	101
Conclusions		121
List of Publications		123
Acknowledgements		125

General Introduction

Introduction

It is well known that structures and properties of transition metal complexes are heavily dependent on supporting ligands both from steric and electronic points of view.[1] Accordingly, the development of supporting ligands that possess unique ligand properties is a crucial subject in organometallic chemistry, often offering the opportunity to discover transition metal complexes with novel structures and reactivities. From the electronic point of view, supporting ligands are roughly categorized into two classes, σ-donors and π-acceptors. The former class covers a wide variety of ligands, including tertiary phosphines, pyridine derivatives, cyclopentadienyl derivatives, and *N*-heterocyclic carbenes. Their steric and electronic properties may be precisely controlled by structural modification, and this situation is essential for designing the most appropriate catalysts for individual organic transformations. In contrast, supporting ligands that exhibit strong π-accepting properties toward transition metals are limited. Although carbon monoxide is a strong π-acceptor, it is often reactive to organometallic species and fundamentally incapable of structural modification. In this context, considerable research efforts have been made over the past two decades on the application of low-coordinate phosphorus compounds as π-accepting ligands in organometallic chemistry.[2] Most of them are two-coordinate phosphorus compounds, such as phosphaalkenes,[3] phosphinines,[4] phospholes,[5] and phosphaferrocenes[5c,6] (Chart 1). Phosphaalkenes with P=C double bonds have attracted particular attention due to their ease of structural modification.[3]

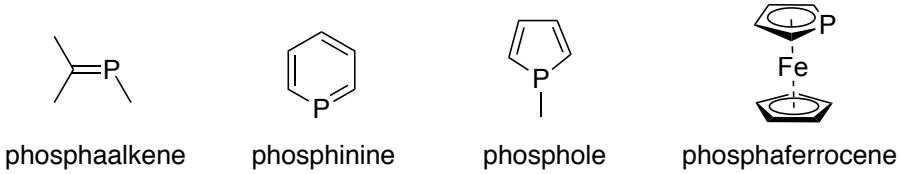

Chart 1. Core structures of low-coordinate phosphorus compounds.

Phosphaalkene Ligands

In 1976, Becker reported the first isolation of phosphaalkenes compounds.[7] It is known that multiple bond compounds including heavier main group elements possess significantly high-lying π orbitals and low-lying π* orbitals, relative to ordinary unsaturated organic molecules. As seen from Figure 1, the π* orbital of $HP=CH_2$ is located more than 2 eV lower than those of CO and $H_2C=NH$, and distributed largely on the phosphorus atom, reflecting the spatial expanse of the 3p orbital.[8] Moreover, the nonbonding orbital including lone pair electrons on the phosphorus atom is present at a high energy level comparable to that of PH_3. Consequently, phosphaalkenes effectively combine with transition metals in an end-on (η^1-coordination) or side-on (η^2-coordination) manner, and behave as strong π-acceptors to form complexes with unique structures and reactivities. Chart 2 shows representative examples of phosphaalkene compounds that have been applied to organometallics chemistry.

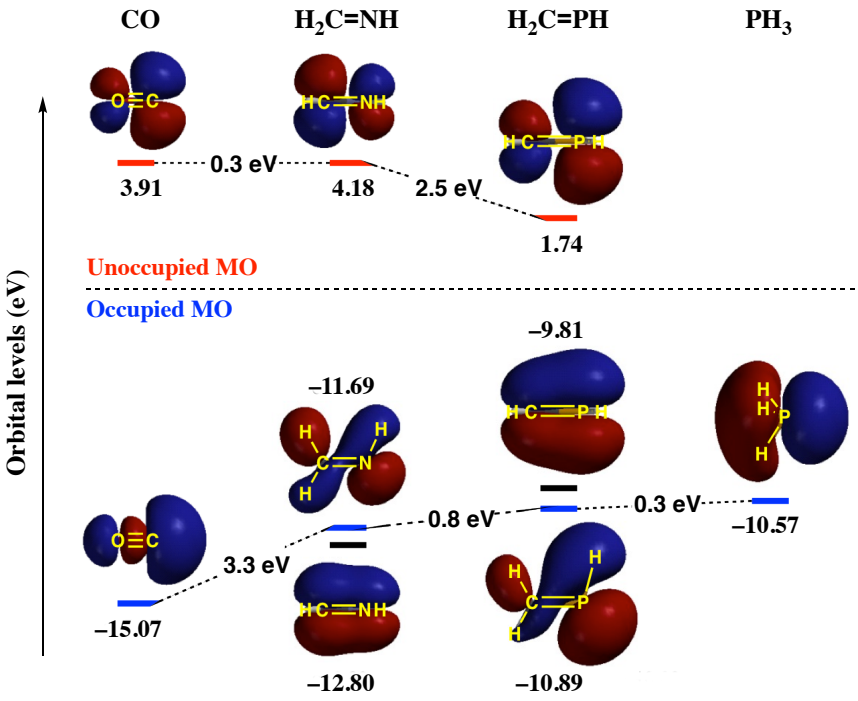

Figure 1. Schematic diagrams for the frontier orbitals of CO, $H_2C=NH$, $H_2C=PH$, and PH_3. The orbital levels were estimated by *ab intio* MO calculations (HF/6-311G(d)).[8]

Bidentate ligands (achiral)

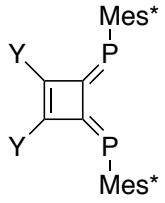

DPCB-Y

Y = Ph
Appel (1987)[15]

Y = $SiMe_3$, *p*-OMe-C_6H_5
p-CF_3-C_6H_5
Yoshifuji (1998)[8,16]

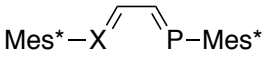

(X = P, N)

1

Brookhart (2002)[22]

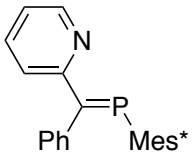

PEP

Bickelhaupt (1997)[25]

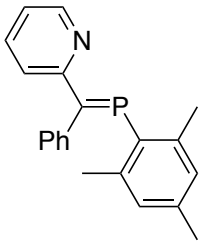

2

Gates (2006)[27]

Bidentate ligands (chiral)

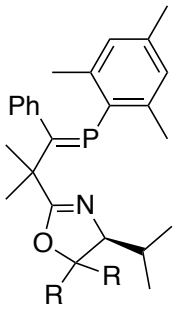

3

R = H, Me
Gates (2008)[38a]

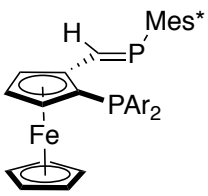

PAr_2 = PPh_2
P(1-naphthyl)Ph

4

Ozawa (2008)[39]

Tridentate ligands

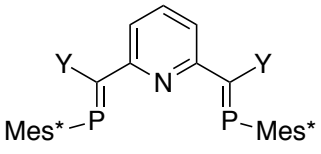

BPEP-Y

Y = H
Geffroy (1992)[29]

Y = Ph
Ozawa (2010)[31]

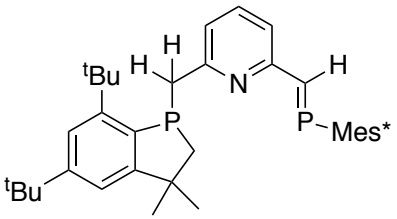

PPEP

Ozawa (2013)[33]

Chart 2. Representative examples of phosphaalkene ligands.

On the other hand, phosphaalkenes with active frontier orbitals possess inherent reactivity to undergo nucleophilic or electrophilic addition to the P=C double bonds to give P–C single bond compounds including oligomers.[9] Thus, the reactivity control of P=C double bonds is a fundamental requirement for the ligand use of phosphaalkenes, and bulky protecting groups are commonly introduced to ensure the kinetic stability. To date, plenty of bulky substituents have been developed for steric protection of multiple bonds of heavier main group elements.[10] Among them, the 2,4,6-tri-*tert*-butylphenyl group (Mes*) has been most frequently utilized for P=C double bonds,[2d,3] including simple phosphaalkenes, such as Mes*P=CH_2[11a] and Mes*P=CHPh.[11b] However, there are precedents of Mes*-substituted phosphaalkene ligands that are still reactive on transition metals. Scheme 1 illustrates phosphaalkene palladium complexes that lose P=C bonds via insertion into a Pd–Me bond[12] and 1,2-addition of alcohol[13] and water.[14]

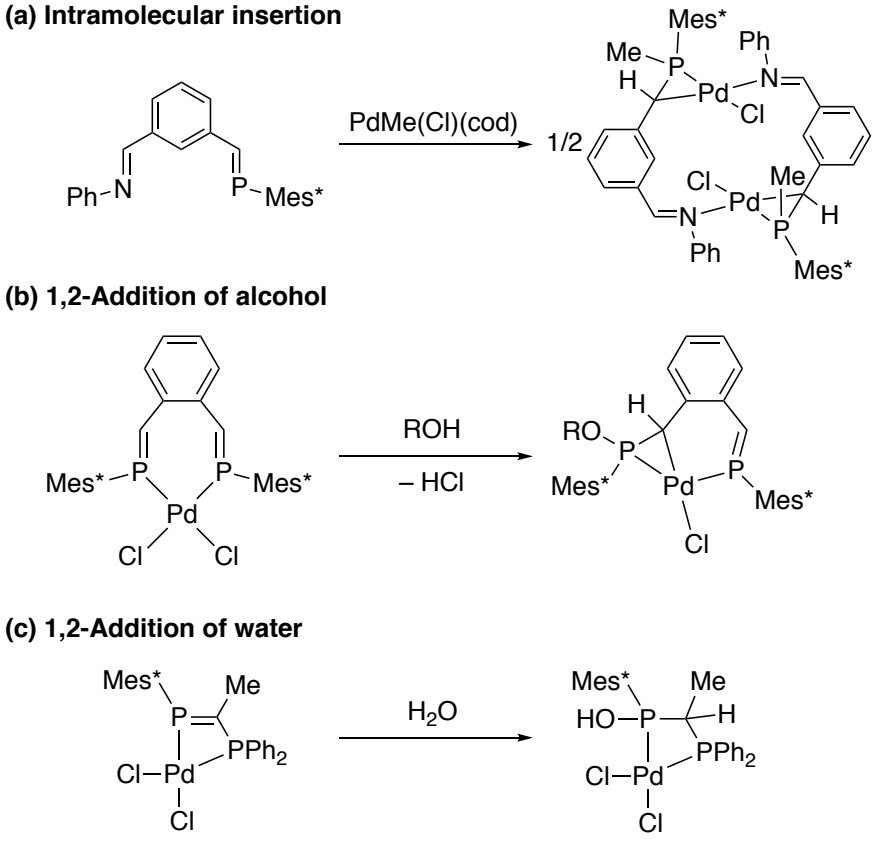

[Mes* = 2,4,6-tri-*tert*-butylphenyl]

Scheme 1. Reactions of P=C double bonds on palladium.

To prevent such undesirable reactions, P=C double bonds are often incorporated into extended π-conjugated systems with the aim of gaining thermodynamic stabilization.[2d] The DPCB-Y ligands given on the top of Chart 2 are representative,[8,15,16] and their P=C double bonds are linked with a 1,2-diarylcyclobutadiene core at the 3,4-positions to constitute a 1,6-diphospha-1,3,5-hexatriene skeleton.[17] The DPCB-Y ligands undergo bidentate coordination with a series of late transition metals to form complexes that are sufficiently stable in catalytic systems.[18]

Phosphaalkene Complexes

In 1981, Nixon *et al*. reported the first example of phosphaalkene complexes, having a Mes-P=CPh_2 ligand (Mes = 2,4,6-trimethylphenyl).[19] In the same year, Bickelhaupt *et al*. reported the first X-ray structure of a phosphaalkene complex, consisting of a Cr(0) center and an η^1-phosphaalkene ligand.[20] Following these reports, several groups examined synthesis and catalytic application of phosphaalkene complexes; however, such attempts have made little success until 2000, due to the chemical instability of P=C double bonds.

In 2000, Ozawa *et al.* reported in collaboration with Yoshifuji's group that dimethyl-palladium complex **5** with a 1,2-phenyl-3,4-diphosphinidenecyclobutadiene ligand (DPCB-H) catalyzed ethylene polymerization in the presence of the Brookhart's acid (Scheme 2).[21] This is the first report on successful catalytic application of phosphaalkene complexes. The same catalytic reaction was reported by Brookhart *et al.* using **1** in Chart 1 as a supporting ligand.[22]

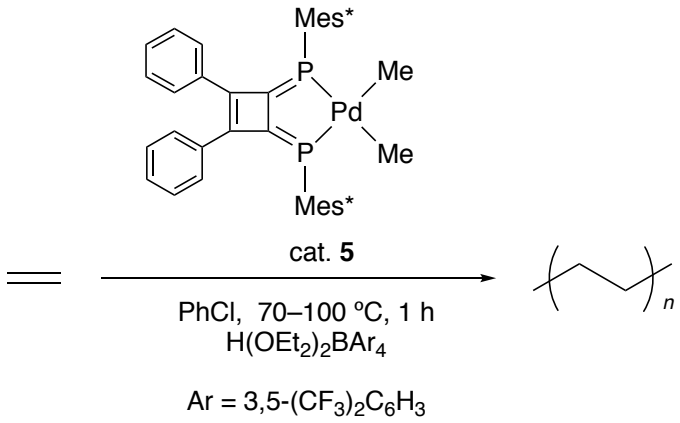

Scheme 2. The first successful application of phosphaalkene complex.[21]

Then, Ozawa and Yoshifuji have demonstrated high catalytic performance of DPCB-Y complexes in a variety of organic transformations,[23,24] including hydroamination of 1,3-dienes,[23a] dehydrative *N*- and *C*-allylation with allylic alcohols,[23b] *Z*-selective hydrosilylation of alkynes, [23c] cyclodehydration of *cis*-2-butene-1,4-diol with active methylene compounds,[23d] conjugate addition of benzyl carbamate to *α,β*-unsaturated ketones,[23e] and cross-coupling reactions.[24] Ozawa *et al.* reported that 2-[1-phenyl-2-(2,4,6-tri-*tert*-butylphenyl)-2-phospha-ethenyl]pyridine as a PN-chelate phosphaalkene ligand (PEP in Chart 2) prepared by Bickelhaupt *et al*.[25] enabled the isolation of a Ni(I) complex (**6**) and a distorted square planar Ni(II) complex (**7**) (Scheme 3).[26] On the other hand, Gates *et al.* reported a PN chelate ligand (**2**) in Chart 2, containing a 2,4,6-trimethylphenyl (Mes)-substituted phosphaalkene unit.[27] This ligand was applied to a Pd(II) complex (**8**), showing high catalytic activity toward Overmann rearrangement (Scheme 4).[28]

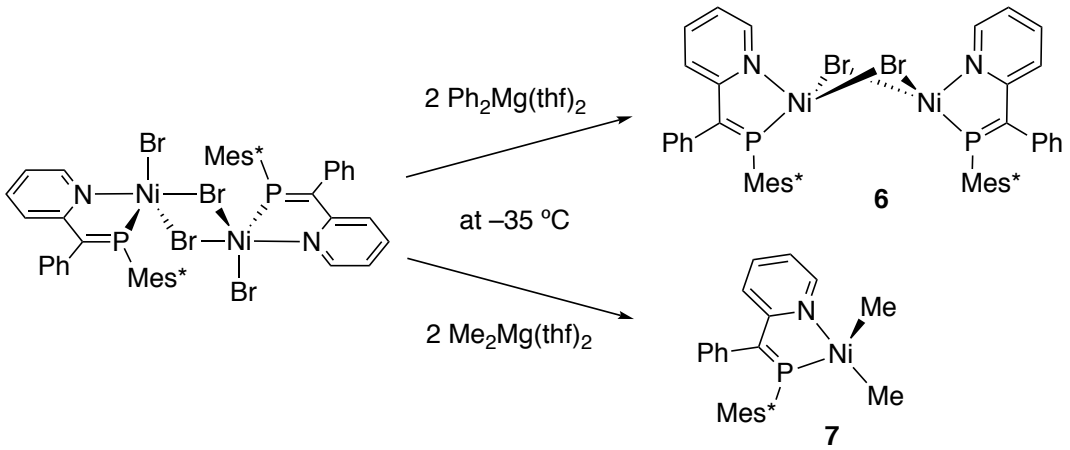

Scheme 3. Synthesis of nickel complexes with a PN-chelate phosphaalkene ligand (PEP).[26]

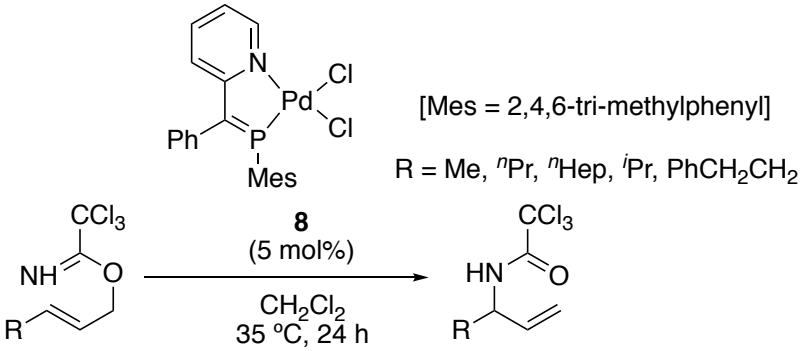

Scheme 4. Overmann rearrangement catalyzed by PN-chelate phosphaalkene complex **8**.[28]

In 1991, Geoffroy *et al.* reported the synthesis of 2,6-bis[2-(2,4,6-tri-*tert*-butylphenyl)-2-phosphaethenyl]pyridine (BPEP-H in Chart 2);[29] however, its application to coordination chemistry has been scarcely documented until 2007. Ozawa *et al.* demonstrated that BPEP-Y (Y = H or Ph in Chart 2) could be utilized as an interesting class of PNP-pincer ligands, which effectively stabilize coordinatively unsaturated complexes of late transition metals.[3a] An early example includes the 15-electron complex of Fe(I) [FeBr(BPEP-Ph)] (**9**), adopting a highly distorted trigonal monopyramidal configuration (Figure 2a).[30] Mössbauer spectroscopy and broken-symmetry DFT calculations revealed a high-spin Fe(I) species (S = 3/2) with a significantly delocalized orbital system including the Fe(I) center and the ligand. These structural features make a sharp contrast to those observed for bis(imino)pyridine (PDI) analogue **10** by Chirik *et al*. (Figure 2b).[31] Complex **10** adopts a square planar configuration and has an Fe(II) center (S = 2) coupled with a ligand-centered radical (S = 1/2). The unusual structure of **9** has been accounted for by the occurrence of strong π-back-bonding between Fe and BPEP-Ph. The BPEP-Ph ligand was also applied to the synthesis of novel T-shaped Cu(I) complexes with strong affinity for PF_6^- and SbF_6^- as uncoordinated anions.[32]

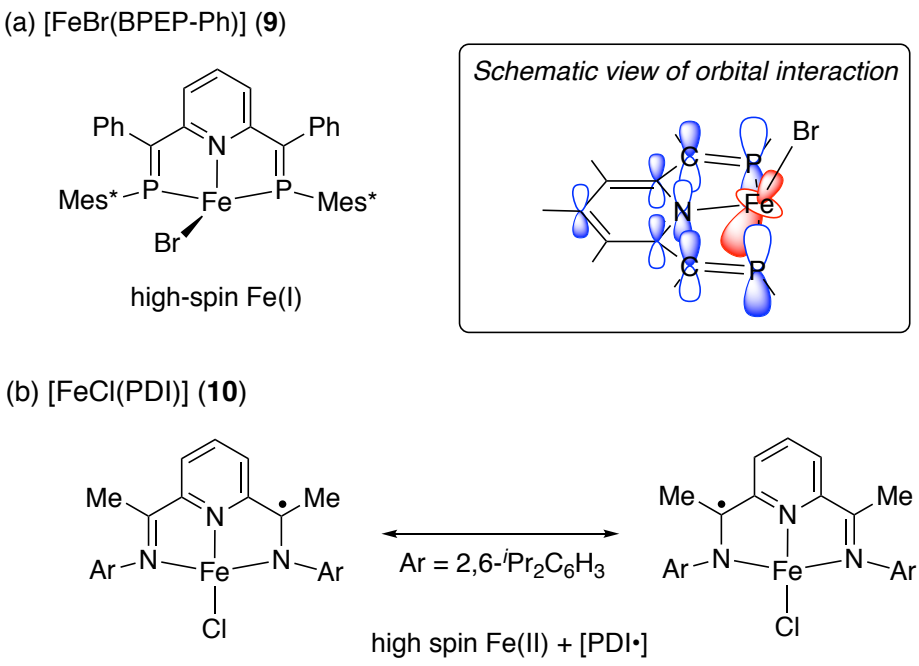

Figure 2. (a) Structure of [FeBr(BPEP-Ph)] (**9**) and a schematic view of the orbital interaction between Fe and BPEP.[30] (b) Electronic structure of [FeCl(PDI)] (**10**).[31]

In 2013, Ozawa *et al.* reported that the Ir(I) complex K[IrCl(PPEP*)] (K[**13**]) with a dearomatized PNP-pincer type phosphaalkene ligand (PPEP*) instantly cleaved the N–H bond of ammonia at ambient temperature via metal–ligand cooperative activation (step c in Scheme 5).[33] Complex K[**13**] is prepared from [IrCl(BPEP)] (**11**) by intramolecular C–H addition/cyclization of one of the Mes*P=CH units (step a), followed by deprotonation from [IrCl(PPEP)] (**12**) (step b). Although metal–ligand cooperative activation of chemical bonds using dearomatized PNP-pincer type phosphine complexes has been documented by Milstein *et al.* and extensively applied to environmentally benign catalytic reactions,[34] there has been no direct observations on the N–H bond cleavage of ammonia.[35] DFT calculations have indicated that the unusually high reactivity of K[**13**] is caused by stabilization of electron-rich intermediates with the aid of strong π-accepting properties of the phosphaalkene ligand. Complex K[**13**] exhibits high catalytic activity toward *N*-alkylation of amines with alcohols under neutral conditions.[36]

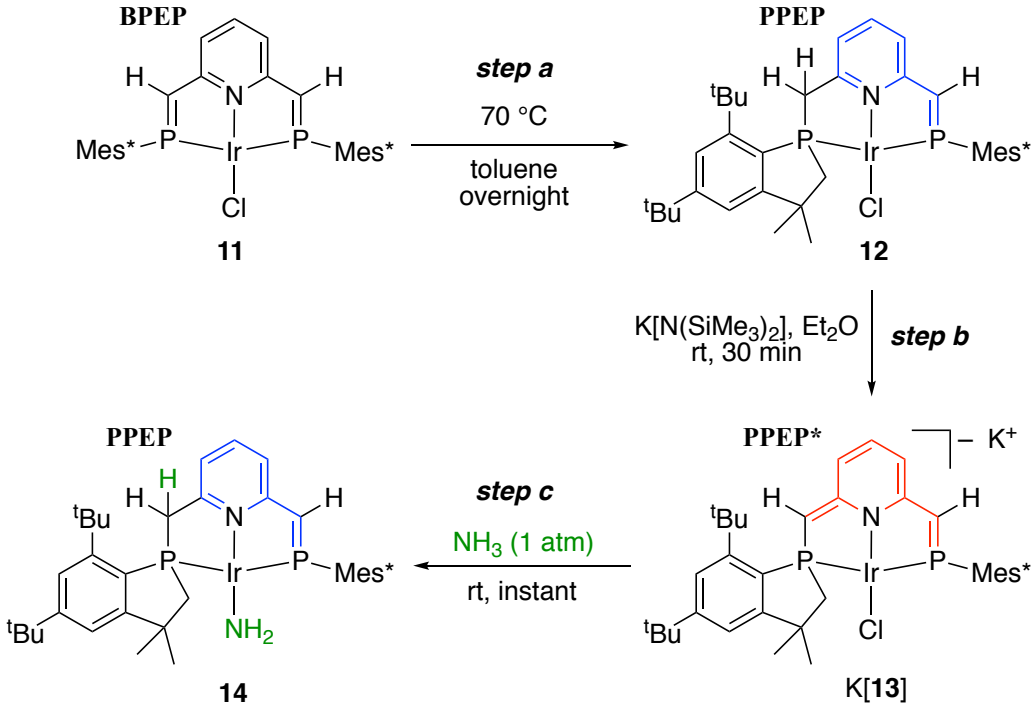

Scheme 5. N–H bond cleavage of ammonia via metal–ligand cooperation by a PNP-pincer type phosphaalkene complex of Ir(I) with a dearomatized pyridine unit (K[**13**]).[33]

There are a limited number of examples of enantiomerically pure phosphaalkene ligands and their transition metal complexes. The first example of a chiral phosphaalkene complex [(*L*-Menthyl){$(CO)_5W$}P=CH(^{i}Pr)] (**15**) was reported by Mathey *et al*. (Scheme 6).[37] This complex has the P=C double bond stabilized by $W(CO)_5$, and its hydrogenation catalyzed by a chiral Rh complex ($[Rh(L^*)]^+$, L* = (–)-chiraphos) forms **16** as an only diastereomer.

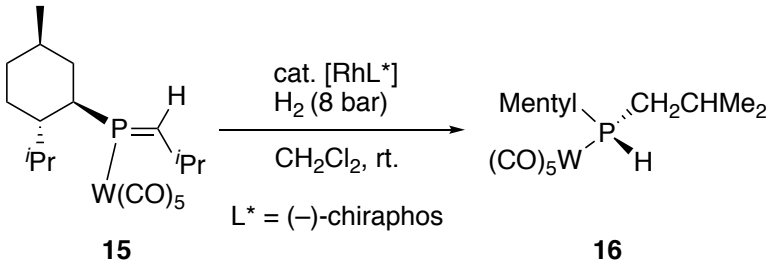

15 **16**

Scheme 6. The first example of an enantiomerically pure phosohaalkene complex.[37]

Two chiral phosphaalkene ligands (**3** and **4** in Chart 2) have been examined in catalytic asymmetric reactions.[38,39] The oxazoline-based ligand **3** developed by Gates *et al.* is particularly effective, and its palladium complex **17** catalyzes asymmetric allylic alkylation with high enantioselectivity (Scheme 7).[38b]

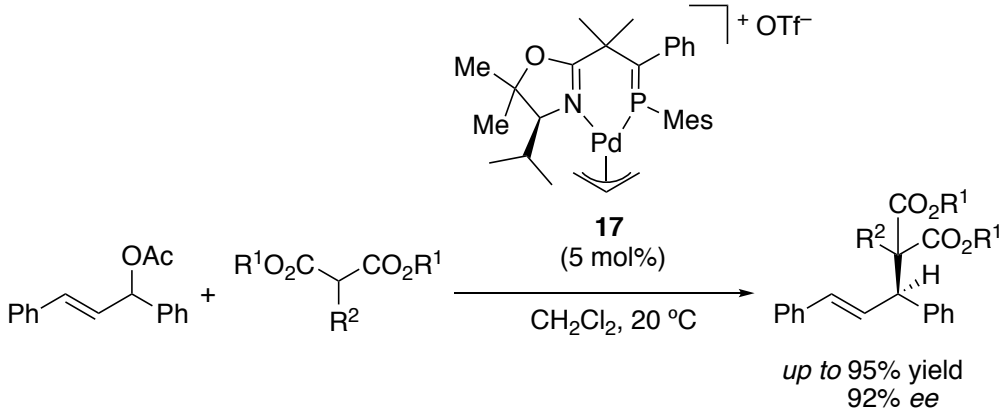

17

Scheme 7. Palladium-catalyzed asymmetric allylic alkylation.[38b]

Contents of the Thesis

As mentioned above, phosphaalkene complexes exhibit novel structures and reactivities, reflecting unique ligand properties of phosphaalkenes with extremely low-lying π* orbitals. In particular, BPEP-Y ligands consisting of a pyridine core and two phosphaethenyl arms at the 2,6-positions effectively stabilize coordinatively unsaturated complexes via meridional coordination. On the other hand, PPEP as an unsymmetrical PNP-pincer ligand with phosphoranylmethyl and phosphaethenyl groups exhibits noninnocent behavior on Ir(I), to facilitate metal–ligand cooperative activation of chemical bonds to a great extent. This author has been interested in these unique functions of PNP-pincer type phosphaalkene ligands, and thus attempted at expanding their utility in organometallic chemistry.

The most serious issue emerged in the previous studies is uncontrollable reactivity of the Mes*P=CH moiety toward intramolecular C–H addition/cyclization. As seen from Scheme 5, this reaction occurs only at one of the Mes*P=CH groups in [IrCl(BPEP)] (**11**), and the resulting complex [IrCl(PPEP)] (**12**) is stable to conversion of the other Mes*P=CH group. In contrast, the Rh(I) analogue of **11** in Scheme 8 undergoes C–H addition/cyclization at both the Mes*P=CH groups and completely loses the P=C double bonds.[40] To the contrary, several BPEP complexes including $[Cu(BPEP)]^+$ are totally inactive to C–H addition/cyclization.[32]

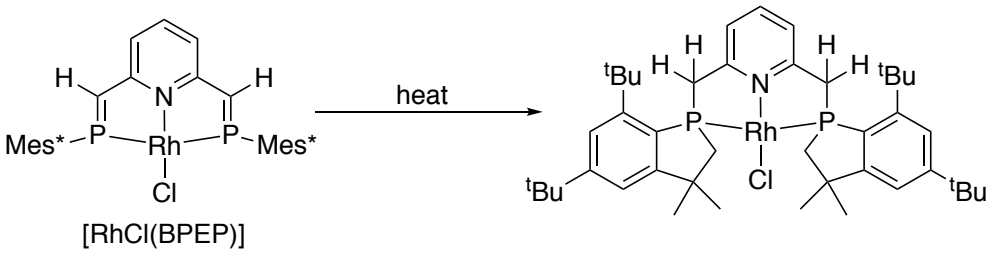

[RhCl(BPEP)]

Scheme 8. The loss of P=C double bonds through intramolecular C–H addition/cyclization.[40]

Thus, the author examined catalytic conversion of BPEP to PPEP, to isolate free PPEP. Moreover, to improve the kinetic stability of P=C double bonds, the author designed novel BPEP and PPEP ligands bearing Rind groups[41] instead of Mes* groups (Figure 3). The Rind groups have been developed by Tamao *et al*. for steric protection of unsaturated compounds of heavier main group elements, such as disilenes,[42a] germanones,[42b] and phosphasilenes.[42c] Among several Rind groups reported, the author has paid particular attention to the

1,1,3,3,5,5,7,7-octaethyl-*s*-hydrindacen-4-yl group (Eind), owing to its easy preparation. The author has expected that the fused-ring bulky Eind group with a rigid conformation could effectively prevent the intramolecular C–H addition/cyclization.

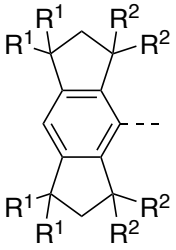

Eind: $R^1 = R^2 = Et$
EMind: R^1 = Et, R^2 = Me
MEind: R^1 = Me, R^2 = Et
MPind: R^1 = Me, R^2 = ^{n}Pr
MPhind: R^1 = Me, R^2 = Ph

Figure 3. Structures of Rind groups.[41]

This thesis consists of the following five chapters. Since the author has employed two kinds of steric protection groups (Mes* and Eind) for P=C double bonds, the phosphaalkene ligands protected by Eind groups will be abbreviated with symbols including "Eind", such as $Eind_2$-BPEP and Eind-PPEP.

In Chapter 1, catalytic synthesis of free PPEP is described. BPEP is converted to PPEP in the presence of a Pt(0)/PCy_3 catalyst (Scheme 9). This reaction involves byproduction of 2,6-bis(phospholanymethyl)pyridine (BPMP) and a Pt(II) phosphanido complex (**18**) having a dearomatized pyridine ring. The catalytic process is discussed based on NMR observations of catalytic intermediates.

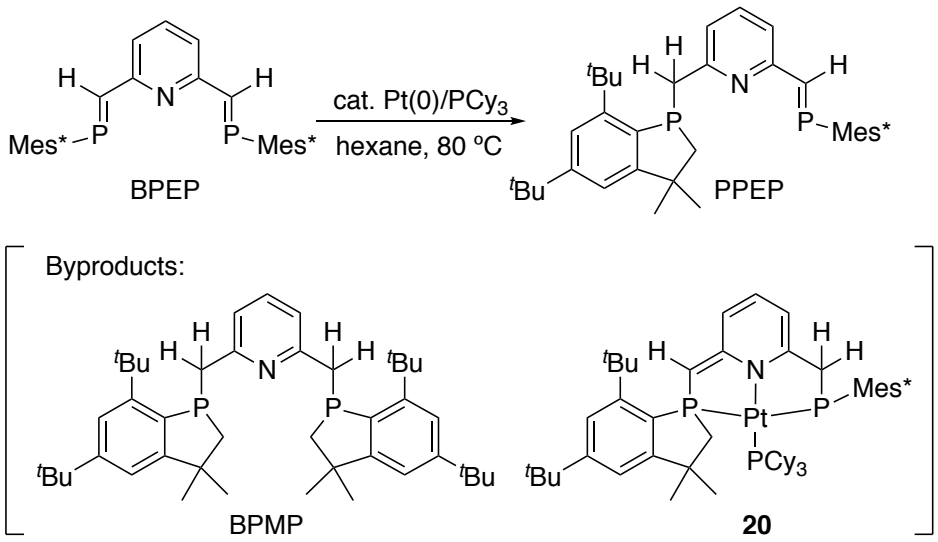

Scheme 9. Catalytic synthesis of free PPEP.

Chapter 2 deals with the synthesis of PNP-pincer type phosphaalkene ligands protected by Eind groups (Scheme 10). The Eind-BPEP ligand, in which the two P=C double bonds are unsymmetrically protected by Mes* and Eind groups, are newly prepared, and introduced to Rh(I) and Ir(I) complexes. The resulting complexes [MCl(Eind-BPEP)] (M = Rh (**19**) and Ir(**20**)) undergo intramolecular C–H addition/cyclization selectively at the Mes*P=CH moiety to afford the corresponding Eind-PPEP complexes **21** (Rh) and **22** (Ir), which are further converted to dearomatized Eind-PPEP* complexes K[**23**] (Rh) and K[**24**] (Ir) by the treatment with K[N(SiMe$_3$)$_2$]. The Eind-PPEP and Eind-PPEP* complexes are successfully stable to C–H addition/cyclization. Reactions of K[**23**] (Rh) and K[**24**] with ammonia are described.

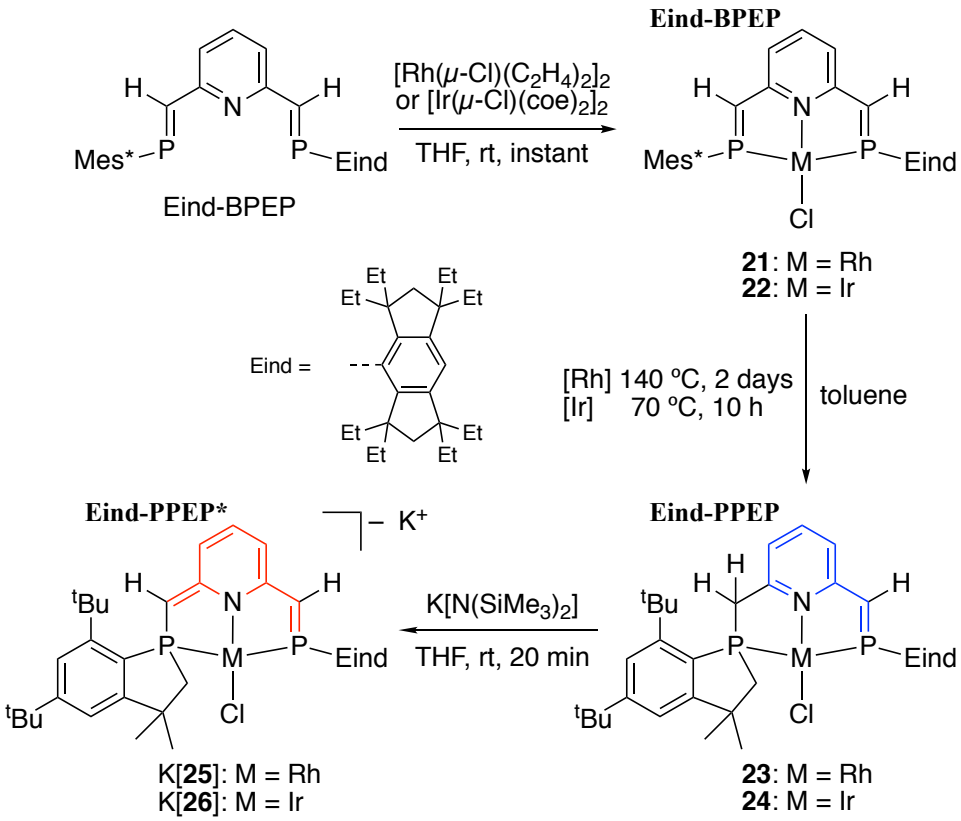

Scheme 10. PNP-Pincer type phosphaalkene complexes of Rh(I) and Ir(I) protected by Eind.

In Chapter 3, high catalytic activity of [K(18-crown-6)][**13**], [K(18-crown-6)][**23**], and [K(18-crown-6)][**24**] toward hydrosilylation of CO_2 is demonstrated. The Ir(I) complexes [K(18-crown-6)][**13**] and [K(18-crown-6)][**24**] are particularly efficient, and the reaction of

CO_2 (1 atm) with $HSiMe_2Ph$ smoothly proceeds at room temperature to give HCO_2SiMe_2Ph in high yield (TON up to 5100 at 40 °C) (Scheme 11). A novel catalytic cycle involving a metal–ligand cooperative activation of hydrosilane will be proposed.

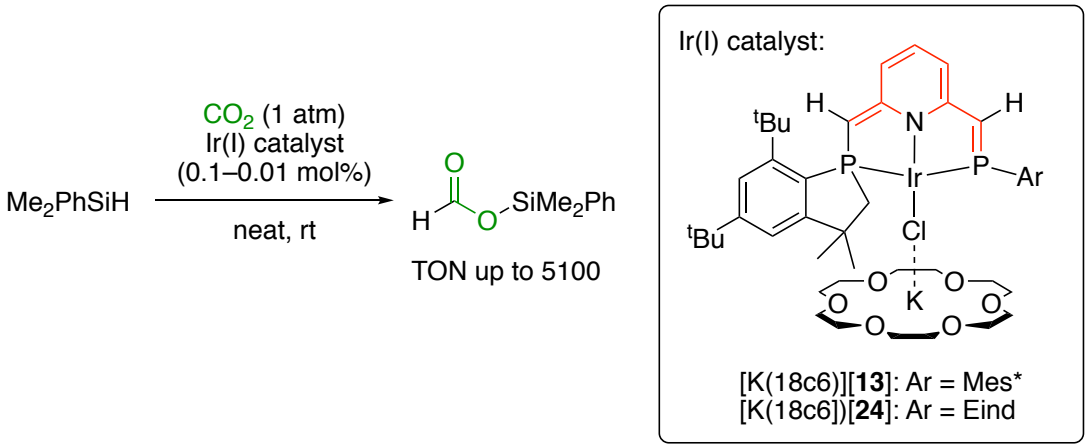

Scheme 11. Hydrosilylation of CO_2 catalyzed by PPEP* and Eind-PPEP* complexes.

Chapter 4 presents a novel Pt(0) complex with a square planar configuration, [Pt(PPh_3)($Eind_2$-BPEP)] (**25**), whose isolation is accomplished by a BPEP ligand stabilized by two Eind groups ($Eind_2$-BPEP). This coordination geometry is very uncommon for formal d^{10} complexes, and the Pd(0) and Ni(0) homologues with the same ligands adopt distorted tetrahedral geometries (Figure 4). DFT calculations indicate that the unique coordination geometry of **25** arises mainly from the two factors: (1) the highly flexible electronic property of $Eind_2$-BPEP with extremely low-lying π* orbitals; (2) the strong hybridization between the atomic 5d and 6s orbitals due to relativistic effects.[43]

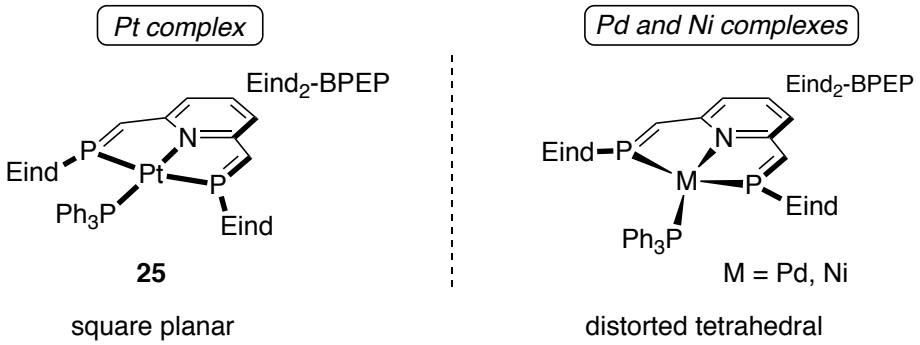

Figure 4. $Eind_2$-BPEP complex of Pt(0) and its Pd(0) and Ni(0) homologues.

Chapter 5 describes the effects of supporting ligands (L) with different electronic properties on coordination geometries of $Eind_2$-BPEP complexes of Pt(0) (Figure 5). While the X-ray structures of a series of [Pt(L)($Eind_2$-BPEP)] complexes display highly planar coordination geometries irrespective of L (τ_4 = 0.20–0.27), the complex having a π-acceptor such as CO gains flexibility toward distortion around Pt. Moreover, the π-accepting L lowers the HOMO level of the complex, and this change in the electronic conditions is clearly reflected in the spectroscopic properties observed by ^{31}P NMR and UV-vis-NIR analysis.

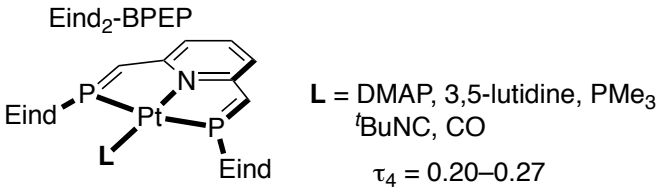

L	DMAP	3,5-lutidine	PMe_3	^{t}BuNC	CO
δ_P(P=C)	95.1	98.2	101.2	110.5	127.3
λ_{max}(nm)	924	907	845	825	776

Figure 5. Geometrical and spectroscopic variations of [Pt(L)($Eind_2$-BPEP)].

References and Notes

(1) (a) Hegedus, L. S. *Transition Metals in the Synthesis of Complex Organic Molecules, 3rd Ed*; University Science Books: Mill Valley, CA, 2009. (b). Hartwig, J. *Organotransition Metal Chemistry: From Bonding to Catalysis*; University Science Books: Mill Valley, USA, 2010. (c) Crabtree, R. H. *The Organometallic Chemistry of the Transition Metals, 6th Ed*; Wiley: Hoboken, USA, 2014.

(2) For related studies on the chemistry of low-coordinate phosphorus compounds, see: (a) Dugal-Tessier, J.; Conrad, E. D.; Dake, G. R.; Gates, D. P. In *Phosphorus(III) Ligands in Homogeneous Catalysis: Design and Synthesis*; Kamer, P. C. J., van Leeuwen, P. W. N. M., Eds.; Wiley: Chichester, U.K., 2012; Chapter 10. (b) Mathey, F. *Angew. Chem. Int. Ed.* **2003**, *42*, 1578–1604. (c) Yoshifuji, M. *Pure Appl. Chem.* **2005**, *77*, 2011–2020. (d) Le Floch, P. *Coord. Chem. Rev.* **2006**, *250*, 627–681. (e) Müller, C.; Sklorz, J. A. W.; de Krom, I.; Loibl, A.; Habicht, M.; Bruce, M.; Pfeifer, G.; Wiecko, J. *Chem. Lett*. **2014**, *43*, 1390–1404. (f) Weber, L. *Angew. Chem., Int. Ed.* **2002**, *41*, 563–572.

(3) For recent reviews, see: (a) Ozawa, F: Nakajima, Y. *Chem. Rec*. **2016**, *16*, 2314–2323. (b) Bates, J. I.; Dugal-Tessier, J.; Gates, D. P. *Dalton Trans.* **2010**, 3151–3159.

(4) For a recent review, see: Müller, C.; Broeckx, L. E. E.; de Krom, I.; Weemers, J. J. M. *Eur. J. Inorg. Chem.* **2013**, 187–202. For recent examples, see: (a) Habicht, M. H.; Wossidlo, F.; Bens, T.; Pidko, E. A.; Müller, C. *Chem. Eur. J.* **2018**, *24*, 944–952. (b) Broeckx, L. E. E.; Bucci, A.; Zuccaccia, C.; Lutz, M.; Macchioni, A.; Müller, C. *Organometallics* **2015**, *34*, 2943−2952. (c) Weemers, J. J. M.; van der Graaff, W. N. P.; Pidko, E. A.; Lutz, M.; Müller, C. *Chem. Eur. J*. **2013**, *19*, 8991–9004.

(5) For recent examples, see: (a) Fourmy, K; Mallet-Ladeira, S; Dechy-Cabaret, O; Gouygou, M. *Dalton Trans*. **2014**, *43*, 6728–6734. (b) Fourmy, K; Mallet-Ladeira, S; Dechy-Cabaret, O; Gouygou, M. *Organometallics* **2013**, *32*, 1571–1574. (c) Ogasawara, M.; Ito, A.; Yoshida, K.; Hayashi, T. *Organometallics* **2006**, *25*, 2715–2718.

(6) For recent examples, see: (a) Tian, R.; Ng, Y.; Ganguly, R.; Mathey, F. *Organometallics* **2012**, *31*, 2486–2488. (b) Escobar, A.; Mathey, F. *Organometallics* **2010**, *29*, 1053–1056. (c) Willms, H.; Frank, W.; Ganter, C. *Organometallics* **2009**, *28*, 3049–3058. (d) Fu, G. C. *Acc. Chem. Res.* **2006**, *39*, 853–860. (e) Shintani, R.; Fu, G. C. *J. Am. Chem. Soc.*

2003, *125*, 10778–10779.

(7) Becker, G. Z. *Anorg. Allg. Chem.* **1976**, *423*, 242–254.

(8) Ozawa, F.; Kawagishi, S.; Ishiyama, T. *Organometallics* **2004**, *23*, 1325–1332.

(9) (a) Appel, R. In *Multiple Bonds and Low Coordination in Phosphorus Chemistry*; Regitz, M.; Scherer, O. J., Eds.; Thieme: Stuttgart, 1990, p 157. (b) Mathey, F. *Acc. Chem. Res.* **1992**, *25*, 90–96.

(10) Yoshifuji, M. *J. Organomet. Chem*. **2000**, *611*, 210–216.

(11) (a) Appel, R.; Casser, C.; Immenkeppel, M.; Knoch, F. *Angew. Chem., Int. Ed.* **1984**, *23*, 895–896. (b) Yoshifuji, M.; Toyota, K.; Inamoto, N. *Tetrahedron Lett*. **1985**, *26*, 1727–1730.

(12) van der Sluis, M.; Beverwijk, V.; Termaten, A.; Bickelhaupt, F; Kooijman, H.; Spek, A. L. *Organometallics* **1999**, *18*, 1402–1407.

(13) Jouaiti, A.; Geoffrey, M .; Bernardinelli, G. *Chem. Commun*. **1996**, 437–438.

(14) Liang, H.; Nishide, K.; Ito, S.; Yoshifuji, M. *Tetrahedron Lett.* **2003**, *44*, 8297–8300.

(15) Appel, R.; Winkhaus, V.; Knoch, F. *Chem. Ber.* **1987**, *120*, 243–245.

(16) Yoshifuji, M.; Ichikawa, Y.; Yamada, N.; Toyota, K. *Chem. Commun.* **1998**, 27–28.

(17) Märkl, G.; Kreitmeier, P.; Nöth, H.; Polborn, K. *Angew. Chem., Int. Ed. Engl.* **1990**, *29*, 927–929.

(18) (a) Ozawa, F.; Yoshifuji, M. *C. R. Chemie* **2004**, *7*, 747–754. (b) Ozawa, F.; Yoshifuji, M. *Dalton Trans.* **2006**, 4987–4995. (c) Ozawa, F. *J. Synth. Org. Chem. Jpn.* **2009**, *67*, 526–539.

(19) Eshtiagh-Hosseihnai, H.; Kroto, H. W.; Nixon, J. F.; Maah, M. J.; Taylor, M. J. *J. Chem. Soc. Chem. Commun.* **1981**, 199–200.

(20) Klebach, T. C.; Lourens, R.; Bickelhaupt, F. *J. Organomet. Chem.* **1981**, *210*, 211–221.

(21) Ikeda, S.; Ohhata, F.; Miyoshi, M.; Tanaka, R.; Minami, T.; Ozawa, F.; Yoshifuji, M. *Angew. Chem., Int. Ed.* **2000**, *39*, 4512–4513.

(22) Daugulis, O.; Brookhart, M.; White, P. S. *Organometallics* **2002**, *21*, 5935–5943.

(23) (a) Minami, T.; Okamoto, H.; Ikeda, S.; Tanaka, R.; Ozawa, F.; Yoshifuji, M. *Angew. Chem., Int. Ed.* **2001**, *40*, 4501–4503. (b) Ozawa, F.; Okamoto, H.; Kawagishi, S.; Yamamoto,

S.; Minami, T.; Yoshifuji, M. *J. Am. Chem. Soc.* **2002**, *124*, 10968–10969. (c) Nagao, M.; Asano, K.; Umeda, K.; Katayama, H.; Ozawa, F. *J. Org. Chem.* **2005**, *70*, 10511–10514. (d) Murakami, H.; Matsui, Y.; Ozawa, F.; Yoshifuji, M. *J. Organomet. Chem.* **2006**, *691*, 3151–3156. (e) Jensen, R. S.; Umeda, K.; Okazaki, M.; Ozawa, F.; Yoshifuji, M. *J. Organomet. Chem.* **2007**, *692*, 286–294.

(24) (a) Toyota, K.; Masaki, K.; Abe, T.; Yoshifuji, M. *Chem. Lett.* **1995**, 221–222. (b) Gajare, A. S.; Toyota, K.; Yoshifuji, M.; Ozawa, F. *J. Org. Chem.,* **2004**, *69*, 6504–6506. (c) Gajare, A. S.; Jensen, R. S.; Toyota, K.; Yoshifuji, M.; Ozawa, F. *Synlett* **2005**, 144–148. (d) Jensen, R. S.; Gajare, A. S.; Toyota, K.; Yoshifuji, M.; Ozawa, F. *Tetrahedron Lett.* **2005**, *46*, 8645–8647. (e) Gajare, A. S.; Toyota, K.; Yoshifuji, M.; Ozawa, F. *Chem. Commun.* **2004**, 1994–1995.

(25) van der Sluis, M.; Beverwijk, V.; Termaten, A.; Gavrilova, E.; Bickelhaupt, F.; Kooijman, H.; Veldman, N.; Spek, A. L. *Organometallics* **1997**, *16*, 1144–1152.

(26) Takeuchi, K.; Minami, A.; Nakajima, Y.; Ozawa, F. *Organometallics* **2014**, *33*, 5365–5370.

(27) Yam, M.; Chong, J. H.; Tsang, C. W.; Patrick, B. O.; Lam, A. E.; Gates, D. P. *Inorg. Chem.* **2006**, *45*, 5225–5234.

(28) Dugal-Tessier, J.; Dake, G. R.; Gates, D. P. *Organometallics* **2007**, *26*, 6481–6486.

(29) Jouaiti, A.; Geoffroy, M.; Bernardinelli, G. *Tetrahedron Lett.* **1992**, *33*, 5071–5074.

(30) Nakajima,Y.; Nakao, Y.; Sakaki, S.; Tamada, Y.; Ono, T.; Ozawa, F. *J. Am. Chem. Soc.* **2010**, *132*, 9934–9936.

(31) Bart, S. C.; Chłopek, K.; Bill, E.; Bouwkamp, M. W.; Lobkovsky, E.; Neese, F.; Wieghardt, K.; Chirik, P. J. *J. Am. Chem. Soc.* **2006**, *128,* 13901–13912.

(32) (a) Nakajima, Y.; Shiraishi, Y.; Tsuchimoto, T.; Ozawa, F. *Chem. Commun.* **2011,** *47*, 6332–6334. (b) Nakajima, Y.; Tsuchimoto, T.; Chang, Y.-H.; Takeuchi, K.; Ozawa, F. *Dalton Trans*. **2016**, *45*, 2079–2084.

(33) Chang, Y.-H.; Nakajima, Y.; Tanaka, H.; Yoshizawa, K.; Ozawa, F. *J. Am. Chem. Soc.* **2013**, *135*, 11791–11794.

(34) For selected reviews, see: (a) Gunanathan, C.; Milstein, D. *Acc. Chem. Res.* **2011**, *44*, 588–602. (b) Gunanathan, C.; Milstein, D. *Science* **2013**, *341*, 249–260. (c) Khusnutdinova, J.

R.; Milstein, D. *Angew. Chem., Int. Ed.* **2015**, *54*, 12236–12273.

(35) Khaskin, E.; Iron, M. A.; Shimon, L. J. W.; Zhang, J.; Milstein, D. *J. Am. Chem. Soc.* **2010**, *132*, 8542–8543.

(36) Chang, Y.-H.; Tanigawa, I.; Taguchi, H.; Takeuchi, K.; Ozawa, F. *Eur. J. Inorg. Chem.* **2016**, 754–760.

(37) de Vaumas, R.; Marinetti, A.; Ricard, L.; Mathey, F. *J. Am. Chem. Soc.* **1992**, *114*, 261–266.

(38) (a) Dugal-Tessier, J.; Dake, G. R.; Gates, D. P. *Angew. Chem., Int. Ed.* **2008**, *47*, 8064–8067. (b) Dugal-Tessier, J.; Dake, G. R.; Gates, D. P. *Org. Lett.* **2010**, *12*, 4667–4669.

(39) Takita, R.; Takada, Y.; Jensen, R. S.; Okazaki, M.; Ozawa, F. *Organometallics* **2008**, *27*, 6279–6285.

(40) The ^{31}P NMR spectroscopy reveals that [RhCl(BPEP)] gives rise to complete loss of P=C bonds under thermal conditions, affording a mixture of diastereomers, *dl*- and *meso*-isomers, via intramolecular C–H addition/cyclization at both the Mes*P=CH units.

(41) (a) Matsuo, T.; Tamao, K. *Bull. Chem. Soc. Jpn.* **2015**, *88*, 1201−1220. (b) Matsuo, T.; Suzuki, K.; Fukawa, T.; Li, B.; Ito, M.; Shoji, Y.; Otani, T.; Li, L.; Kobayashi, M.; Hachiya, M.; Tahara, Y.; Hashizume, D.;Fukunaga, T.; Fukazawa, A.; Li, Y.; Tsuji, H.; Tamao, K. *Bull. Chem. Soc. Jpn.* **2011**, *84,* 1178−1191.

(42) (a) Kobayashi, M. Matsuo, T.; Fukunaga, T.; Hashizume, D.; Fueno, H.; Tanaka, K.; Tamao, K. *J. Am. Chem. Soc.* **2010**, *132*, 15162–1516. (b) Li, L.; Fukawa, T.; Matsuo, T.; Hashizume, D.; Fueno, H.; Tanaka, K.; Tamao, K. *Nat. Chem.* **2012**, *4*, 361–365. (c) Li, B.; Matsuo, T.; Hashizume, D.; Fueno, H.; Tanaka, K.; Tamao, K. *J. Am. Chem. Soc.* **2009**, *131*, 13222–13223.

(43) Li, J.; Schreckenbach, G.; Ziegler, T. *Inorg. Chem.* **1995**, *34*, 3245–3252.

Chapter 1

Catalytic Synthesis of an Unsymmetrical PNP-Pincer Type Phosphaalkene Ligand

Abstract

An unsymmetrical PNP-pincer type phosphaalkene ligand, 2-(phospholanylmethyl)-6-(2-phosphaethenyl)pyridine (PPEP), has been prepared from 2,6-bis(2-phosphaethenyl)pyridine (BPEP) by intramolecular C–H addition/cyclization of the 2-phosphaethenyl group with a 2,4,6-tri-*tert*-butylphenyl substituent (Mes*P=CH). The reaction proceeds in hexane in the presence of a catalytic amount of $[Pt(PCy_3)_2]$ and PCy_3 (both 20 mol%) at 80 °C in a sealed tube, giving PPEP in 32% isolated yield, along with by-production of 2,6-bis(phospholanylmethyl)-pyridine (BPMP) and a Pt(II) phosphanido complex (**5**). The PPEP ligand reacts with $[Rh(\mu\text{-}Cl)(C_2H_4)_2]_2$ and $[RuCl_2(PPh_3)_3]$ to afford [RhCl(PPEP)] (**6**) and $[RuCl_2(PPh_3)(PPEP)]$ (**8**), respectively. Complex **6** easily undergoes C–H addition/cyclization at the other Mes*P=CH group to afford the 2,6-bis(phospholanylmethyl)pyridine complex [RhCl(BPMP)] (**7**), whereas **8** is stable against C–H addition/cyclization. Treatment of **8** with ^{t}BuOK forms $[RuCl(PPh_3)(PPEP^*)]$ (**9**), coordinated with an unsymmetrical PNP-pincer type phosphaalkene ligand containing a dearomatized pyridine unit (PPEP*). The X-ray structures of **5** and **9** are reported. The reaction processes from BPEP to PPEP and to **5** are discussed based on NMR observations.

Introduction

Metal–ligand cooperative activation of chemical bonds has attracted much attention as a powerful approach to highly active catalysis.[1,2] A key to this elementary process is the rational design of functional ligands. In this context, Milstein *et al.* have demonstrated a particular function of pyridine-based PNP-pincer ligands causing heterolytic cleavage of various chemical bonds via metal–ligand cooperation involving aromatization/dearomatization of the pyridine ring.[3,4] This novel ligand system has been applied to catalytic organic transformations that meet the criteria of green and sustainable chemistry.

Recently, Ozawa *et al.* found that the reactivity of a PNP-pincer complex of iridium towards N–H bond cleavage of ammonia is dramatically enhanced by introducing a phosphaalkene unit to the pyridine-based ligand.[5] As shown in Scheme 1, dearomatized PNP-pincer type phosphaalkene complex **3**, derived from 2,6-bis(2-phosphaethenyl)pyridine complex **1** by a two-step procedure, instantly reacts with ammonia (1 atm) at room temperature to afford parent amido complex **4** quantitatively. Phosphaalkene is a low-coordinate phosphorus compound with a P=C bond, which possesses an extremely low-lying π* orbital and thus serves as an extremely strong π-acceptor towards transition metals.[6] DFT calculations revealed a remarkable situation where the phosphaalkene ligands (PPEP/PPEP*) stabilize reaction intermediates and transition states via effective dπ–pπ interactions, leading

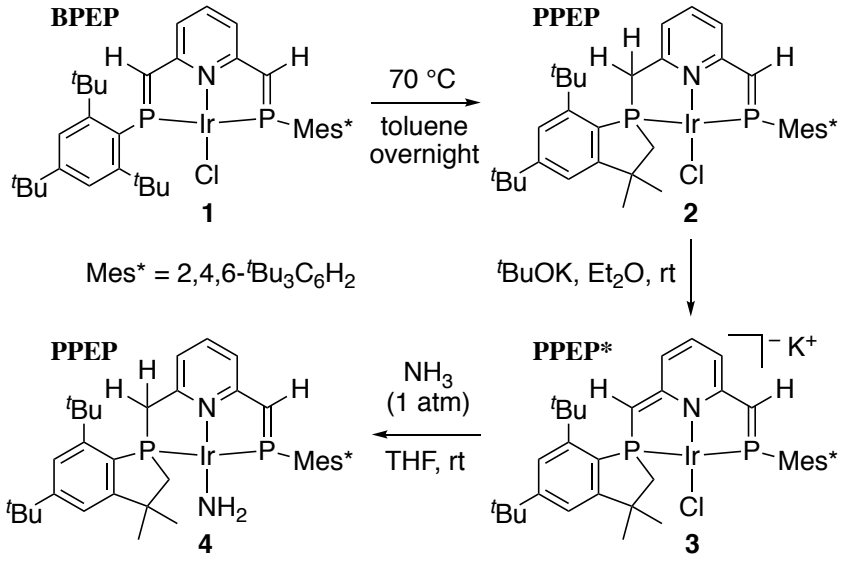

Scheme 1. PNP-pincer type phosphaalkene complexes of Ir(I).[5a]

to extremely high reactivity towards ammonia. In this study, the author attempted to prepare 2-(phospholanylmethyl)-6-(2-phosphaethenyl)pyridine (PPEP) in a free state, with expectations of expanding the utility of this particular ligand system in organometallic chemistry.

As seen from Scheme 1, the PPEP ligand is formed from 2,6-bis(2-phosphaethenyl)-pyridine (BPEP) by C–H addition/cyclization at one of the 2-phosphaethenyl groups with a 2,4,6-tri-*tert*-butylphenyl substituent (Mes*P=CH). Since the conversion of BPEP to PPEP on iridium (**1** → **2**) did not proceed catalytically, the author examined a platinum-catalyzed reaction, referring to a closely related study on catalytic conversion of 1,5-bis(2-phosphaethenyl)benzene (**I**) to 1,5-bis(2-phospholanylmethyl)benzene (**II**) (Scheme 2).[7] Although the C–H addition/cyclization of the benzene analogue proceeds successively at both phosphaalkene units, the reaction of BPEP proceeds in a stepwise manner, leading to the isolation of free PPEP.

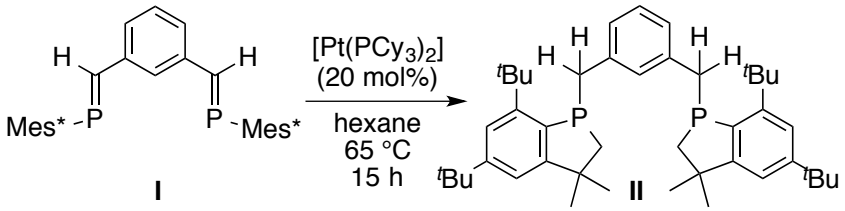

Scheme 2. Platinum-catalyzed C–H addition/cyclization of 2,6-bis(2-phosphaethenyl)benzene.[7]

Results and Discussion

Catalytic Conversion of BPEP to PPEP. The BPEP ligand (9.8 mg) was treated with a catalytic amount of [$Pt(PCy_3)_2$] (20 mol%) in hexane at 80 °C in a sealed NMR sample tube for 12 h (Scheme 3), and the reaction system was examined by NMR spectroscopy. The result is given in entry 1 in Table 1. This reaction also formed a solid product of **5** (vide infra), but its amount was too small to confirm (< 1 mg). Therefore, the product ratio observed in the solution is reported.

The $^{31}P\{^{1}H\}$ NMR spectrum exhibited the signals arising from BPEP (δ 283.5), PPEP (δ 283.4 and –6.5), and 2,6-bis(phospholanylmethyl)pyridine (BPMP; δ –6.2 and –6.4, a 1:1 mixture of diastereomers) in a 39:55:6 ratio (entry 1). The reaction did not proceed with

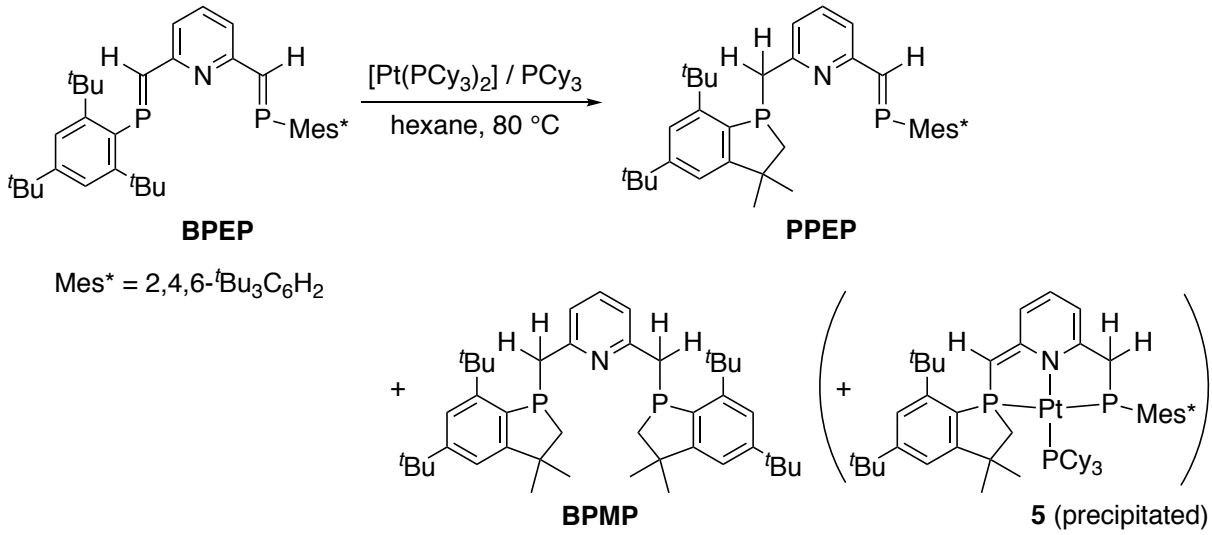

Scheme 3. Platinum-catalyzed C–H addition/cyclization of 2,6-bis(2-phosphaethenyl)pyridine (BPEP).

Table 1. Catalytic Conversion of BPEP under Various Conditions [a]

entry	catalyst	additive (equiv/Pt)	time (h)	ratio[b]		
				BPEP	BPEP	BPEP
1	$[Pt(PCy_3)_2]$	–	12	39	55	6
2	$[Pt(cod)_2]$	–	40	100	0	0
3	$[Pt(cod)_2]$	PCy_3 (2)	12	42	53	5
4	$[Pt(PCy_3)_2]$	PCy_3 (1)	12	27	65	8
5	$[Pt(PCy_3)_2]$	PCy_3 (1)	24	9	71	20
6	$[Pt(PCy_3)_2]$	PCy_3 (1)	264	0	0	100
7	$[PtMe_2(\mu\text{-}SMe_2)]_2$	PCy_3 (2)	12	100	0	0
8	$[PtCl_2(PCy_3)_2]$	PCy_3 (2)	12	100	0	0

[a] All reactions were run in hexane (0.5 mL) at 80 °C, using BPEP (0.015 mmol), catalyst (20 mol%), and additive. [b] The product ratio in solution as confirmed by $^{31}P\{^1H\}$ NMR analysis.

[$Pt(cod)_2$] (entry 2), but addition of free PCy_3 resulted in the formation of PPEP in comparable selectivity to entry 1 (entry 3). The conversion of BPEP was improved, keeping the selectivity for PPEP, when 1 equiv/Pt of PCy_3 was added to [$Pt(PCy_3)_2$] (entry 4). The conversion was further enhanced in a prolonged reaction time; however, the product ratio of PPEP gradually decreased (entry 5), and eventually the doubly cyclized compound (BPMP) became the sole product (entry 6). Unlike the Pt(0) catalysts, Pt(II) complexes did not show the catalytic activity (entries 7 and 8).

Next, the author attempted to isolate free PPEP under the catalytic conditions of entry 4 in Table 1. BPEP (131 mg) was heated with [$Pt(PCy_3)_2$] and PCy_3 (both 20 mol%) in hexane (3.5 mL) at 80 °C in a sealed Schlenk tube for 12 h, where a small quantity of orange solid (11 mg) was precipitated from the solution. As described in the next section, this solid was identified as phosphanido complex **5** depicted in Scheme 3. The solution part was concentrated to dryness and subjected to column chromatography, giving free PPEP as a white solid in 32% yield. This product contained small amounts of BPEP and the *Z*-isomer of PPEP, but was successfully applied to the synthesis of PPEP complexes of ruthenium and rhodium (vide infra).

Identification of 5. Figure 1 shows the X-ray structure of **5**, demonstrating a distorted square planar configuration around platinum. The PNP-pincer ligand adopts a meridional coordination with the P1–Pt–P2 angle of 162.89(4)°, whereas PCy_3 is located trans to the pyridine unit. The P1–C1 bond (1.747(4) Å) is clearly shorter than typical P–C single bonds, and the C1–C3 bond (1.382(6) Å) is between those expected for a single and double bond. These bond variations are characteristic of PNP-pincer ligands with a dearomatized pyridine unit.[4,5]

The most remarkable feature of **5** is a significantly pyramidalized geometry around P2. Because the P2–C2 bond is saturated (1.879(2) Å), the P2 unit can be identified as a phosphanido ligand, formed by protonation at the C2 atom of parent phosphaethenyl group. The sum of the bond angles around P2 is 298.81°; this value is among the smallest of terminal phosphanido complexes of platinum (306–333°).[8] Moreover, since the C2–P2–Pt bond bends to nearly 90° (89.30(13)°), the least contribution of the s-orbital of phosphorus to Pt–P2 bond

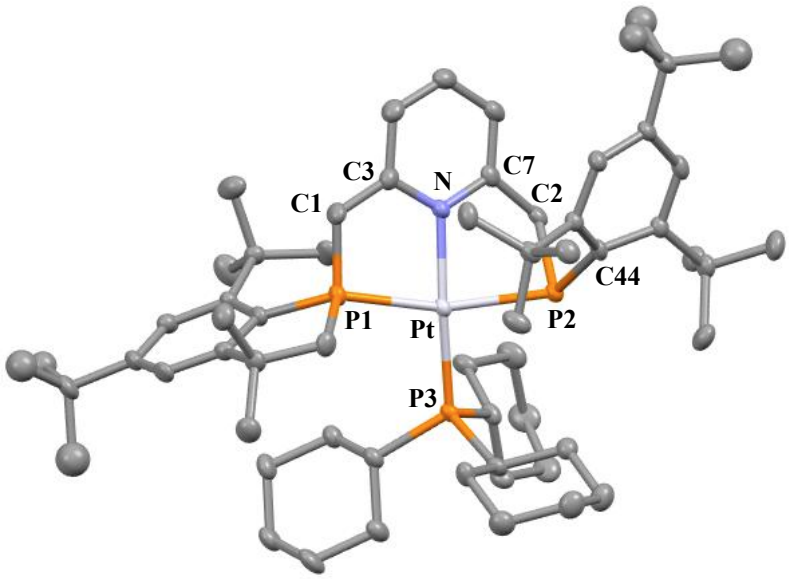

Figure 1. Molecular structure of **5** with 50% probability ellipsoids. Hydrogen atoms and disordered carbon atoms (^{t}Bu) are omitted for clarity. Selected bond distances (Å) and angles (deg): Pt–N 2.073(3), Pt–P1 2.3259(11), Pt–P2 2.3892(11), Pt–P3 2.2839(11), P1–C1 1.747(4), P2–C2 1.879(2), C1–C3 1.382(6), C2–C7 1.486(6), N–Pt–P3 167.49(10), P1–Pt–P2 162.89(4), C2–P2–Pt 89.30(13), C2–P2–C44 92.33(18), C44–P2–Pt 117.18(13).

is suggested. Indeed, the $^{31}P\{^1H\}$ NMR signal of P2 (δ 35.3) exhibited an extremely small coupling to platinum ($^1J_{PtP}$ = 599 Hz). On the other hand, the $^1J_{PtP}$ couplings for P1 (δ 26.6, $^1J_{PtP}$ = 1986 Hz) and P3 (δ 14.7, $^1J_{PtP}$ = 3515 Hz) were consistent with the phosphorus ligands trans to the anionic phosphanido and neutral pyridine ligand, respectively. The ^1H NMR spectrum displayed characteristic signals of a dearomatized pyridine unit at δ 6.24, 6.00, and 4.98 (pyridine ring protons) and at δ 3.73 (vinylic proton).[4,5]

Study on the Formation Process of PPEP from BPEP. Complex **5** gradually decomposed in toluene in the presence of 1 equiv of PCy_3 at 80 °C, but did not generate free PPEP. Thus, the author concluded that this complex is a dead-end side-product, responsible for the relatively large catalyst loading (20 mol%). Scheme 4 shows a plausible catalytic process for the formation of PPEP from BPEP, including the side reaction to afford **5**. Although Le Floch *et al*. previously reported DFT calculations showing a C–H addition/cyclization process via a π-coordinated phosphaalkene intermediate,[7] the author could obtain an evidence for the

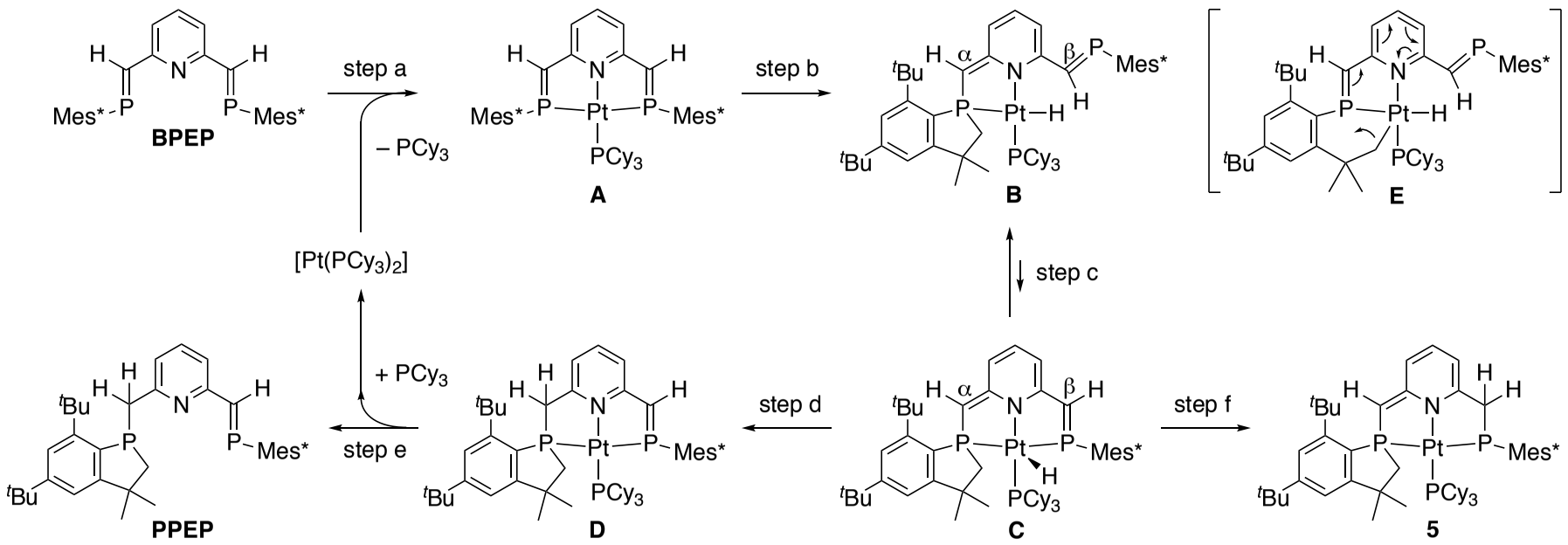

Scheme 4. Plausible catalytic process for the formation of PPEP from BPEP.

catalytic process involving meridional coordination of PNP-pincer ligands.

The first step is the coordination of BPEP to platinum along with liberation of PCy_3 (step a). To gain structural information about [Pt(PCy_3)(BPEP)] (**A**), a 1:1 mixture of [Pt(PCy_3)$_2$] and BPEP were dissolved in toluene-d^8 at –78 °C, and examined by $^{31}P\{^1H\}$ NMR spectroscopy at –10 °C, showing the signals assignable to coordinated BPEP and PCy_3 at δ 113.7 (d, $^2J_{PP}$ = 31 Hz, $^1J_{PtP}$ = 1543 Hz) and 17.9 (t, $^2J_{PP}$ = 31 Hz, $^1J_{PtP}$ = 4154 Hz) in a 2:1 ratio. In this case, since the chemical shift of BPEP (δ 113.7) was too upfield for a phosphaalkene ligand (ca. δ 240–260),[6] its reason was investigated by DFT calculations.

Figure 2(a) shows the optimized structure for model compound **A1**, in which the 2,4,6-^{t}Bu$_3$C$_6$H$_2$ (Mes*) groups and PCy_3 ligand in **A** are replaced with 2,6-^{t}Bu$_2$C$_6$H$_3$ (Ar) and PMe_3, respectively. Although this complex is formally a Pt(0) species, the platinum center adopts a square planer configuration typical of Pt(II) species; the sum of the four bond angles around Pt is 361.3°. Moreover, the P1–C1 bond (1.73 Å) is clearly elongated compared with ordinary phosphaalkene ligands (1.68 Å). Thus, it is reasonable that the complex possesses a great contribution of canonical structures **A1'** and **A1"** in Figure 2(b), in which one of the phospha-alkene ligands changes to an anionic phosphanido ligand along with dearomatization of the

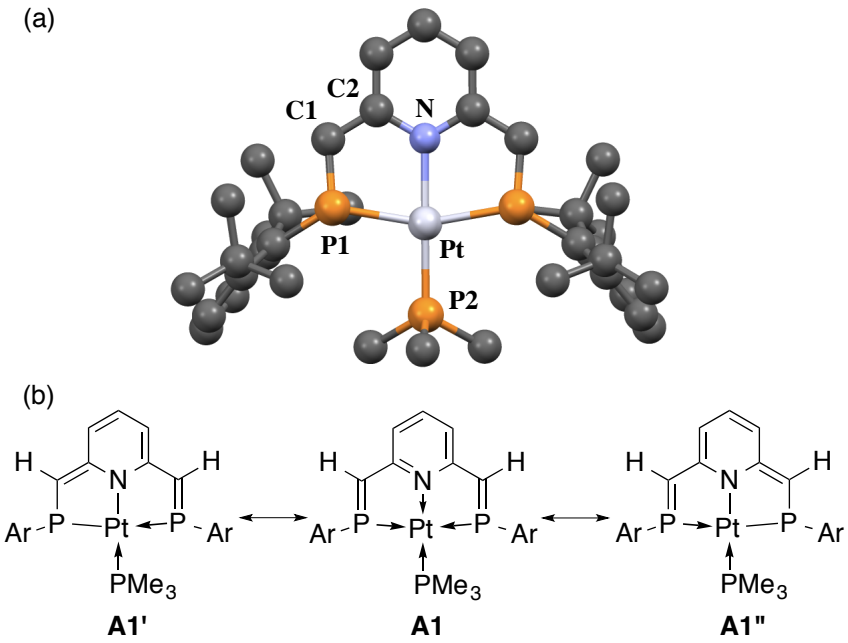

Figure 2. (a) Optimized structure of [Pt(PMe_3)(BPEP')] (**A1**). (b) Resonance structures of **A1** (Ar = 2,6-^{t}Bu$_2$C$_6$H$_3$). Selected bond distances (Å) and angles (deg): Pt–N 2.11, Pt–P1 2.35, Pt–P2 2.29, P1–C1 1.73, C1–C2 1.41, N–Pt–P1 80.5, N–Pt–P2 174.6.

pyridine unit. The ^{31}P NMR chemical shift estimated by the GIAO method (δ 102.7) was in good agreement with the observed value for the real complex **A** (δ 113.7).

When the solution of **A** was allowed to stand at room temperature, the $^{31}P\{^{1}H\}$ NMR signals of **A** decreased, and three signals with nearly the same intensities increased at δ 247.4, 28.2 ($^{1}J_{PtP}$ = 3480 Hz), and 25.3 ($^{1}J_{PtP}$ = 1985 Hz). These signals were assigned to hydrido complex **B**, formed by C–H oxidative addition of a ^{t}Bu group, followed by P–C reductive elimination from intermediate **E**, based on the following NMR observations (step b in Scheme 4). The presence of a hydrido ligand was evidenced by the appearance of a double doublet signal at δ –6.82 in the ^{1}H NMR spectrum. This signal involved two sets of $^{2}J_{PH}$ couplings (182 and 16 Hz) and ^{195}Pt satellites (996 Hz); the large and small $^{2}J_{PH}$ values are consistent with trans and cis arrangements of the hydrido ligand to phosphorus ligands in a square planar configuration. The ^{31}P NMR signal at δ 247.4 did not involve ^{195}Pt satellites, showing dissociation of the phosphaalkene unit. On the other hand, the ^{31}P NMR signals at δ 28.2 and 25.3 involved ^{195}Pt satellites. In this case, the relatively large coupling for the former signal (3480 Hz) was consistent with the PCy_3 ligand trans to the pyridine unit, whereas the small coupling for the latter signal (1985 Hz) was in accord with the phospholanyl group trans to the hydrido ligand with strong trans influence.

The next step is the 1,3-shift of the hydrido ligand to the *exo*-methylene carbon or phosphaalkene carbon of the dearomatized PNP-pincer ligand (step c → step d or f in Scheme 4). In this step, the hydrido ligand very probably changes the coordination site from the equatorial to apical position (**B** → **C** in step c), to ensure the orbital interaction between the Pt–H bond and π* orbitals on the carbon atoms. Migration of the hydrido ligand to the α-position on **C** forms PPEP complex **D**, which subsequently undergoes ligand substitution with free PCy_3 to give free PPEP and $[Pt(PCy_3)_2]$ (step d → step e). On the other hand, migration to the β-position affords **5** (step f).

Synthesis of PPEP Complex of Rh(I). Next, the author introduced free PPEP to rhodium and ruthenium complexes (Scheme 5). The reaction of $[Rh(\mu\text{-}Cl)(C_2H_4)_2]_2$ with PPEP (1 equiv/Rh) in THF-d^8 readily proceeded at –70 °C to form [RhCl(PPEP)] (**6**) exclusively (path a). The $^{31}P\{^{1}H\}$ NMR signals appeared at δ 243.4 (dd, $^{2}J_{PP}$ = 463 Hz, $^{1}J_{RhP}$ = 186 Hz) and

26.0 (dd, $^{2}J_{PP}$ = 463 Hz, $^{1}J_{RhP}$ = 167 Hz); the chemical shifts and coupling patterns were consistent with complex **6** coordinated with PPEP as an unsymmetrical PNP-pincer type phosphaalkene ligand. However, this complex could not be isolated due to the high reactivity of the phospha-ethenyl unit (Mes*P=CH) to C–H addition/cyclization. Instead, the doubly cyclized complex [RhCl(BPMP)] (**7**) was obtained in 71% yield as a 5:1 mixture of diastereomers (path b).[9]

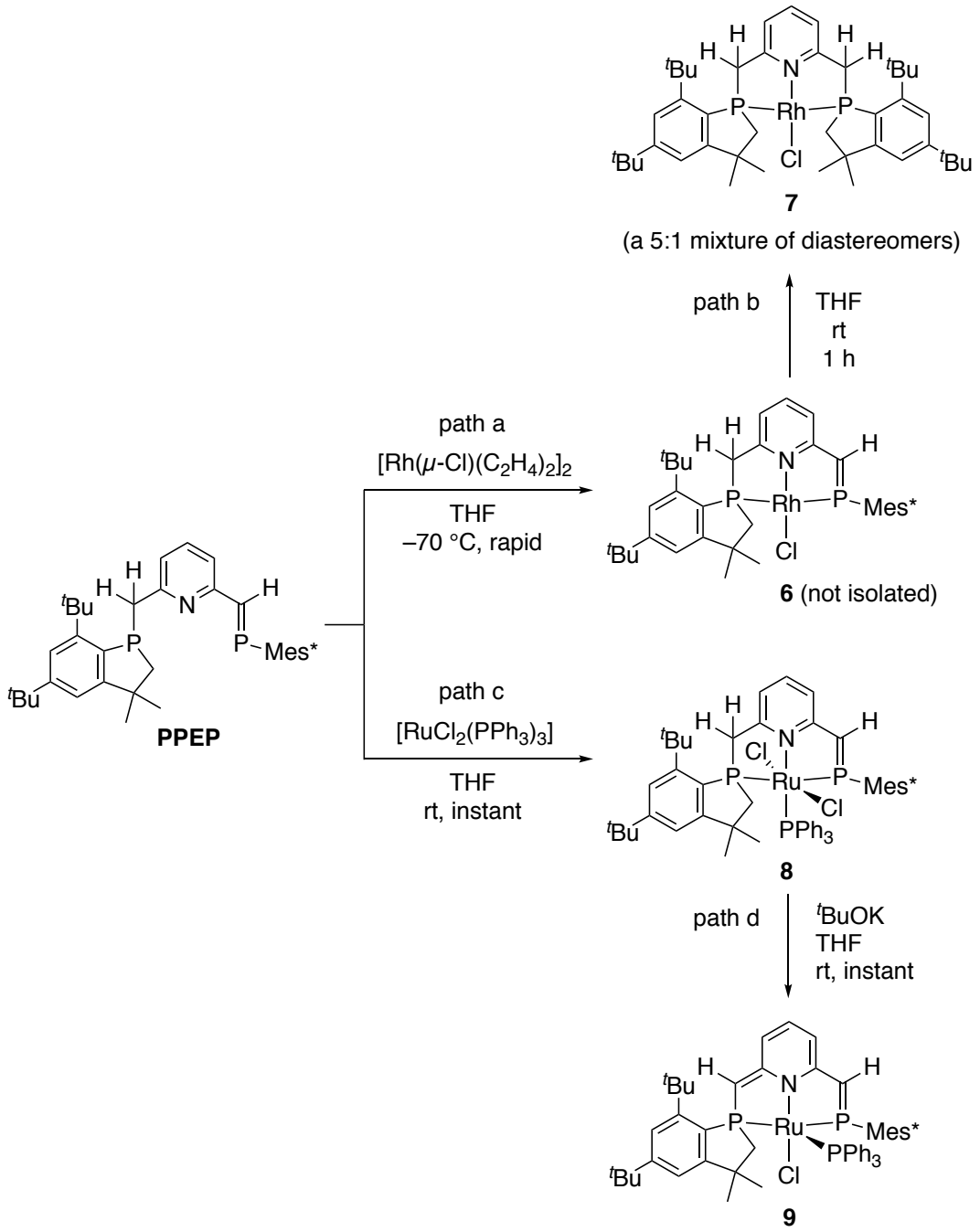

Scheme 5. Synthesis of PPEP complexes of Rh(I) and Ru(II).

Synthesis of PPEP Complex of Ru(II). Treatment of $[RuCl_2(PPh_3)_3]$ with PPEP (1 equiv/Ru) in THF at room temperature led to $[RuCl_2(PPh_3)(PPEP)]$ (**8**) quantitatively. Unlike the rhodium complex **6**, this ruthenium complex was stable enough for isolation as a purple solid in 69% yield (path c in Scheme 5). The $^{31}P\{^1H\}$ NMR spectrum showed three sets of signals arising from PPEP (δ 292.0 (dd) and 50.5 (dd); $^2J_{PP}$ = 411 and 29 Hz) and PPh_3 (δ 34.8 (t), $^2J_{PP}$ = 29 Hz).

Complex **8** reacted with ^{t}BuOK in THF at room temperature to give $[RuCl(PPh_3)(PPEP^*)]$ (**9**) as a dearomatized complex, which was isolated as dark green crystals in 69% yield (path d). The ^1H NMR signals of the dearomatized pyridine unit were observed at δ 6.06, 5.78, and 5.25 (pyridine ring protons) and at δ 3.76 (vinylic proton). The $^{31}P\{^1H\}$ NMR signals appeared at δ 217.9 (dd, $^2J_{PP}$ = 298 and 24 Hz), 58.4 (dd, $^2J_{PP}$ = 40 and 24 Hz), and 46.7 (dd, $^2J_{PP}$ = 298 and 40 Hz). The signals at δ 217.9 and 46.7 ppm with a large $^2J_{PP}$ coupling (298 Hz) are due to PPEP, whereas the signal at δ 58.4 with small $^2J_{PP}$ couplings (40 and 24 Hz) is due to PPh_3 located cis to the PPEP ligand.

Figure 3 shows the X-ray structure of **9**, which adopts a square pyramidal configuration around Ru (τ = 0.12).[10] The PPh_3 ligand is accommodated at the apical position, whereas the Cl ligand is located trans to the pyridine unit on the basal plane. The bond lengths of Ru–N (2.0990(18) Å), Ru–P1 (2.2974(6) A), and Ru–P3 (2.2534(6) A) are ordinary for a five-coordinated Ru(II) complex, whereas the Ru–P2 bond (2.5208(6) Å) is clearly elongated as compared with the analogous complex $[RuCl(CO)_2(PPEP^*\text{-}Ph)]$ (2.3571(14)Å).[11] The elongation of Ru–P2 bond may be caused by steric repulsion between PPh_3 and bulky substituents of PPEP*. In any event, the elongation of Ru–P2 bond results in weakening of π-back-donation from ruthenium to the P=C bond. Actually, the P2–C2 bond length (1.672(2) Å) was in agreement with that of a non-activated P=C double bond (1.66–1.68 Å). Moreover, the P1–C1 (1.753(2) Å) and C1–C3 (1.379(3) Å) bond lengths were typical of PNP-pincer ligands with a dearomatized pyridine unit.[4]

Conclusion

In summary, the author succeeded in platinum-catalyzed synthesis of an unsymmetrical PNP-pincer type phosphaalkene ligand (PPEP) from bis(phosphaethenyl)pyridine (BPEP) via

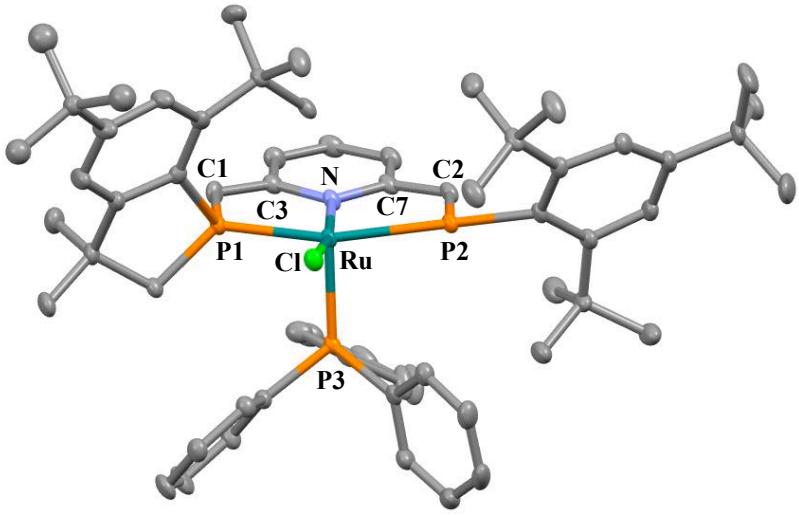

Figure 3. Molecular structure of **9** with 50% probability ellipsoids. Hydrogen atoms, a crystal solvent (pentane), and disordered carbon atoms (^{t}Bu) are omitted for clarity. Selected bond distances (Å) and angles (deg): Ru–N 2.0990(18), Ru–P1 2.2974(6), Ru–P2 2.5208(6), Ru–P3 2.2534(6), Ru–Cl 2.4120(6), P1–C1 1.753(2), P2–C2 1.672(2), C1–C3 1.379(3), C2–C7 1.438(3), N–Ru–Cl 167.51(6), P1–Ru–P2 160.39(2), N–Ru–P3 96.99(5).

intramolecular C–H addition/cyclization of the Mes*P=CH group. Unlike the reaction of benzene analogue **I** in Scheme 2, the reaction of BPEP proceeded in a stepwise manner, and the desired product (free PPEP) could be isolated in moderate yield (32%). The PPEP ligand reacted with Rh(I) and Ru(II) precursors to afford [RhCl(PPEP)] (**6**) and [$RuCl_2(PPh_3)$(PPEP)] (**8**), respectively. The Mes*P=CH group in **6** was still reactive to C–H addition/cyclization giving [RhCl(BPMP)] (**7**) with a doubly cyclized PNP-pincer ligand (BPMP). On the other hand, ruthenium complex **8** was sufficiently stable for isolation, and underwent the abstraction of a benzylic proton with ^{t}BuOK to form [$RuCl(PPh_3)$(PPEP*)] (**9**) with a dearomatized PNP-pincer type phosphaalkene ligand (PPEP*).

Plausible intermediates **A** and **B** in the catalytic conversion of BPEP to PPEP could be detected by NMR spectroscopy. The $^{31}P\{^1H\}$ NMR signal of **A** appeared at an extremely high magnetic field. This is possibly due to the occurrence of strong π-back-donation from platinum to phosphaalkene units. DFT calculations for the model compound (**A1**) revealed a square planar configuration around platinum despite the formal Pt(0) species. Complex **B** was assignable to a four-coordinated platinum hydride with an uncoordinated phosphaalkene unit

and a dearomatized pyridine unit. It was rationalized that **B** undergoes coordination of the phosphaalkene unit, followed by 1,3-shift of the hydrido ligand to the *exo*-methylene carbon of the dearomatized pyridine unit, giving [Pt(PCy_3)(PPEP)] (**D**), which subsequently releases PPEP by ligand substitution with PCy_3. On the other hand, 1,3-shift to the phosphaalkene carbon forms a novel phosphanido complex (**5**), whose structure was confirmed by X-ray diffraction analysis.

Experimental Section

General Considerations. All manipulations were carried under a nitrogen atmosphere using standard Schlenk techniques or a glove box. Nitrogen gas was dried by passing through a P_2O_5 column. THF, Et_2O, hexane, and pentane (dehydrated) were used as received. C_6D_6 and THF-d_8 were dried over sodium/benzophenone, distilled, and stored over activated MS4A. 2,6-Bis(phosphaethenylpyridine) (BPEP),[12] [Pt(PCy_3)$_2$],[13] [$PtCl_2(PCy_3)_2$],[13] [Rh(μ-Cl)-$(C_2H_4)_2]_2$,[14] and [$RuCl_2(PPh_3)_3$][15] were prepared according to the literature. The other chemicals were obtained from commercial sources and used without purification. NMR spectra were recorded on a 400 MHz spectrometer. Chemical shifts are reported in δ (ppm), referenced to ^{1}H (residual) and ^{13}C signals of deuterated solvents as internal standards or to the ^{31}P signal of 85% H_3PO_4 as an external standard. Elemental analysis was performed by ICR Analytical Laboratory, Kyoto University.

Catalytic Conversion of BPEP to PPEP (Table 1). A typical procedure (entry 2) is as follows. A hexane solution (0.2 mL) of BPEP (9.8 mg, 15 μmol) and PCy_3 (0.8 mg, 3.0 μmol) was added dropwise to a suspension of [Pt(PCy_3)$_2$] (2.3 mg, 3.0 μmol) in hexane (0.3 mL) at room temperature. The mixture was heated at 80 ºC for 12 h, and the ratio of BPEP, PPEP, and BPMP were determined by ^{31}P{^{1}H} NMR analysis at room temperature.

Preparation of PPEP and 5. A mixture of BPEP (131 mg, 0.20 mmol), [Pt(PCy_3)$_2$] (30 mg, 0.040 mmol), and PCy_3 (11 mg, 0.040 mmol) in hexane (3.5 mL) was heated at 80 °C for 12 h. The color of the solution gradually changed from green to brown, and orange crystals of **5** were precipitated. The solution was separated by decantation, and the crystals of **5** were washed with hexane (1 mL × 3) and dried under vacuum (11 mg, 25% yield/Pt). The solution part was concentrated to dryness, and subjected to column chromatography on 3-

aminopropyl-functionalized silica gel using hexane as the eluent, to afford PPEP as a white solid (41 mg, 0.063 mmol, 32%). This product contained small amounts of impurities including BPEP and the *Z*-isomer of PPEP, as confirmed by NMR analysis.

PPEP: ^{1}H NMR (C_6D_6, 25 °C): δ 8.27 (d, $^{2}J_{PH}$ = 25.6 Hz, 1H, P=C*H*), 7.63 (s, 2H, Ar), 7.55 (dd, $^{4}J_{PH}$ = 4.0, $^{4}J_{HH}$ = 1.7 Hz, 1H, Ar), 7.24 (d, $^{4}J_{HH}$ = 1.7 Hz, 1H, Ar), 6.98 (t, $^{3}J_{HH}$ = 7.7 Hz, 1H, 4-Py), 6.75 (d, $^{3}J_{HH}$ = 7.7 Hz, 2H, 3,5-Py), 3.38 (dd, $^{2}J_{PH}$ = 3.6, $^{2}J_{HH}$ = 12.8 Hz, 1H, PyC*H*$_2$P), 3.32 (dd, $^{2}J_{PH}$ = 4.8, $^{2}J_{HH}$ = 12.8 Hz, 1H, PyC*H*$_2$P), 2.59 (dd, $^{2}J_{PH}$ = 2.0, $^{2}J_{HH}$ = 14.7 Hz, 1H, PC*H*$_2$), 1.95 (dd, $^{2}J_{PH}$ = 22.5, $^{2}J_{HH}$ = 14.7 Hz, 1H, PC*H*$_2$), 1.73 (s, 3H, C*H*$_3$), 1.66 (s, 9H, C*H*$_3$ of ^{t}Bu), 1.62 (s, 18H, C*H*$_3$ of ^{t}Bu), 1.36 (s, 9H, C*H*$_3$ of ^{t}Bu), 1.34 (s, 9H, C*H*$_3$ of ^{t}Bu), 1.30 (s, 3H, C*H*$_3$). ^{13}C{^{1}H} NMR (C_6D_6, 25 °C): δ 176.1 (d, J_{PC} = 35 Hz), 160.5 (d, J_{PC} = 6 Hz), 160.1 (s), 158.1 (d, J_{PC} = 12 Hz), 155.1 (s), 153.1 (d, J_{PC} = 15 Hz), 152.9 (s), 150.4 (s), 141.3 (d, J_{PC} = 54 Hz), 137.1 (s), 136.7 (d, J_{PC} = 23 Hz), 122.6 (s), 122.4 (t, J_{PC} = 5 Hz), 119.7 (s), 118.7 (d, J_{PC} = 16 Hz), 47.6 (d, J_{PC} = 7 Hz), 40.8 (d, J_{PC} = 27 Hz), 39.0 (s), 38.1 (d, J_{PC} = 2 Hz), 36.9 (d, J_{PC} = 10 Hz), 35.6 (d, J_{PC} = 2 Hz), 35.0 (d, J_{PC} = 4 Hz), 34.6 (d, J_{PC} = 7 Hz), 34.2 (s), 33.2 (d, J_{PC} = 9 Hz), 32.1 (s), 32.0 (s). ^{31}P{^{1}H} NMR (C_6D_6, 25 °C): δ 282.5 (s), –7.4 (s). HRMS (ESI): Calcd for $C_{43}H_{64}NP_2$ 656.4509 ([M+H]$^{+}$); Found 656.4509.

[5]: ^{1}H NMR (THF-d_8, 25 °C): δ 7.49 (dd, $^{4}J_{PH}$ = 4.2 Hz, $^{4}J_{HH}$ = 1.7 Hz, 1H, Ar), 7.33 (br t, $^{4}J_{PH}$ = 2.9 Hz, $^{4}J_{HH}$ = 2.2 Hz, 1H, Ar), 7.22 (d, $^{4}J_{HH}$ = 1.7 Hz, 1H, Ar), 7.16 (d, $^{4}J_{HH}$ = 2.2 Hz, 1H, Ar), 6.24 (ddd, $^{3}J_{HH}$ = 8.6 and 6.6 Hz, $^{5}J_{PH}$ = 1.8 Hz, 1H, Py), 6.00 (br d, $^{3}J_{HH}$ = 8.6, 1H, Py), 4.98 (br, $^{3}J_{HH}$ = 6.6 Hz, 1H, Py), 3.73 (vt, J_{app} = 2.4 Hz, 1H, Py=C*H*P), 2.90 (dd, $^{2}J_{PH}$ = 26.2 Hz, $^{2}J_{HH}$ = 14.9 Hz, 1H, PyC*H*$_2$P), 2.84 (d, $^{2}J_{HH}$ = 14.9 Hz, 1H, PC*H*$_2$), 2.17 (dd, $^{2}J_{HH}$ = 14.9 Hz, $^{2}J_{PH}$ = 5.3 Hz, 1H, PyC*H*$_2$P), 1.94 (dd, $^{2}J_{HH}$ = 14.9 Hz, $^{2}J_{PH}$ = 7.8 Hz, 1H, PC*H*$_2$), 1.92-1.98 (br, 3 H, PCy$_3$), 1.75 (s, 9H, C*H*$_3$ of ^{t}Bu), 1.54 (s, 3H, C*H*$_3$), 1.57 (s, 9H, C*H*$_3$ of ^{t}Bu), 1.47 (s, 9H, C*H*$_3$ of ^{t}Bu), 1.32 (s, 9H, C*H*$_3$ of ^{t}Bu), 1.33 (s, 3H, C*H*$_3$), 1.29 (s, 9H, C*H*$_3$ of ^{t}Bu), 1.25-1.34 (br, 18 H, PCy$_3$), 1.10-1.24 (br, 12 H, PCy$_3$). The ^{13}C{^{1}H} NMR spectrum was not recorded because of the low solubility of **5**. ^{31}P{^{1}H} NMR (THF-d_8, 25 °C): δ 35.3 (br d, $^{2}J_{PP}$ = 65 Hz, $^{1}J_{PtP}$ = 599 Hz), 26.6 (dd, $^{2}J_{PP}$ = 65 and 19 Hz, $^{1}J_{PtP}$ = 1986 Hz), 14.7 (d, $^{2}J_{PP}$ = 19 Hz, $^{1}J_{PtP}$ = 3515 Hz). Anal. Calcd for $C_{61}H_{96}NP_3Pt$: C, 64.75; H, 8.55; N, 1.24. Found: C, 64.34; H, 8.77; N, 1.39.

Preparation of BPMP. A toluene solution (2 mL) of BPEP (131 mg, 0.20 mmol) and PCy_3 (11 mg, 0.040 mmol) was added to a suspension of $[Pt(PCy_3)_2]$ (30 mg, 0.040 mmol) in toluene (1.5 mL) at room temperature. The solution was heated at 100 °C for 50 h, and concentrated to dryness under reduced pressure. The crude product was purified by column chromatography on 3-aminopropyl-functionalized silica gel using hexane as the eluent, to give a white solid of BPMP as a 6:4 mixture of diastereomers (48 mg, 0.073 mmol, 36%). With consideration of the steric conditions, the major isomer was assigned to the *dl*-isomer. Anal. Calcd for $C_{43}H_{63}NP_2$: C, 78.74; H, 9.68; N, 2.14. Found: C, 78.45; H, 9.94; N, 2.20.

***dl*-BPMP:** ^{1}H NMR (C_6D_6, 25 °C): δ 7.57 (d, $^4J_{HH}$ = 2.9 Hz, 2H, Ar), 7.25 (d, $^4J_{HH}$ = 1.7 Hz, 2H, Ar), 7.07 (t, $^3J_{HH}$ = 6.7 Hz, 1H, 4-Py), 6.81 (d, $^3J_{HH}$ = 7.6 Hz, 2H, 3,5-Py), 3.29–3.42 (m, 4H, PyCH_2P), 2.46 (dd, $^2J_{PH}$ = 1.8, $^2J_{HH}$ = 14.6 Hz, 2H, PCH_2), 2.02 (dd, $^2J_{PH}$ = 22.4, $^2J_{HH}$ = 14.7 Hz, 2H, PCH_2), 1.69 (s, 18H, CH_3 of ^{t}Bu), 1.66 (s, 6H, CH_3), 1.35 (s, 18H, CH_3 of ^{t}Bu), 1.29 (s, 6H, CH_3). ^{13}C{^{1}H} NMR (C_6D_6, 25 °C): 160.3 (d, J_{PC} = 8 Hz), 159.8 (s), 153.1 (s), 152.9 (s), 136.9 (d, J_{PC} = 19 Hz), 136.8 (s), 122.5 (d, J_{PC} = 5 Hz), 121.0 (d, J_{PC} = 4 Hz), 119.6 (s), 47.6 (d, J_{PC} = 7 Hz), 41.3 (d, J_{PC} = 25 Hz), 38.2 (s), 37.9 (d, J_{PC} = 10 Hz), 35.6 (s), 34.9 (s), 34.4 (s), 33.3 (s), 32.1 (s). ^{31}P{^{1}H} NMR (C_6D_6, 25 °C): δ –7.0 (s).

***meso*-BPMP:** ^{1}H NMR (C_6D_6, 25 °C): δ 7.58 (d, $^4J_{HH}$ = 2.8 Hz, 2H, Ar), 7.27 (d, $^4J_{HH}$ = 1.6 Hz, 2H, Ar), 7.08 (t, $^3J_{HH}$ = 6.7 Hz, 1H, 4-Py), 6.81 (d, $^3J_{HH}$ = 7.6 Hz, 2H, 3,5-Py), 3.29–3.42 (m, 4H, PyCH_2P), 2.42 (dd, $^2J_{PH}$ = 1.7, $^2J_{HH}$ = 14.8 Hz, 2H, PCH_2), 1.96 (dd, $^2J_{PH}$ = 24.1, $^2J_{HH}$ = 14.7 Hz, 2H, PCH_2), 1.71 (s, 18H, CH_3 of ^{t}Bu), 1.66 (s, 6H, CH_3), 1.35 (s, 18H, CH_3 of ^{t}Bu), 1.29 (s, 6H, CH_3). ^{13}C{^{1}H} NMR (C_6D_6, 25 °C): 160.1 (d, J_{PC} = 8 Hz), 159.9 (s), 153.2 (s), 152.9 (s), 136.9 (d, J_{PC} = 19 Hz), 136.8 (s), 122.4 (d, J_{PC} = 5 Hz), 121.0 (d, J_{PC} = 4 Hz), 119.7 (s), 47.6 (d, J_{PC} = 7 Hz), 41.1 (d, J_{PC} = 25 Hz), 38.2 (s), 37.2 (d, J_{PC} = 10 Hz), 35.6 (s), 34.9 (s), 34.4 (s), 33.2 (s), 32.1 (s). ^{31}P{^{1}H} NMR (C_6D_6, 25 °C): δ –7.1 (s).

Stoichiometric Reaction of BPEP with $[Pt(PCy_3)_2]$. A solution of BPEP (10 mg, 0.015 mmol) and $[Pt(PCy_3)_2]$ (11 mg, 0.015 mmol) in toluene-d_8 (0.5 ml) was prepared in an NMR sample tube at –78 °C. After 5 min at –10 °C, the ^{31}P{^{1}H} NMR spectrum exhibited two sets of signals assignable to **A** at δ 113.7 (br d, $^2J_{PP}$ = 31 Hz, $^1J_{PtP}$ = 1543 Hz) and 17.9 (br t, $^2J_{PP}$ = 31 Hz, $^1J_{PtP}$ = 4154 Hz), along with the signal of free PCy_3 at δ 9.8 (s). After 3 h at room temperature, the ^{31}P{^{1}H} NMR signals of **A** vanished, and three new signals appeared at

δ 247.4 (br), 28.2 (br, $^{1}J_{PtP}$ = 3480 Hz), and 25.3 (br, $^{1}J_{PtP}$ = 1985 Hz) in almost the same intensity. Moreover, the ^{1}H NMR spectrum exhibited the signals assignable to Pt–H at δ –6.82 (dd, $^{2}J_{PH}$ = 182 and 16 Hz, $^{1}J_{PtH}$ = 996 Hz) and to P=CH at δ 9.15 (d, $^{2}J_{PH}$ = 24.4 Hz) in almost the same intensity.

Reaction of PPEP with [Rh(*μ*-Cl)(C_2H_4)$_2$]$_2$. A solution of PPEP (21 mg, 0.032 mmol) and [Rh(*μ*-Cl)(C_2H_4)$_2$]$_2$ (6.2 mg, 0.016 mmol) in THF-d_8 (0.6 ml) was prepared in an NMR sample tube at –78 °C. The color of the solution instantly changed to reddish brown. The ^{1}H and ^{31}P{^{1}H} NMR spectra indicated selective formation of [RhCl(PPEP)] (**6**).

[6]: ^{1}H NMR (THF-d_8, –70 °C): δ 7.68 (d, $^{2}J_{PH}$ = 17.6 Hz, 1H, P=C*H*), 7.64 (t, $^{3}J_{HH}$ = 7.6 Hz, 1H, Py), 7.56 (s, 1H, Ar), 7.55 (s, 1H, Ar), 7.45 (s, 1H, Ar), 7.35 (s, 1H, Ar), 7.17 (d, $^{3}J_{HH}$ = 7.6 Hz, 1H, Py), 7.03 (d, $^{3}J_{HH}$ = 7.6 Hz, 1H, Py), 4.41 (dd, $^{2}J_{HH}$ = 18.4, $^{2}J_{PH}$ = 9.4 Hz, 1H, PyC*H*$_2$P), 4.14 (dd, $^{2}J_{HH}$ = 18.4, $^{2}J_{PH}$ = 9.4 Hz, 1H, PyC*H*$_2$P), 2.67 (br d, $^{2}J_{HH}$ = 14.8, 1H, PC*H*$_2$), 2.47 (br d, $^{2}J_{HH}$ = 14.8 Hz, 1H, PC*H*$_2$), 1.78 (s, 9H, C*H*$_3$ of ^{t}Bu), 1.55 (br, 9H, C*H*$_3$ of ^{t}Bu), 1.45 (s, 3H, C*H*$_3$), 1.41 (s, 3H, C*H*$_3$), 1.39 (s, 9H, C*H*$_3$ of ^{t}Bu), 1.36 (s, 18H, C*H*$_3$ of ^{t}Bu). ^{31}P{^{1}H} NMR (THF-d_8, –70 °C): δ 243.4 (dd, $^{2}J_{PP}$ = 463 Hz, $^{1}J_{RhP}$ = 186 Hz), 26.0 (dd, $^{2}J_{PP}$ = 463 Hz, $^{1}J_{RhP}$ = 167 Hz).

Upon standing the sample at room temperature for 1 h, the ^{31}P{^{1}H} NMR signals of **6** disappeared, and two doublet signals at δ 29.5 ($^{1}J_{RhP}$ = 151 Hz) and 26.8 ($^{1}J_{RhP}$ = 154 Hz), assignable to a 5:1 mixture of diastereomers of [RhCl(BPMP)] (**7**), appeared. Dry up the reaction mixture under vacuum gave an orange solid of **7** as a 5:1 mixture of diastereomers (18 mg, 0.023 mmol, 71%). With consideration of the steric conditions, the major isomer was assigned to the *dl*-isomer. HRMS (ESI): Calcd for $C_{43}H_{63}NP_2Rh$ 792.3096 ([M–H]$^{+}$); Found 792.3092.

***dl*-[7]:** ^{1}H NMR (THF-d_8, 25 °C): δ 7.46 (s, 2H, Ar), 7.42 (t, $^{3}J_{HH}$ = 7.6 Hz, 1H, 4-Py), 7.21 (s, 2H, Ar), 6.93 (d, $^{3}J_{HH}$ = 7.6 Hz, 2H, 3,5-Py), 3.62 (s, 4H, PyC*H*$_2$P), 2.79 (d, $^{2}J_{HH}$ = 14.4 Hz, 2H, PC*H*$_2$), 2.18 (d, $^{2}J_{HH}$ = 14.4 Hz, 2H, PC*H*$_2$), 1.83 (s, 18H, C*H*$_3$ of ^{t}Bu × 2), 1.46 (s, 6H, C*H*$_3$), 1.39 (s, 6H, C*H*$_3$), 1.35 (s, 18H, CH$_3$ of ^{t}Bu). ^{13}C{^{1}H} NMR (THF-d_8, 25 ºC): δ 164.0 (br), 159.9 (br d, J_{PC} = 7 Hz), 154.7 (s), 154.2 (s), 131.5 (s), 130.5 (br), 123.7 (s), 121.4 (br), 119.3 (s), 49.3 (br), 44.8 (s), 43.0 (br), 39.1 (s), 35.9 (s), 34.2 (br), 34.0 (s), 32.6 (s), 31.9 (s). ^{31}P{^{1}H} NMR (C_6D_6, 25 °C): δ 28.9 (br d, $^{1}J_{RhP}$ = 150 Hz).

***meso*-[7]:** ^{1}H NMR (THF-d_8, 25 °C): 7.24 (t, $^{3}J_{HH}$ = 7.6 Hz, 1H, 4-Py), 7.40 (s, 2H, Ar), 7.21 (s, 2H, Ar), 6.91 (d, $^{3}J_{HH}$ = 7.6 Hz, 2H, 3,5-Py), 3.89 (dvt, $^{2}J_{HH}$ = 18.5, J_{app} = 3.8 Hz, 2H, PyCH_2P), 3.52 (dvt, $^{2}J_{HH}$ = 18.5, J_{app} = 3.8 Hz, 2H, PyCH_2P), 2.95 (d, $^{2}J_{HH}$ = 14.7 Hz, 2H, PCH_2), 2.18 (d, $^{2}J_{HH}$ = 14.7 Hz, 2H, PCH_2), 1.63 (s, 18H, CH_3 of ^{t}Bu), 1.50 (s, 6H, CH_3), 1.41 (s, 6H, CH_3), 1.34 (s, 18H, CH_3 of ^{t}Bu). ^{13}C{^{1}H} NMR (THF-d_8, 25 °C): 164.6 (br), 159.5 (br), 154.7 (s), 154.1 (s), 131.3 (s), 130.5 (br), 123.0 (s), 121.2 (s), 119.3 (s), 49.6 (br), 45.0 (s), 43.5 (br), 38.1 (s), 33.6 (s, two signals are overlapped), 33.4 (s), 31.8 (s). ^{31}P{^{1}H} NMR (C_6D_6, 25 °C): δ 25.8 (d, $^{1}J_{RhP}$ = 152 Hz).

Preparation of [$RuCl_2(PPh_3)$(PPEP)] (8). A THF solution (0.3 mL) of PPEP (13 mg, 0.020 mmol) was added to a suspension of [$RuCl_2(PPh_3)_3$] (19 mg, 0.020 mmol) in THF (0.2 mL) at room temperature. The color of the mixture instantly changed to bluish purple. After stirring for 30 min, solvent was removed under reduced pressure. The residue was washed with pentane (5 mL) to remove free PPh_3, and dissolved in THF (5 mL). The solution was concentrated, layered with pentane, and allowed to stand at room temperature overnight to give purple crystals of **8** (15 mg, 0.013 mmol, 69%). The same reaction was performed in a large scale using a 262 mg of PPEP, and a 248 mg of **8** (63%) was isolated.

^{1}H NMR (THF-d_8, 25 °C): δ 7.72–7.65 (m, 3H, PyCH=P + Ar), 7.54–7.50 (m, 7H, PPh_3 + 4-Py), 7.47 (br, 1H, Ar), 7.29 (br d, $^{3}J_{HH}$ = 8.4 Hz, 2H, 3,5-Py), 7.07 (t, $^{3}J_{HH}$ = 7.2 Hz, 3H, *p*-PPh_3), 6.81 (t, $^{3}J_{HH}$ = 7.2 Hz, 3H, *m*-PPh_3), 6.78 (d, $^{4}J_{HH}$ = 1.7 Hz, 1H, Ar), 4.74 (dd, $^{2}J_{HH}$ = 16.2, $^{2}J_{PH}$ = 10.4 Hz, 1H, PyCH_2P), 4.21 (dd, $^{2}J_{HH}$ = 16.2, $^{2}J_{PH}$ = 9.8 Hz, 1H, PyCH_2P), 3.35 (dd, $^{2}J_{HH}$ = 15.2, $^{2}J_{PH}$ = 5.5 Hz, 1H, PCH_2), 2.57 (br d, $^{2}J_{HH}$ = 15.2 Hz, 1H, PCH_2), 1.46 (s, 9H, CH_3 of ^{t}Bu), 1.43 (s, 9H, CH_3 of ^{t}Bu), 1.39 (s, 9H, CH_3 of ^{t}Bu), 1.34 (s, 9H, CH_3 of ^{t}Bu), 1.17 (s, 9H, CH_3 of ^{t}Bu), 1.11 (s, 3H, CH_3), 0.80 (s, 3H, CH_3). ^{13}C{^{1}H} NMR (THF-d_8, 25 °C): δ 167.9 (d, J_{PC} = 4 Hz), 165.1 (s), 162.5 (d, J_{PC} = 39 Hz), 160.0 (dd, J_{PC} = 14 and 3 Hz), 157.2 (s), 157.1 (d, J_{PC} = 9 Hz), 157.0 (d, J_{PC} = 1 Hz), 156.52 (s), 156.49 (s), 153.3 (d, J_{PC} = 2 Hz), 151.9 (s), 138.4 (d, J_{PC} = 39 Hz, P=CH), 135.9 (s), 135.8 (s), 134.7 (d, J_{PC} = 20 Hz), 129.5 (s), 127.8 (d, J_{PC} = 9 Hz), 127.5 (d, J_{PC} = 8 Hz), 126.3 (d, J_{PC} = 4 Hz), 122.7 (d, J_{PC} = 6 Hz), 121.6 (d, J_{PC} = 26 Hz), 119.2 (d, J_{PC} = 8 Hz), 118.8 (t, J_{PC} = 10 Hz), 51.1 (d, J_{PC} = 20 Hz), 43.9 (d, J_{PC} = 5 Hz), 43.5 (d, J_{PC} = 33 Hz), 39.5 (s), 38.9 (s), 38.8 (s), 36.3 (s), 35.9 (s), 35.6 (s), 35.4 (s), 35.3 (s), 34.5 (s), 31.8 (s), 31.7 (s), 29.9 (d, J_{PC} = 10 Hz). ^{31}P{^{1}H} NMR (THF-d_8,

25 °C): δ 292.0 (dd, $^{2}J_{PP}$ = 411 and 29 Hz), 50.5 (dd, $^{2}J_{PP}$ = 411 and 29 Hz), 34.8 (t, $^{2}J_{PP}$ = 29 Hz). Anal. Calcd for $C_{61}H_{78}Cl_2NP_3Ru$: C, 67.21; H, 7.21; N, 1.28. Found: C, 67.42; H, 7.14; N, 1.26.

Preparation of [RuCl(PPh$_3$)(PPEP*)] (9). A THF solution (2 mL) of ^{t}BuOK (18 mg, 0.16 mmol) was added dropwise to a THF solution (1.5 mL) of **8** (134 mg, 0.12 mmol) at room temperature. The color of the solution changed from purple to dark green. The reaction mixture was allowed to stand for 30 min, and filtered through a Celite pad to remove the precipitate of KCl. The solvent was removed under reduced pressure, and the residue was dissolved in Et_2O (0.6 mL), and allowed to stand at room temperature to afford dark-green crystals of **9** (87 mg, 0.083 mmol, 69%). Single crystals for X-ray diffraction analysis were grown from a THF/pentane (1:1) solution.

^{1}H NMR (THF-d_8, −20 °C): δ 8.49−7.48 (br, 6H, PPh$_3$), 7.53 (br, 1H, Ar), 7.41 (dd, 1H, $^{4}J_{PH}$ = 4.3 Hz, $^{4}J_{HH}$ = 1.3 Hz, 1H, Ar), 7.39 (br, 1H, Ar), 7.36–7.05 (br, 9H, PPh$_3$), 7.13 (d, $^{4}J_{HH}$ = 1.3 Hz, 1H, Ar), 6.99 (d, $^{2}J_{PH}$ = 20.4 Hz, 1H, P=C*H*), 6.06 (ddd, $^{3}J_{HH}$ = 8.6 and 6.5 Hz, $^{5}J_{PH}$ = 1.2 Hz, 1H, Py), 5.78 (dd, $^{3}J_{HH}$ = 8.6 Hz, $^{4}J_{PH}$ = 4.9 Hz, 1H, Py), 5.25 (t, $^{3}J_{HH}$ = 6.5 Hz, $^{4}J_{PH}$ = 5.9 Hz, 1H, Py), 3.76 (vt, J_{app} = 2.7 Hz, 1H, Py=C*H*P), 1.90 (s, 9H, CH_3 of ^{t}Bu), 1.67 (br dd, $^{2}J_{HH}$ = 14.5 Hz, $^{2}J_{PH}$ = 12.7 Hz, 1H, PCH_2), 1.34 (s, 9H, CH_3 of ^{t}Bu), 1.32 (s, 9H, CH_3 of ^{t}Bu), 1.25 (s, 3H, CH_3), 1.09 (s, 3H, CH_3), 1.03 (s, 9H, CH_3 of ^{t}Bu), 0.91 (s, 9H, CH_3 of ^{t}Bu), 0.72 (dd, $^{2}J_{HH}$ = 14.5 Hz, $^{2}J_{PH}$ = 2.6 Hz, 1H, PCH_2). ^{13}C{^{1}H} NMR (THF-d_8, –20 °C): δ 179.1 (d, J_{PC} = 31 Hz, P=*C*H), 174.1 (d, J_{PC} = 16 Hz), 160.4 (s), 158.2 (br d, J_{PC} = 2 Hz), 157.7 (dd, J_{PC} = 15 and 3 Hz), 157.0 (s), 152.8 (d, J_{PC} = 2 Hz), 151.4 (s), 151.3 (s), 151.0 (s), 137.3 (br, PPh$_3$), 135.4 (dd, J_{PC} = 38 and 18 Hz), 134.2 (br, PPh$_3$), 130.5 (br), 130.2 (br, PPh$_3$), 129.5 (dd, J_{PC} = 39 and 5 Hz), 128.2 (br, PPh$_3$), 126.6 (s), 125.6 (d, J_{PC} = 8 Hz), 121.3 (d, J_{PC} = 4 Hz), 119.1 (d, J_{PC} = 8 Hz), 117.2 (dd, J_{PC} = 18 and 14 Hz), 111.0 (d, J_{PC} = 32 Hz), 78.9 (d, J_{PC} = 55 Hz), 43.5 (dd, J_{PC} = 5 and 3 Hz), 40.6 (d, J_{PC} = 39 Hz), 39.4 (s), 38.8 (s), 36.2 (s), 35.6 (s), 35.5 (s), 35.1 (s), 33.8 (s), 33.5 (s), 32.0 (d, J_{PC} = 10 Hz), 31.8 (s), 31.6 (s), 30.1 (d, J_{PC} = 4 Hz). ^{31}P{^{1}H} NMR (THF-d_8, −20 °C): δ 216.9 (dd, $^{2}J_{PP}$ = 299 and 23 Hz), 57.7 (dd, $^{2}J_{PP}$ = 40 and 23 Hz), 46.2 (dd, $^{2}J_{PP}$ = 299 and 40 Hz). Anal. Calcd for $C_{61}H_{77}ClNP_3Ru$: C, 69.53; H, 7.37; N, 1.33. Found: C, 69.71; H, 7.63; N, 1.30.

X-ray Structural Analysis. The intensity data were collected at 103 K on a Rugaku VariMax diffractometer using graphite-monochromated Mo Kα radiation (λ = 0.71075 Å). The intensity data were corrected for Lorentz and polarization effects and for absorption. The structures were solved by direct methods (SHELXS-97)[16] and refined by least-squares calculations on F^2 for all reflections (SHELXL-97).[16] Non-hydrogen atoms, except for disordered groups in **5** (^{t}Bu), were refined anisotropically. Hydrogen atoms were placed at calculated positions using AFIX instructions, and included in least-squares calculations without refinement of their parameters. The crystallographic data and the summary of solution and refinement are listed in Table 2.

DFT Calculations. All calculations were carried out with the Gaussian 09 program package.[17] The geometric optimization of **A1** was performed with the DFT method using the B3LYP functional. The Pt was described with the LANL2TZ(f) basis set.[18] The 6-31G(d) basis sets were applied to other atoms. The NMR chemical shifts were evaluated by the GIAO method using the B3LYP functional with the LANL2TZ(f) basis set[18] for Pt and 6-311+G(2d,p) basis sets for other atoms. As a result, the ^{31}P NMR chemical shifts of **A1** were estimated to be δ 102.7 (BPEP) and 10.7 (PMe_3).

Table 2. Crystal Data and Details of Structure Determination for **5** and **9**

complex	**5**	**9**
empirical formula	$C_{61}H_{96}NP_3Pt$	$C_{61}H_{77}ClNP_3Ru \cdot 0.5(C_5H_{12})$
formula weight	1131.39	1089.74
T (K)	103(2)	103(2)
crystal system	Monoclinic	Triclinic
space group	$P2_1/c$	$P\bar{1}$
a (Å)	17.281(2)	10.4778(11)
b (Å)	11.8806(14)	16.0104(18)
c (Å)	28.514(4)	18.230(2)
a (°)	90	82.466(4)
b (°)	104.322(2)	75.797(4)
g (°)	90	72.530(4)
V (Å^3)	5672.3(12)	2822.5(6)
Z	4	2
d_{calc} (g/cm^3)	1.325	1.282
μ(Mo Ka) (mm^{-1})	2.596	0.450
F(000)	2368	1154
crystal size	0.19 × 0.09 × 0.03	0.14 × 0.12 × 0.05
θ range (°)	2.10 to 27.50	2.60 to 27.50
reflections collected	44831	22982
independent reflections (R_{int})	13016 (0.0432)	12454 (0.0241)
absorption correction	multi-scan	numerical
max. and min. transmission	1.0000 and 0.8566	0.9926 and 0.9579
data / restraints / parameters	13016 / 0 / 614	12454 / 7 / 643
GOF on F^2	1.168	1.032
$R1$, $wR2$ [$I > 2\sigma(I)$]	0.0434, 0.0951	0.0401, 0.0846
$R1$, $wR2$ (all data)	0.0512, 0.0996	0.0497, 0.0911
largest peak and hole (e Å^3)	2.071 and –1.313	1.045 and –0.584

References and Notes

(1) (a) Blum, Y.; Czarkie, D.; Rahamim, Y.; Shvo, Y. *Organometallics* **1985**, *4*, 1459–1461. (b) Grützmacher, H. *Angew. Chem., Int. Ed.* **2008**, *47*, 1814–1818. (c) van der Vlugt, J. I.; Reek, J. N. H. *Angew. Chem., Int. Ed.* **2009**, *48*, 8832–8846. (d) Crabtree, R. H. *New J. Chem.* **2011**, *35*, 18–23. (e) van der Vlugt, J. I. *Eur. J. Inorg. Chem.* **2012**, 363–375. (f) Schneider, S.; Meiners, J.; Askevold, B. *Eur. J. Inorg. Chem.* **2012**, 412–429.

(2) (a) Noyori, R.; Ohkuma, T. *Angew. Chem., Int. Ed.* **2001**, *40*, 40–73. (b) Ikariya, T.; Murata, K.; Noyori, R. *Org. Biomol. Chem.* **2006**, *4*, 393–406. (c) Ikariya, T.; Blacker, A. J. *Acc. Chem. Res.* **2007**, *40*, 1300–1308. (d) Samec, J. S. M.; Bäckvall, J.-E.; Andersson, P. G.; Brandt, P. *Chem. Soc. Rev.* **2006**, *35*, 237–248. (e) Ito, J.; Nishiyama, H. *Top. Organomet. Chem.* **2011**, *37*, 185–205. (f) Kuwata, S.; Ikariya, T. *Chem. Eur. J.* **2011**, *17*, 3542–3556. (g) Annibale, V. T.; Song, D. *RSC Adv.* **2013**, *3*, 11432–11449.

(3) For reviews, see: (a) Gunanathan, C.; Milstein, D. *Science* **2013**, *341*, 249–260. (b) Gunanathan, C.; Milstein, D. In *Pincer and Pincer-Type Complexes: Applications in Organic Synthesis and Catalysis*; Szabó, K. J., Wendt, O. F., Eds.; Wiley-VCH: Weinheim, Germany, 2014; Chapter I. (c) Gunanathan, C.; Milstein, D. *Chem. Rev.* **2014**, *114*, 12024–12087.

(4) For representative examples, see: (a) Zhang, J.; Gandelman, M.; Shimon, L. J. W.; Rozenberg, H.; Milstein, D. *Organometallics* **2004**, *23*, 4026–4033. (b) Zhang, J.; Leitus, G.; Ben-David, Y.; Milstein, D. *J. Am. Chem. Soc.* **2005**, *127*, 10840–10841. (c) Zhang, J.; Leitus, G.; Ben-David, Y.; Milstein, D. *Angew. Chem., Int. Ed.* **2006**, *45*, 1113–1115. (d) Gunanathan, C.; Ben-David, Y.; Milstein, D. *Science* **2007**, *317*, 790–792. (e) Gunanathan, C.; Milstein, D. *Angew. Chem., Int. Ed.* **2008**, *47*, 8661–8664. (f) Gunanathan, C; Shimon, L. J. W.; Milstein, D. *J. Am. Chem. Soc.* **2009**, *131*, 3146–3147. (g) Gnanaprakasam, B.; Zhang, J.; Milstein, D. *Angew. Chem., Int. Ed.* **2010**, *49*, 1468–1471. (h) Khaskin, E.; Iron, M. A.; Shimon, L. J. W.; Zhang, J.; Milstein, D. *J. Am. Chem. Soc.* **2010**, *132*, 8542–8543. (i) Balaraman, E.; Gunanathan, C.; Zhang, J.; Shimon, L. J. W.; Milstein, D. *Nat. Chem.* **2011**, *3*, 609–614. (j) Balaraman, E.; Fogler, E.; Milstein, D. *Chem. Commun.* **2012**, *48*, 1111–1113. (k) Feller, M.; Diskin-Posner, Y.; Shimon, L. J. W.; Ben-Ari, E.; Milstein, D. *Organometallics* **2012**, *31*, 4083–4101. (l) Anaby, A.; Butschke, B.; Ben-David, Y.; Shimon, L. J. W.; Leitus, G.; Feller, M.; Milstein, D. *Organometallics* **2014**, *33*, 3716–3726.

(5) (a) Chang, Y.-H.; Nakajima, Y.; Tanaka, H.; Yoshizawa, K.; Ozawa, F. *J. Am. Chem. Soc.* **2013**, *135*, 11791–11794. (b) Chang, Y.-H.; Nakajima, Y.; Tanaka, H.; Yoshizawa, K.; Ozawa, F. *Organometallics* **2014**, *33*, 715–721.

(6) (a) Dugal-Tessier, J.; Conrad, E. D.; Dake, G. R.; Gates, D. P. In *Phosphorus(III) Ligands in Homogeneous Catalysis: Design and Synthesis*; Kamer, P. C. J., van Leeuwen, P. W. N. M., Eds.; Wiley: Chichester, U.K., 2012; Chapter 10. (b) Le Floch, P. *Coord. Chem. Rev.* **2006**, *250*, 627–681. (c) Ozawa, F.; Yoshifuji, M. *Dalton Trans.* **2006**, 4987–4995. (d) Weber, L. *Coord. Chem. Rev.* **2005**, *249*, 741–763. (e) Mathey, F. *Angew. Chem., Int. Ed.* **2003**, *42*, 1578–1604.

(7) Houdard, R.; Mézailles, N.; Le Goff, X.-F.; Le Floch, P. *Organometallics* **2009**, *28*, 5952–5959.

(8) For review, see: Mastrorilli, P. *Eur. J. Inorg. Chem.* **2008**, 4835–4850. See also for a phosphanido platinum complex with a Mes* substituent: Waterman, R.; Mindiola, D. J.; Clough, C. R.; Hillhouse, G. L. *Inorg. Chim. Acta* **2014**, *422*, 57–64.

(9) With consideration of the steric conditions, the author presumes the major product to be the *dl*-isomer.

(10) Addison, A. W.; Rao, T. N.; Reedijk, J.; van Rijn, J.; Verschoor, G. C. *J. Chem. Soc., Dalton Trans.* **1984**, 1349–1356.

(11) Nakajima, Y.; Okamoto, Y.; Chang, Y.-H.; Ozawa, F. *Organometallics* **2013**, *32*, 2918–2925. PPEP*-Ph stands for a PPEP* ligand substituted with Ph groups at the *exo*-methylene and phosphaalkene carbons.

(12) Jouaiti, A.; Geoffroy, M.; Bernardinelli, G. *Tetrahedron Lett.* **1992**, *33*, 5071–5074.

(13) Yoshida, T.; Otsuka, S.; Jones, D. G.; Spencer, J. L.; Binger, P.; Brinkmann, A. *Inorg. Synth.* **1990**, *28*, 113–119.

(14) Cramer, R.; McCleverty, J. A.; Bray, J. *Inorg. Synth.* **1974**, *15*, 14–18.

(15) Hallman, P. S.; Stephenson, T. A.; Wilkinson, G. *Inorg. Synth.* **1970**, *12*, 237–240.

(16) Sheldrick, G. M. SHELXL-97; University of Göttingen, Göttingen, Germany, 1997.

(17) Gaussian 09, Revision C.01, Frisch, M. J.; Trucks, G. W.; Schlegel, H. B.; Scuseria, G. E.; Robb, M. A.; Cheeseman, J. R.; Scalmani, G.; Barone, V.; Mennucci, B.; Petersson, G. A.; Nakatsuji, H.; Caricato, M.; Li, X.; Hratchian, H. P.; Izmaylov, A. F.; Bloino, J.; Zheng, G.;

Sonnenberg, J. L.; Hada, M.; Ehara, M.; Toyota, K.; Fukuda, R.; Hasegawa, J.; Ishida, M.; Nakajima, T.; Honda, Y.; Kitao, O.; Nakai, H.; Vreven, T.; Montgomery, J. A., Jr.; Peralta, J. E.; Ogliaro, F.; Bearpark, M.; Heyd, J. J.; Brothers, E.; Kudin, K. N.; Staroverov, V. N.; Kobayashi, R.; Normand, J.; Raghavachari, K.; Rendell, A.; Burant, J. C.; Iyengar, S. S.; Tomasi, J.; Cossi, M.; Rega, N.; Millam, N. J.; Klene, M.; Knox, J. E.; Cross, J. B.; Bakken, V.; Adamo, C.; Jaramillo, J.; Gomperts, R.; Stratmann, R. E.; Yazyev, O.; Austin, A. J.; Cammi, R.; Pomelli, C.; Ochterski, J. W.; Martin, R. L.; Morokuma, K.; Zakrzewski, V. G.; Voth, G. A.; Salvador, P.; Dannenberg, J. J.; Dapprich, S.; Daniels, A. D.; Farkas, Ö.; Foresman, J. B.; Ortiz, J. V.; Cioslowski, J.; Fox, D. J. Gaussian, Inc., Wallingford CT, 2009.

(18) (a) Hay, P. J.; Wadt, W. R. *J. Chem. Phys.* **1985**, *82*, 299–310. (b) Ehlers, A. W.; Bohme, M.; Dapprich, S.; Gobbi, A.; Hollwarth, A.; Jonas, V.; Kohler, K. F.; Stegmann, R.; Veldkamp, A.; Frenking, G. *Chem. Phys. Lett.* **1993**, *208*, 111–114. (c) Roy, L. E.; Hay, P. J.; Martin, R. L. *J. Chem. Theory Comput.* **2008**, *4*, 1029–1031.

Chapter 2

Unsymmetrical PNP-Pincer Type Phosphaalkene Ligands Protected by a Fused-Ring Bulky Eind Group: Synthesis and Applications to Rh(I) and Ir(I) Complexes

Abstract

It has been reported that 2-(phospholanylmethyl)-6-(2-phosphaethenyl)pyridine (PPEP) with a 2,4,6-tri-*tert*-butylphenyl group (Mes*) as steric protection of the P=C bond serves as a noninnocent ligand on Ir(I), leading to extremely high reactivity towards metal–ligand cooperative activation of ammonia and acetonitrile. The high reactivity is largely due to the strong π-accepting properties of P=C bond. However, PPEP had a stability problem that provokes the loss of P=C bond on other transition metals including Rh(I) and restricts its utilization. This chapter describes the synthesis of Eind-PPEP protected by an octaethyl-*s*-hydrindacen-4-yl group (Eind) instead of Mes*. The fused-ring bulky Eind group successfully prevents the loss of P=C bond, and allows the author to compare the reactivity of Rh(I) and Ir(I) complexes towards ammonia. The complex K[RhCl(Eind-PPEP*)] bearing a dearomatized Eind-PPEP* ligand undergoes simple ligand displacement to give [Rh(NH_3)(Eind-PPEP*)], whereas the iridium analogue K[IrCl(Eind-PPEP*)] causes N–H bond cleavage to form [Ir(NH_2)(Eind-PPEP)]. DFT calculations indicate a thermodynamic cause of the metal-dependent product change.

Introduction

Phosphaalkenes with a P=C double bond are an interesting class of phosphorus compounds, which possess an extremely low-lying π*-orbital and thus serve as strong π-acceptors towards transition metals.[1] This particular ligand property has been shown to be useful in organometallic chemistry.[2–4] In this chapter, the author examined the synthesis of a novel pyridine-based PNP-pincer type phosphaalkene ligand that exhibits noninnocent behavior on group 9 metals.

Metal–ligand cooperative activation of chemical bonds aided by noninnocent behavior of pyridine-based pincer ligands has found wide application in catalytic transformations.[5] PNP- and PNN-pincer complexes with a phosphanylmethyl group on the pyridine core undergo deprotonation at the benzylic position to cause dearomatization of the pyridine ring. The dearomatized complex cleaves chemical bonds in a heterolytic manner, along with regeneration of the aromatic pyridine ring, where the metal center and the dearomatized ligand serve as a Lewis acid and a Brønsted base, respectively.

Recently, Chang *et al.* found that the reactivity of dearomatized PNP-pincer complexes of Ir(I) towards metal–ligand cooperation could be remarkably enhanced by incorporating a phosphaalkene unit into the PNP-pincer scaffold.[3d–g] For example, complex K[**3b**] in Scheme 1 bearing a dearomatized PNP-pincer type phosphaalkene ligand (PPEP*) causes instant cleavage of the N–H bond of ammonia (1 atm) at room temperature.[3d] DFT calculations have revealed that the reactivity is effectively enhanced by strong π-back donation from the metal to the phosphaalkene unit.

Complex K[**3b**] is prepared from **1b** bearing a 2,6-bis(phosphaethenyl)pyridine ligand (BPEP), as illustrated in Scheme 1.[3d] While the Mes* substituent is commonly used for steric protection of P=C bonds, the Mes*P=CH group has been known to undergo C–H addition/cyclization on transition metals to form a phospholanylmethyl group in some instances.[6] The conversion of BPEP into the unsymmetrical PNP-pincer ligand (PPEP) in Scheme 1 (**1b** → **2b**) proceeds via this process. A crucial requirement is that BPEP undergoes C–H addition/cyclization exclusively at one of the Mes*P=CH groups. The reaction of Ir(I) complex **1b** proceeded in perfect selectivity, and the resulting **2b** was totally stable to further C–H addition/cyclization. On the other hand, attempts at other transition metal complexes

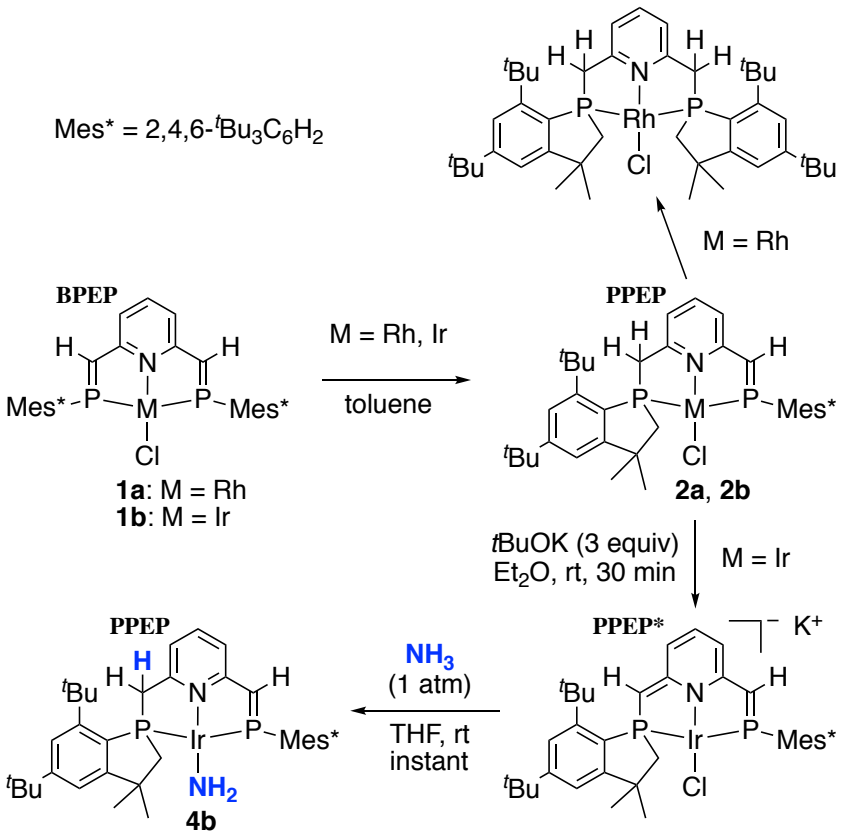

Scheme 1. Reactions of PNP-pincer type phosphaalkene complexes of Rh(I) and Ir(I) having 2,4,6-^{t}Bu$_3$C$_6$H$_2$ groups as steric protection of P=C bonds.[3d,3f]

including Rh(I) complex **1a** were unsuccessful due to the occurrence of successive C–H addition/cyclization at both Mes*P=CH groups, giving rise to completely loss of P=C bonds.[3f]

In this study, the author examined the synthesis of a novel BPEP ligand that can be selectively converted to PPEP on various metals. In this case, the most reliable way is the introduction of a steric protection group that is stable to C–H addition/cyclization into one of the phosphaalkene units. The author found that the 1,1,3,3,5,5,7,7-octaethyl-*s*-hydrindacen-4-yl group (Eind)[7] having a fused-ring bulky structure could effectively prevent the undesirable loss of the P=C bond. Moreover, using the newly synthesized phosphaalkene ligand (Eind-PPEP), the author could observe a distinct change in the reaction products of K[M(Cl)(Eind-PPEP*)] (M = Rh, Ir) and ammonia depending on the metals.

Results and Discussion

Synthesis of Eind-BPEP (7). Compound **7** having Mes*P=CH and Eind-P=CH groups at the 2,6-positions of pyridine was synthesized by two-step procedure starting from 2,6-pyridinedicarboxaldehyde (**5**) (Scheme 2). While phosphaalkene units may be constructed either by the phospha-Peterson reaction[8] or by the phospha-Wittig reaction,[9] the author chose the phospha-Wittig reaction because of the difficulty of preparing the phospha-Peterson reagent, Eind-P($SiMe_3$)Li. The first step is the treatment of **5** with Eind-P=PMe_3, in situ generated from Eind-PCl_2,[10] PMe_3, and zinc dust in THF. The phospha-Wittig reaction took place selectively at one of the formyl groups, and the desired compound **6** was isolated as a pale yellow powder in 74% yield by column chromatography.

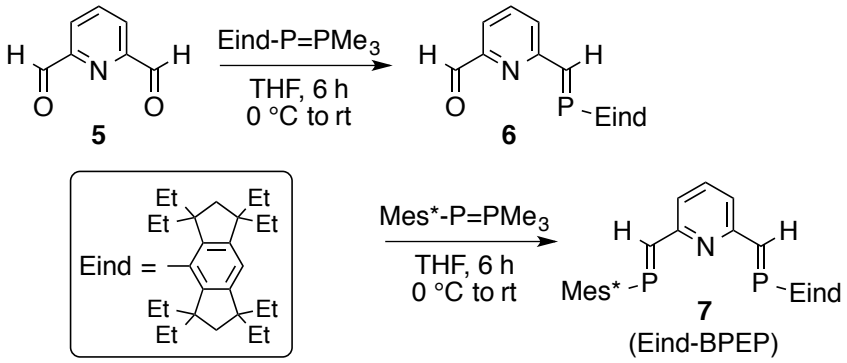

Scheme 2. Synthetic route to Eind-BPEP.

Compound **6** was then treated with Mes*P=PMe_3 in THF, and Eind-BPEP (**7**) was obtained in 97% yield. This product was contaminated with a small amount of Mes*-PH_2, which could not be removed by repeating chromatographic purifications. Accordingly, compound **7** was identified by NMR spectroscopy and mass spectrometry, and used for complex formation without further purification. The $^{31}P\{^1H\}$ NMR spectrum displayed two singlet signals at δ_P 285.8 and 275.2, consistent with the unsymmetrical structure of **7** having different substituents on phosphorus atoms.

Synthesis of Eind-BPEP Complexes (8 and 9). Eind-BPEP (**7**) was coordinated with rhodium and iridium chlorides by the reactions with [Rh(μ-Cl)(η^2-C_2H_4)$_2$]$_2$ and [Ir(μ-Cl)(η^2-

coe)$_2$]$_2$, respectively (Scheme 3). Both reactions took place instantly at room temperature to give [RhCl(Eind-BPEP)] (**8**) and [IrCl(Eind-BPEP)] (**9**) quantitatively, as confirmed by NMR spectroscopy.

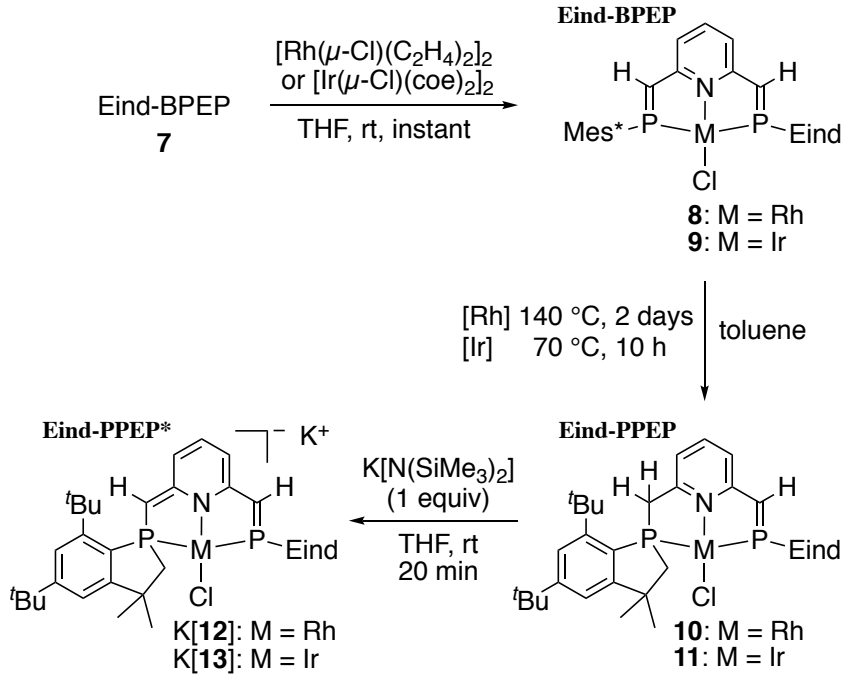

Scheme 3. Synthetic route to Eind-BPEP complexes of Rh(I) and Ir(I).

The $^{31}P\{^1H\}$ NMR spectrum of rhodium complex **8** displayed two sets of doublet of doublets at δ_P 239.2 ($^2J_{PP}$ = 519 Hz, $^1J_{RhP}$ = 207 Hz) and 231.2 ($^2J_{PP}$ = 519 Hz, $^1J_{RhP}$ = 204 Hz), which were assigned to Mes*P=CH and Eind-P=CH groups, respectively, referring to the chemical shifts of [RhCl(BPEP)] (δ_P 242.4)[11] and [RhCl(Eind-PPEP)] (**10**, δ_P 230.5). Similarly, complex **9** showed two sets of doublets at δ_P 249.3 and 237.2 ($^2J_{PP}$ = 560 Hz), assignable to Mes*P=CH and Eind-P=CH groups, respectively. The large $^2J_{PP}$ couplings are consistent with the trans arrangement of two phosphorus atoms. Moreover, the $^1J_{RhP}$ values of **8** are reasonable for a Rh(I) complex.

Complexes **8** and **9** were isolated as crystalline solids, suitable for X-ray diffraction analysis, in 60 and 84% yields, respectively. Figure 1 shows the crystal structures, which are superimposable to one another. Both complexes adopt a square planar geometry around the metal: Σ(Rh) = 360.1°, Σ(Ir) = 360.0°. The Eind-BPEP ligand adopts meridional coordination, and the chlorido ligand occupies the forth coordination site. The Mes* and Eind groups are

oriented nearly perpendicular to the coordination plane. The C2–P2–C26(Eind) and C1–P1–C8(Mes*) bond angles are comparable to each other for both complexes. The bond lengths of P1–C1 and P2–C2 in **8** (1.646(10) and 1.668(10) Å) and in **9** (1.671(3) and 1.673(3) Å) are typical of P=C double bonds. The Rh–P1, Rh–P2, Rh–N, and Rh–Cl lengths of **8** are comparable to those of [RhCl(BPEP)].[11] Moreover, the Ir–P1, Ir–P2, Ir–N, and Ir–Cl lengths of **9** are nearly the same as those of [IrCl(BPEP)].[3c]

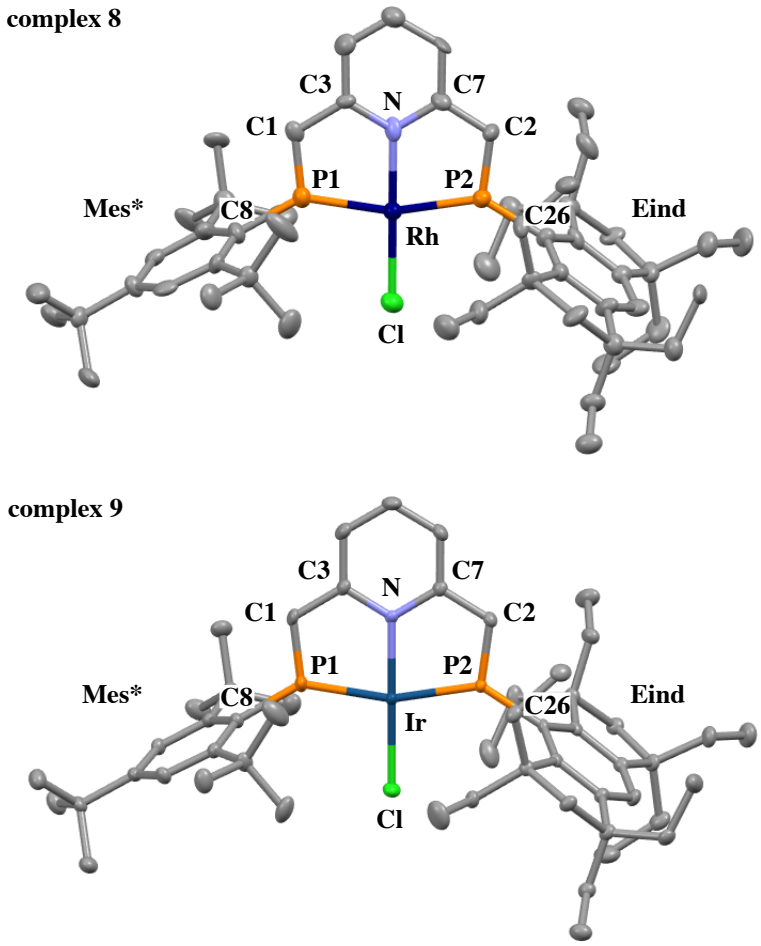

Figure 1. Molecular structures of [RhCl(Eind-BPEP)] (**8**) and [IrCl(Eind-BPEP)] (**9**) with 50% probability ellipsoids. Hydrogen atoms are omitted for clarity. Selected bond distances (Å) and angles (deg): [**8**] Rh−P1 2.243(3), Rh−P2 2.205(3), Rh−N 2.061(9), Rh–Cl 2.318(3), P1−C1 1.646(10), P2−C2 1.668(10), C1−C3 1.465(13), C2−C7 1.436(13), P1−Rh−P2 161.83(10), N−Rh−Cl 178.3(2), C1–P1–C8 112.8(5), C2–P2–C26 113.5(5); [**9**] Ir−P1 2.2349(9), Ir−P2 2.2128(8), Ir−N 2.047(3), Ir–Cl 2.3099(9), P1−C1 1.671(3), P2−C2 1.673(3), C1−C3 1.446(5), C2−C7 1.441(4), P1−Ir−P2 161.32(3), N−Ir−Cl 177.73(8), C1–P1–C8 113.37(16), C2–P2–C26 114.40(16).

Synthesis of Eind-PPEP Complexes (10 and 11). Complexes **8** and **9** were converted to [RhCl(Eind-PPEP)] (**10**) and [IrCl(Eind-PPEP)] (**11**) by C–H addition/cyclization of the Mes*P=CH group, respectively (Scheme 3). Although **8** and **9** have very similar structures, their reactivity was significantly different from each other. Heating iridium complex **9** in toluene at 70 °C overnight led to quantitative formation of **11**; the reactivity was comparable to that of [IrCl(BPEP)] (**1**) in Scheme 1.[3d] In contrast, rhodium complex **8** was stable at this temperature, and converted to **10** by heating at 140 °C for 2 days in a sealed tube.

Complexes **10** and **11** were isolated in quantitative yields, and identified by NMR spectroscopy and elemental analysis. The $^{31}P\{^{1}H\}$ NMR spectrum of **10** exhibited two sets of doublet of doublets at δ_P 230.5 ($^{2}J_{PP}$ = 461 Hz, $^{1}J_{RhP}$ = 183 Hz) and 26.0 ($^{2}J_{PP}$ = 461 Hz, $^{1}J_{RhP}$ = 168 Hz); the chemical shifts are consistent with the unsymmetrical structure of PPEP bearing phosphaethenyl and phospholanylmethyl groups. Likewise, complex **11** displayed two sets of doubles at δ_P 232.7 and 25.4 ($^{2}J_{PP}$ = 480 Hz) in the $^{31}P\{^{1}H\}$ NMR spectrum.

The occurrence of C–H addition/cyclization giving a phospholanylmethyl group was supported by the appearance of benzylic proton and carbon signals in the ^{1}H and $^{13}C\{^{1}H\}$ NMR spectra: [**10**] δ_H 4.32 (dd, $^{2}J_{HH}$ = 18.4 Hz, $^{2}J_{PH}$ = 9.6 Hz, 1H), 4.10 (dd, $^{2}J_{HH}$ = 18.4 Hz, $^{2}J_{PH}$ = 9.7 Hz, 1H); δ_C 50.6 (s, $^{1}J_{PC}$ = 18 Hz); [**11**] δ_H 4.02 (dd, $^{2}J_{HH}$ = 18.8 Hz, $^{2}J_{PH}$ = 9.9 Hz, 1H), 4.01 (dd, $^{2}J_{HH}$ = 18.8 Hz, $^{2}J_{PH}$ = 10.2 Hz, 1H); δ_C 51.1 (s, $^{1}J_{PC}$ = 26 Hz). Two benzylic protons are diastereotopic with each other, showing two sets of signals with a large $^{2}J_{HH}$ coupling (ca. 18 Hz). This signal pattern is consistent with the structure of Eind-PPEP having a chiral phospholanylmethyl group.

Synthesis of Dearomatized Eind-PPEP* Complexes (12 and 13). Treatment of Eind-PPEP complexes **10** and **11** with K[N(SiMe$_3$)$_2$] (1 equiv) in THF at room temperature resulted in deprotonation at the benzylic position to give dearomatized complexes K[RhCl(Eind-PPEP*)] (K[**12**]) and K[IrCl(Eind-PPEP*)] (K[**13**]), respectively. Similarly, complexes **10** and **11** reacted with ^{t}BuOK in THF in the presence of 18-crown-6 (18C6) to form [K(18C6)][**12**] and [K(18C6)][**13**], respectively. The anionic parts showed the same NMR spectrum irrespective of the kinds of counter ions. Since the crown ether adducts were easily crystallized in high yields (both 80%), [K(18C6)][**12**] and [K(18C6)][**13**] were characterized

by NMR and X-ray analysis in detail.

The $^{31}P\{^{1}H\}$ NMR signals of **12** appeared at δ_P 211.3 ($^{2}J_{PP}$ = 433 Hz, $^{1}J_{RhP}$ = 182 Hz) and 19.2 ($^{2}J_{PP}$ = 433 Hz, $^{1}J_{RhP}$ = 169 Hz) as two sets of doublet of doublets. These signals were

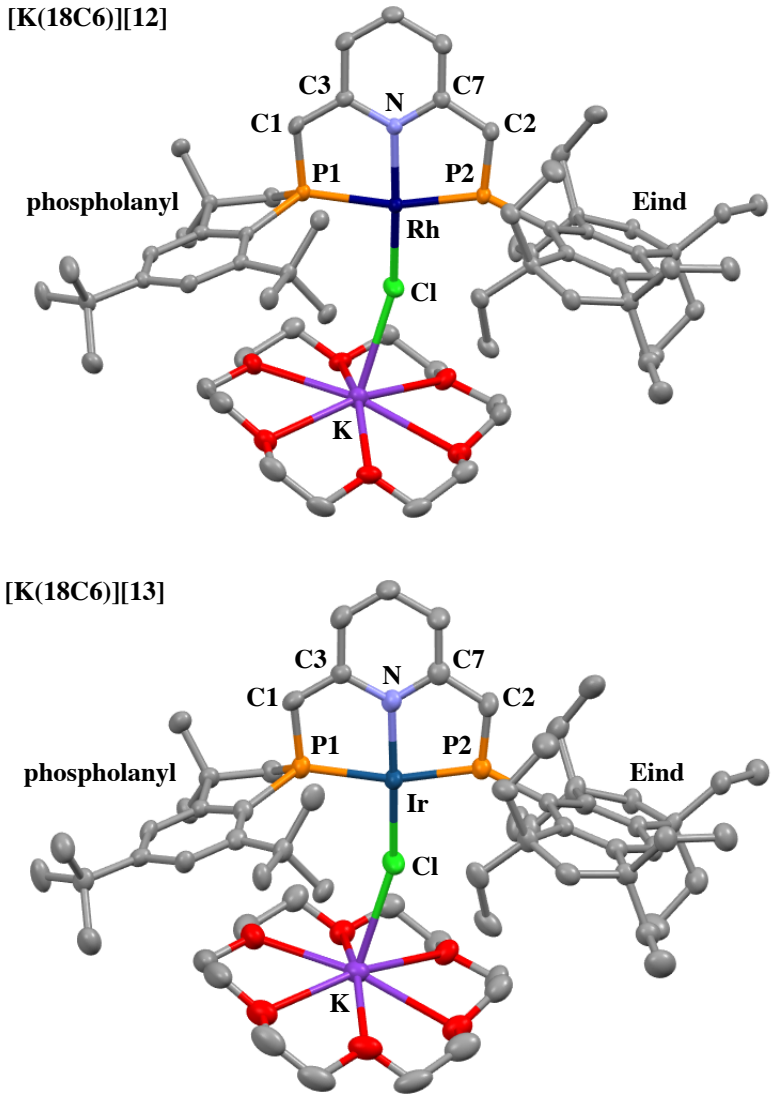

Figure 2. Molecular structures of [K(18-crown-6)][RhCl(Eind-PPEP*)] ([K(18C6)][**12**]) and [K(18-crown-6)][IrCl(Eind-PPEP*)] ([K(18C6)][**13**]) with 50% probability ellipsoids. Hydrogen atoms are omitted for clarity. Selected bond distances (Å) and angles (deg): [K(18C6)][**12**] Rh–P1 2.2800(7), Rh–P2 2.2192(7), Rh–N1 2.067(2), Rh–Cl 2.3382(7), P1–C1 1.751(3), P2–C2 1.673(3), C1–C3 1.383(4), C2–C7 1.437(4), Cl–K 2.9570(10), P1–Rh–P2 162.61(3), N–Rh–Cl 171.32(6); [K(18C6)][**13**] Ir–P1 2.2869(16), Ir–P2 2.2174(17), Ir–N 2.068(5), Ir–Cl 2.3557(16), P1–C1 1.750(6), P2–C2 1.675(6), C1–C3 1.379(9), C2–C7 1.434(8), Cl–K 2.994(2), P1–Ir–P2 162.59(6), N–Ir–Cl 172.36(15).

clearly shifted upfield compared with the parent complex **10**. Similarly, the signals of iridium complex **13** (δ_P 218.8 and 18.9, $^2J_{PP}$ = 458 Hz) appeared in a higher magnetic field than those of **11**. The presence of a dearomatized pyridine unit in complex **12** was indicated by three characteristic signals of ring protons at δ_H 6.03, 5.92, and 5.49. While the vinylic proton signal of Eind-PPEP* overlapped with a residual proton signal of the solvent (THF-d_8) as confirmed by HMQC experiments, the vinylic carbon signal was observed at δ_C 74.7 (d, $^1J_{PC}$ = 51 Hz). On the other hand, the vinylic proton and carbon signals of iridium complex **13** appeared at δ_H 3.89 (virtual triplet, J_{app} = 3.8 Hz) and δ_C 73.1 ($^1J_{PC}$ = 64 Hz), respectively.

Figure 2 shows the X-ray structures of [K(18C6)][**12**] and [K(18C6)][**13**], adopting a square planar configuration around the metals: Σ(Rh) = 360.5°, Σ(Ir) = 360.3°. The bond lengths of Rh–Cl in **12** (2.3382(7) Å) and of Ir–Cl in **13** (2.3557(16) Å) are consistent with dative bonding, whereas the Cl and K atoms are significantly distant from each other (2.9570(10) and 2.994(2) Å). Thus, the rhodium and iridium complexes may be described as anionic species bearing electrostatic interactions with the [K(18C6)] cation.

The P1–C1 bonds in **12** (1.751(3) Å) and **13** (1.750(6) Å) are clearly shorter than normal P–C single bonds, whereas the C1–C3 bond lengths (1.383(4) and 1.379(9) Å) are between those expected for a single and double bond. These variations are characteristic of dearomatized PNP-pincer ligands.[5] On the other hand, the P2–C2 bond lengths (1.673(3) and 1.675(6) Å) are typical of P=C double bonds.

Reactions of Dearomatized Eind-PPEP* Complexes with Ammonia. The rhodium and iridium complexes coordinated with Eind-PPEP* were subjected to the reactions with ammonia (1 atm) in THF-d_8 at room temperature (Scheme 4). Due to the difficulty in separating reaction products from [K(18C6)]Cl, the reactions were conducted with K[MCl(Eind-PPEP*)] (M = Rh and Ir), in situ generated from **10** and **11** by the treatment with K[N(SiMe$_3$)$_2$]. The resulting complexes **14** and **15** were isolated as analytically pure compounds in 98 and 99% yields, respectively, and characterized by NMR spectroscopy and elemental analysis.

The reaction of rhodium complex K[**12**] with ammonia was instantly completed, to form ammine complex **14** in almost quantitative yield. Thus, the simple displacement of the Cl^-

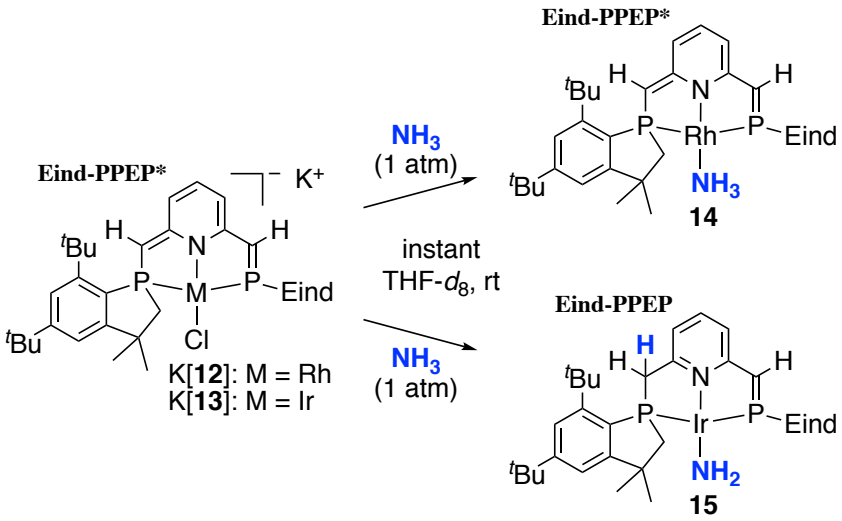

Scheme 4. Reactions of Eind-PPEP* complexes with ammonia.

ligand with ammonia took place. The dearomatized pyridine unit was preserved as indicated by three characteristic signals of ring protons at δ_H 6.04, 5.91, and 5.49 and of a vinylic proton at δ_H 3.48 in the ^{1}H NMR spectrum. A broad signal arising from the ammine ligand was observed at δ_H 2.13. Complex **14** was also examined by X-ray diffraction analysis. While the data quality was insufficient for detailed discussion of structural parameters ($R1$ = 0.1458), the existence of a dearomatized pyridine ring with a phospholanylmethylidene substituent was evidenced by characteristic bond lengths of P1–C1 (1.74(1) Å) and C1–C3 (1.38 Å), which were comparable to those of [K(18C6)][**12**] (1.751(3) and 1.383(4) Å) in Figure 2. Moreover, the P2–C2 bond length (1.65(1) Å) was appropriate for a phosphaalkene unit.

On the other hand, iridium complex K[**13**] led to metal–ligand cooperative activation of the N–H bond of ammonia, to afford a quantitative yield of parent amido complex **15** bearing an aromatized pyridine ring. The ^{1}H NMR spectrum showed a broad signal assignable to the amido ligand at δ_H 3.95; the chemical shift was similar to that observed for PPEP amido complex **4** (δ_H 3.82).[3d] The benzylic proton signals appeared at δ_H 4.15 and 4.14 as two sets of doublet of doublets with a large geminal coupling ($^2J_{HH}$ = 20.3 Hz).

Thus, the author could observe a dramatic change in the reaction courses depending on the metals. Since both reactions in Scheme 4 were completed instantly at room temperature, it would be reasonable that the distinct change is mainly due to thermodynamic reasons. The author therefore compared the relative stability of ammine and amido complexes by DFT

calculations. The calculations were performed with the B3LYP-D functional and triple-zeta quality basis sets for the whole molecules without omission of any substituents. Solvent effects (THF) were included by PCM calculations.

As a result, it was found that the rhodium ammine complex (**14**, Rh^{NH3}) is more stable than the amido complex [Rh(NH_2)(Eind-PPEP)] (Rh^{NH2}) (eq 1); to the contrary, the iridium ammine complex [Ir(NH_3)(Eind-PPEP*)] (Ir^{NH3}) is less stable than the amido complex (**15**, Ir^{NH2}) (eq 2). The energy differences between two species (ΔG_{298} = –2.4 and +2.2 kcal/mol) correspond to the ratios of Rh^{NH3}/Rh^{NH2} = 58/1 and Ir^{NH3}/Ir^{NH2} = 1/41, respectively. Thus, while the energy differences are somewhat smaller than those expected for the experimental observations showing selective formation of either complex, the tendencies were reproduced by DFT calculations.

$$[Rh(NH_3)(\text{Eind-PPEP*})] \quad > \quad [Rh(NH_2)(\text{Eind-PPEP})] \qquad (1)$$
$$\Delta G_{298}\,([Rh^{NH3}] - [Rh^{NH2}]) = -2.4 \text{ kcal/mol}$$

$$[Ir(NH_3)(\text{Eind-PPEP*})] \quad < \quad [Ir(NH_2)(\text{Eind-PPEP})] \qquad (2)$$
$$\Delta G_{298}\,([Ir^{NH3}] - [Ir^{NH2}]) = +2.2 \text{ kcal/mol}$$

Conclusion

In this study, the author could synthesize a novel PNP-pincer type phosphaalkene ligand (Eind-PPEP) that functions as a noninnocent ligand on transition metals. Unlike PPEP bearing Mes* as a steric protecting group of the P=C bond, Eind-PPEP protected by a fused-ring bulky Eind group was sufficiently stable against C–H addition/cyclization even on a Rh(I) center. Therefore, the author could compare the reactivity of K[MCl(Eind-PPEP*)] (M = Rh and Ir) towards ammonia, and found a dramatic change in the reaction courses depending on the metals. It is worth noting that the reactivity of iridium complex K[**13**] towards N–H bond cleavage of ammonia is comparable to that of PPEP* complex K[**3b**]. This observation indicates that, while the Eind group seems sterically more demanding than the Mes* group, the highly reactive nature of dearomatized phosphaalkene complex towards metal–ligand cooperative activation is successfully preserved after structural modification using Eind.

Experimental Section

General Considerations. All manipulations were performed under a nitrogen atmosphere using a glove box and Schlenk techniques. Eind-PCl_2 was prepared as previously reported.[10] The other chemicals were obtained from commercial sources. NMR spectra were recorded on a 400 MHz spectrometer. Chemical shifts are reported in δ (ppm), referenced to ^{1}H (residual) and ^{13}C signals of deuterated solvents as internal standards or to the ^{31}P signal of 85% H_3PO_4 as an external standard. The assignments of ^{13}C signals are based on HMQC experiments. Elemental analysis was performed by ICR Analytical Laboratory, Kyoto University.

Synthesis of Eind-BPEP (7). (i) Synthesis of 6. To a mixture of zinc dust (348 mg, 5.3 mmol) and Eind-PCl_2 (300 mg, 0.62 mmol) in THF (4 mL), was added a 1.0 M THF solution of PMe_3 (1.5 mL, 1.5 mmol) at room temperature. After stirring for 1 h, the reaction mixture was added dropwise to a THF solution (6 mL) of **5** (86 mg, 0.64 mmol) by a cannula at 0 °C over 10 min. The mixture was stirred at room temperature for 6 h, and solvent was removed under reduced pressure. The residue was suspended in hexane (600 mL), and filtrated through a Celite pad to remove zinc dust, $ZnCl_2$, and Me_3PO. The filtrate was concentrated to half in volume, and purified by gel filtration using a 1,2-dihydroxy-3-propoxypropyl-modified silica gel and hexane as the eluent to afford **6** as a pale-yellow powder (241 mg, 0.45 mmol, 74%).

6: ^{1}H NMR (C_6D_6, 25 °C): δ 10.05 (s, 1H, C*H*O), 9.21 (d, $^{2}J_{PH}$ = 25.5 Hz, 1H, P=C*H*), 7.48 (d, $^{3}J_{HH}$ = 7.7 Hz, 1H, 4-Py), 7.31 (d, $^{3}J_{HH}$ = 7.7 Hz, 1H, 5-Py), 6.88 (t, $^{3}J_{HH}$ = 7.7 Hz, 1H, 3-Py), 6.86 (s, 1H, *p*-Eind), 2.07 (dq, $^{2}J_{HH}$ = 14.2 Hz, $^{3}J_{HH}$ = 7.4 Hz, 4H, CH*H*), 1.94 (dq, $^{2}J_{HH}$ = 14.2 Hz, $^{3}J_{HH}$ = 7.4 Hz, 4H, CH*H*), 1.78 (s, 4H, ind-CH_2), 1.73 (dq, $^{2}J_{HH}$ = 14.2 Hz, $^{3}J_{HH}$ = 7.4 Hz, 4H, CH*H*), 1.62 (dq, $^{2}J_{HH}$ = 14.2 Hz, $^{3}J_{HH}$ = 7.4 Hz, 4H, CH*H*), 0.90 (t, $^{3}J_{HH}$ = 7.4 Hz, 12H, CH_3), 0.86 (t, $^{3}J_{HH}$ = 7.4 Hz, 12H, CH_3). $^{13}C\{^{1}H\}$ NMR (C_6D_6, 25 °C): δ 193.3 (s, *C*HO), 180.3 (d, $^{1}J_{PC}$ = 36 Hz, P=*C*H), 158.8 (d, J_{PC} = 15 Hz), 153.9 (s), 150.7 (d, J_{PC} = 3 Hz), 150.2 (s), 137.8 (s), 136.3 (d, $^{1}J_{PC}$ = 48 Hz, *ipso*-Eind), 124.3 (d, J_{PC} = 18 Hz), 121.5 (s, *p*-Eind), 120.1 (d, J_{PC} = 6 Hz), 53.7 (s), 49.0 (s), 42.9 (s, *C*H_2), 34.4 (br s, *C*H_2CH$_3$), 33.7 (br s, *C*H_2CH$_3$), 10.1 (s, CH$_2$*C*H$_3$), 9.8 (s, CH$_2$*C*H$_3$). $^{31}P\{^{1}H\}$ NMR (C_6D_6, 25 °C): δ 284.2 (s). Anal. Calcd for $C_{35}H_{50}NOP$: C, 79.05; H, 9.48; N, 2.63. Found: C, 79.10; H, 9.62; N, 2.65.

(ii) Synthesis of 7. To a mixture of zinc dust (235 mg, 3.6 mmol) and Mes*-PCl_2 (119 mg, 0.33 mmol) in THF (3.5 mL), was added a 1.0 M THF solution of PMe_3 (0.9 mL, 0.9 mmol)

at room temperature. After stirring for 3 h, the reaction mixture was added dropwise to a THF solution (7 mL) of **6** (174 mg, 0.33 mmol) by a cannula at 0 °C. The mixture was stirred at room temperature for 6 h, and volatiles were removed under reduced pressure. The residue was suspended in hexane (30 mL), and filtrated through a Celite pad to remove zinc dust, $ZnCl_2$, and Me_3PO. The filtrate was concentrated to dryness under reduced pressure to afford Eind-BPEP (**7**) as a yellow solid (259 mg, 0.32 mmol, 97%). The crude product was purified by column chromatography using deactivated neutral alumina and hexane as the eluent to remove a small amount of Mes*PH_2 formed by decomposition of the phopha-Wittig reagent (Mes*P=PMe_3).

7: ^{1}H NMR (CD_2Cl_2, 25 °C): δ 8.86 (d, $^2J_{PH}$ = 25.6 Hz, 1H, EindP=C*H*), 8.13 (d, $^2J_{PH}$ = 25.3 Hz, 1H, Mes*P=C*H*), 7.58 (t, $^3J_{HH}$ = 7.8 Hz, 1H, Py), 7.55 (d, $^3J_{HH}$ = 7.8 Hz, 1H, Py), 7.45 (s, 2H, *m*-Mes*), 7.39 (d, $^3J_{HH}$ = 7.8 Hz, 1H, Py), 6.73 (s, 1H, *p*-Eind), 1.91–1.76 (m, 8H, C*H*$_2$CH$_3$), 1.81 (s, 4H, 2 × C*H*$_2$), 1.74–1.55 (m, 8H, C*H*$_2$CH$_3$), 1.53 (s, 18H, *o*-C(C*H*$_3$)$_3$), 1.36 (s, 9H, *p*-C(C*H*$_3$)$_3$), 0.85 (t, $^3J_{HH}$ = 7.4 Hz, 12H, CH$_2$C*H*$_3$), 0.77 (t, $^3J_{HH}$ = 7.4 Hz, 12H, CH$_2$C*H*$_3$). ^{13}C{^{1}H} NMR (CD_2Cl_2, 25 °C): δ 181.8 (d, $^1J_{PC}$ = 34 Hz, EindP=*C*H), 175.9 (d, $^1J_{PC}$ = 35 Hz, Mes*P=*C*H), 158.7 (d, J_{PC} = 28 Hz), 158.6 (d, J_{PC} = 27 Hz), 154.7 (s), 150.6 (s), 150.4 (s), 150.0 (s), 139.6 (d, $^1J_{PC}$ = 54 Hz, *ipso*-Ar), 137.3 (s), 136.3 (d, $^1J_{PC}$ = 48 Hz, *ipso*-Ar), 122.6 (s, *m*-Mes*), 121.3 (s, *p*-Eind), 119.8 (t, J_{PC} = 18 Hz), 119.7 (t, J_{PC} = 17 Hz), 53.6 (s), 48.8 (s), 42.7 (s, *C*H$_2$), 38.8 (s), 35.6 (s), 34.4 (d, $^4J_{PC}$ = 7 Hz, *o*-C(*C*H$_3$)$_3$), 34.1 (br, *C*H$_2$CH$_3$), 33.5 (br, *C*H$_2$CH$_3$), 31.8 (s, *p*-C(*C*H$_3$)$_3$), 10.0 (s, CH$_2$*C*H$_3$), 9.6 (s, CH$_2$*C*H$_3$). ^{31}P{^{1}H} NMR (CD_2Cl_2, 25 °C): δ 285.8 (s), 275.2 (s). HRMS (APCI): Calcd for $C_{53}H_{79}NP_2$ 792.5761 ([M + H]$^+$); Found 792.5774.

Synthesis of Eind-BPEP Complexes (8 and 9). A typical synthetic procedure is described for [RhCl(Eind-BPEP)] (**8**). The complex [Rh(*μ*-Cl)(C_2H_4)$_2$]$_2$ (26 mg, 0.067 mmol) was suspended in THF (2 mL), and a solution (1 mL) of Eind-BPEP (122 mg, 0.15 mmol) in THF (1 mL) was added at room temperature. The mixture was instantly changed into a greenish brown solution. The solution was stirred for 30 min, and concentrated under reduced pressure. Addition of Et_2O (0.5 mL) led to the formation of a dark green crystalline solid of **8**, which was collected by filtration, washed with Et_2O (0.3 mL × 5), and dried under vacuum (75 mg, 0.080 mmol, 60%). The complex [IrCl(Eind-BPEP)] (**2**) was similarly prepared from [Ir(*μ*-

Cl)(coe)$_2$]$_2$, and isolated as a greenish brown crystalline solid (84%).

[8]: ^{1}H NMR (CD_2Cl_2, 25 °C): δ 7.66 (dd, $^2J_{PH}$ = 17.5 Hz, $^3J_{RhH}$ = 3.6 Hz, 1H, EindP=C*H*), 7.59 (d, $^4J_{PH}$ = 2.5 Hz, 2H, *m*-Mes*), 7.28–7.23 (m, 1H, Py), 7.19 (dd, $^2J_{PH}$ = 18.1 Hz, $^3J_{RhH}$ = 3.6 Hz, 1H, Mes*P=C*H*), 6.91 (d, $^5J_{PH}$ = 3.3 Hz, 1H, *p*-Eind), 6.72–6.68 (m, 2H, Py), 2.39–2.24 (m, 4H, CH_2CH$_3$), 2.18–2.11 (m, 2H, CH_2CH$_3$), 1.97–1.88 (m, 2H, CH_2CH$_3$), 1.93 (d, $^2J_{HH}$ = 14.0 Hz, 2H, CH_2), 1.84 (d, $^2J_{HH}$ = 14.0 Hz, 2H, CH_2), 1.74 (s, 18H, *o*-C(CH_3)$_3$), 1.72–1.52 (m, 8H, CH_2CH$_3$), 1.38 (s, 9H, *p*-C(CH_3)$_3$), 0.90 (t, $^3J_{HH}$ = 7.4 Hz, 6H, CH$_2$CH_3), 0.85 (t, $^3J_{HH}$ = 7.4 Hz, 6H, CH$_2$CH_3), 0.83 (t, $^3J_{HH}$ = 7.6 Hz, 6H, CH$_2$CH_3), 0.77 (t, $^3J_{HH}$ = 7.3 Hz, 6H, CH$_2$CH_3). ^{13}C{^{1}H} NMR (CD_2Cl_2, 25 °C): δ 168.5 (d, J_{PC} = 8 Hz), 157.2 (s), 153.7 (d, J_{PC} = 2 Hz), 153.3 (s), 151.0 (s), 150.9 (s), 149.3 (dd, $^1J_{PC}$ = 36 Hz, $^2J_{RhC}$ = 4 Hz, EindP=*C*H), 148.1 (dd, $^1J_{PC}$ = 36 Hz, $^2J_{RhC}$ = 4 Hz, Mes*P=*C*H), 134.4 (s), 126.8–126.4 (m, *ipso*-Ar), 124.3–123.9 (m, *ipso*-Ar), 123.7 (d, $^4J_{PC}$ = 2 Hz, *p*-Eind), 123.4 (d, $^3J_{PC}$ = 7 Hz, *m*-Mes*), 114.6 (t, J_{PC} = 8 Hz, J_{RhC} = 8 Hz), 114.3 (t, J_{PC} = 8 Hz, J_{RhC} = 8 Hz), 54.2 (s), 48.8 (s), 43.0 (s, *C*H$_2$), 39.5 (s), 35.9(s), 35.0 (d, $^4J_{PC}$ = 2 Hz, *C*H$_2$CH$_3$), 34.8 (d, $^4J_{PC}$ = 2 Hz, *o*-C(*C*H$_3$)$_3$), 34.4 (s, *C*H$_2$CH$_3$), 33.7 (s, *C*H$_2$CH$_3$), 33.5 (s, *C*H$_2$CH$_3$), 31.6 (s, *p*-C(*C*H$_3$)$_3$), 10.5 (s, CH$_2$*C*H$_3$), 10.4 (s, CH$_2$*C*H$_3$), 9.6 (s, 2 × CH$_2$*C*H$_3$). ^{31}P{^{1}H} NMR (CD_2Cl_2, 25 °C): δ 239.2 (dd, $^2J_{PP}$ = 519 Hz, $^1J_{RhP}$ = 207 Hz), 231.2 (dd, $^2J_{PP}$ = 519 Hz, $^1J_{RhP}$ = 204 Hz). Anal. Calcd for $C_{53}H_{79}ClNP_2Rh$: C, 68.41; H, 8.56; N, 1.51. Found: C, 68.32; H, 8.65; N, 1.65.

[9]: ^{1}H NMR (CD_2Cl_2, 25 °C): δ 8.96 (dd, $^2J_{PH}$ = 13.3 Hz, $^4J_{PH}$ = 5.4 Hz, 1H, EindP=C*H*), 8.50 (dd, $^2J_{PH}$ = 14.1 Hz, $^4J_{PH}$ = 5.1 Hz, 1H, Mes*P=C*H*), 7.79–7.74 (m, 1H, Py), 7.65 (d, $^4J_{PH}$ = 2.9 Hz, 2H, *m*-Mes*), 7.05–7.03 (m, 1H, Py), 7.00–6.98 (m, 1H, Py), 6.95 (d, $^5J_{PH}$ = 1.7 Hz, 1H, *p*-Eind), 2.35–2.24 (m. 4H, CH_2CH$_3$), 2.14–2.06 (m, 2H, CH_2CH$_3$), 1.94 (d, $^2J_{HH}$ = 14.0 Hz, 2H, CH_2), 1.94–1.81 (m, 2H, CH_2CH$_3$), 1.85 (d, $^2J_{HH}$ = 14.0 Hz, 2H, CH_2), 1.79–1.58 (m, 8H, CH_2CH$_3$), 1.72 (s, 18H, *o*-C(CH_3)$_3$), 1.41 (s, 9H, *p*-C(CH_3)$_3$), 0.92 (t, $^3J_{HH}$ = 7.4 Hz, 6H, CH$_2$CH_3), 0.862 (t, $^3J_{HH}$ = 7.2 Hz, 6H, CH$_2$CH_3), 0.857 (t, $^3J_{HH}$ = 7.2 Hz, 6H, CH$_2$CH_3), 0.71 (t, $^3J_{HH}$ = 7.3 Hz, 6H, CH$_2$CH_3). ^{13}C{^{1}H} NMR (CD_2Cl_2, 25 °C): δ 174.6 (dd, J_{PC} = 9 and 4 Hz), 157.4 (vt, J_{app} = 2 Hz), 154.0 (d, J_{PC} = 2 Hz), 153.3 (s), 151.2 (s), 151.1 (s), 143.2 (d, $^1J_{PC}$ = 53 Hz, Mes*P=*C*H), 142.6 (d, $^1J_{PC}$ = 53 Hz, EindP=*C*H), 135.8 (vt, J_{app} = 3 Hz, Py), 127.3 (d, $^1J_{PC}$ = 21 Hz, *ipso*-Ar), 124.5 (dd, $^1J_{PC}$ = 21 Hz, $^3J_{PC}$ = 5 Hz, *ipso*-Ar), 124.0 (d, $^4J_{PC}$ = 3 Hz, *p*-Eind), 123.5 (d, $^3J_{PC}$ = 8 Hz, *m*-Mes*), 108.0 (dd, J_{PC} = 7 and 6 Hz),

107.8 (dd, J_{PC} = 7 and 6 Hz), 54.3 (s), 48.7 (s), 43.0 (s, *C*H_2), 39.5 (s), 36.0 (s), 34.6 (s, *C*H_2CH$_3$), 34.4 (d, $^4J_{PC}$ = 1 Hz, *o*-C(*C*H$_3$)$_3$), 33.9 (s, *C*H_2CH$_3$), 33.6 (s, 2 × *C*H_2CH$_3$), 31.6 (s, *p*-C(*C*H$_3$)$_3$), 10.5 (s, CH$_2$*C*H$_3$), 10.3 (s, CH$_2$*C*H$_3$), 9.6 (s, 2 × CH$_2$*C*H$_3$). ^{31}P{^{1}H} NMR (CD_2Cl_2, 25 °C): δ 249.3 (d, $^2J_{PP}$ = 560 Hz), 237.2 (d, $^2J_{PP}$ = 560 Hz). Anal. Calcd for $C_{53}H_{79}ClNP_2Ir$: C, 62.42; H, 7.81; N, 1.37. Found: C, 62.28; H, 7.88; N, 1.32.

Synthesis of Eind-PPEP Complexes (10 and 11). The complex [RhCl(Eind-BPEP)] (**8**) (14 mg, 0.015 mmol) was dissolved in toluene-d_8 (0.6 mL), and heated at 140 °C for 2 days in a sealed NMR sample tube. The color of the solution gradually changed from dark green to dark red. ^{1}H and ^{31}P{^{1}H} NMR analysis revealed the complete conversion of **8** to **10**. The solution was filtered through a Celite pad to remove a small amount of black solids, and concentrated to dryness to give a dark red crystalline solid of **10** (14 mg, 100%), which was analytical pure. Iridium Eind-PPEP complex **11** was prepared by heating a toluene solution of **9** at 70 °C for 10 h, and isolated as a pure brown crystalline solid in quantitative yield.

[10]: ^{1}H NMR (THF-d_8, 25 °C): δ 8.06 (dd, $^2J_{PH}$ = 17.0 Hz, $^3J_{RhH}$ = 3.6 Hz, 1H, EindP=C*H*), 7.58 (br t, $^3J_{HH}$ = 7.7 Hz, 1H, Py), 7.46 (dd, $^4J_{PH}$ = 4.8 Hz, $^4J_{HH}$ = 1.7 Hz, 1H, Ar), 7.27 (d, $^4J_{HH}$ = 1.7 Hz, 1H, Ar), 7.13–7.10 (m, 1H, Py), 7.02 (br d, $^3J_{HH}$ = 6.4 Hz, 1H, Py), 6.92 (s, 1H, *p*-Eind), 4.32 (dd, $^2J_{HH}$ = 18.4 Hz, $^2J_{PH}$ = 9.6 Hz, 1H, PyC*H*$_2$P), 4.10 (dd, $^2J_{HH}$ = 18.4 Hz, $^2J_{PH}$ = 9.7 Hz, 1H, PyC*H*$_2$P), 2.83–2.71 (m, 2H, PC*H*$_2$ + C*H*$_2$CH$_3$), 2.57–2.47 (m, 1H, C*H*$_2$CH$_3$), 2.36 (dd, $^2J_{HH}$ =14.8 Hz, $^2J_{PH}$ = 2.1 Hz, 1H, PC*H*$_2$), 2.25–2.14 (m, 3H, C*H*$_2$CH$_3$), 2.06–1.93 (m, 4H, C*H*$_2$CH$_3$ + C*H*$_2$), 1.89–1.83 (m, 3H, C*H*$_2$CH$_3$ + C*H*$_2$), 1.79–1.58 (m, 8H, C*H*$_2$CH$_3$), 1.53 (s, 9H, C(C*H*$_3$)$_3$), 1.51 (s, 3H, C*H*$_3$), 1.46 (s, 3H, C*H*$_3$), 1.35 (s, 9H, C(C*H*$_3$)$_3$), 0.93 (t, $^3J_{HH}$ = 6.8 Hz, 6H, CH$_2$C*H*$_3$), 0.90–0.82 (m, 12H, CH$_2$C*H*$_3$), 0.82–0.75 (m, 6H, CH$_2$C*H*$_3$). ^{13}C{^{1}H} NMR (THF-d_8, 25 °C): δ 166.3 (d, J_{PC} = 10 Hz), 164.0 (d, J_{PC} = 10 Hz), 160.1 (dd, J_{PC} = 11 and 5 Hz), 154.9 (d, J_{PC} = 2 Hz), 154.7 (d, J_{PC} = 11 Hz), 153.3 (d, J_{PC} = 2 Hz), 153.0 (s), 150.8 (d, J_{PC} = 6 Hz), 150.7 (d, J_{PC} = 6 Hz), 149.0 (dd, $^1J_{PC}$ = 32 Hz, $^2J_{RhC}$ = 3 Hz, EindP=*C*H), 132.5 (s), 129.3–129.0 (m), 128.6 (dt, J_{RhC} = 19 Hz, J_{PC} = 19 and 7 Hz), 123.9 (d, $^3J_{PC}$ = 8 Hz, Ar), 123.2 (s, *p*-Eind), 120.8 (d, J_{PC} = 25 Hz), 119.6 (d, $^3J_{PC}$ = 8 Hz, Ar), 118.9 (dd, J_{PC} = 13 and 8 Hz), 54.9 (s), 54.7 (s), 50.6 (d, $^1J_{PC}$ = 18 Hz, Py*C*H$_2$P), 49.2 (s), 45.4–45.2 (m), 43.7 (s, *C*H_2), 43.6 (s, *C*H_2), 43.2 (s), 42.3 (d, $^1J_{PC}$ = 27 Hz, P*C*H$_2$), 38.3 (s), 36.1 (s), 35.5 (s, *C*H_2CH$_3$), 35.3 (s, *C*H_2CH$_3$), 35.1 (d, $^4J_{PC}$ = 3 Hz, *C*H_2CH$_3$), 34.8 (s,

*C*H$_2$CH$_3$), 34.7 (s, *C*H$_2$CH$_3$), 34.6 (d, $^4J_{PC}$ = 2 Hz, *C*H$_2$CH$_3$), 33.8 (d, $^4J_{PC}$ = 3 Hz, C(*C*H$_3$)$_3$), 33.7 (s, *C*H$_3$), 33.3 (s, *C*H$_2$CH$_3$), 33.2 (s, *C*H$_2$CH$_3$), 32.1 (d, $^3J_{PC}$ = 9 Hz, *C*H$_3$), 31.9 (s, C(*C*H$_3$)$_3$), 11.02 (s, CH$_2$*C*H$_3$), 10.99 (s, CH$_2$*C*H$_3$), 10.7 (s, CH$_2$*C*H$_3$), 10.6 (s, CH$_2$*C*H$_3$), 9.8 (s, 4 × CH$_2$*C*H$_3$). ^{31}P{^{1}H} NMR (THF-d_8, 25 °C): δ 230.5 (dd, $^2J_{PP}$ = 461 Hz, $^1J_{RhP}$ = 183 Hz), 26.0 (dd, $^2J_{PP}$ = 461 Hz, $^1J_{RhP}$ = 168 Hz). Anal. Calcd for $C_{53}H_{79}ClNP_2Rh$: C, 68.41; H, 8.56; N, 1.51. Found: C, 68.68; H, 8.83; N, 1.73.

[11]: ^{1}H NMR (THF-d_8, 25 °C): δ 8.94 (dd, $^2J_{PH}$ = 12.7 Hz, $^4J_{PH}$ = 4.1 Hz, 1H, EindP=C*H*), 7.99 (td, $^3J_{HH}$ = 7.6 Hz, $^5J_{PH}$ = 1.7 Hz, 1 H, Py), 7.47 (dd, $^4J_{PH}$ = 4.8 Hz, $^4J_{HH}$ = 1.7 Hz, 1H, Ar), 7.30 (d, $^4J_{HH}$ = 1.7 Hz, 1H, Ar), 6.96 (br d, $^3J_{HH}$ = 7.2 Hz, 1H, Py), 6.95 (s, 1H, *p*-Eind), 6.90 (br d, $^3J_{HH}$ = 7.6 Hz, 1H, Py), 4.02 (dd, $^2J_{HH}$ = 18.8 Hz, $^2J_{PH}$ = 9.9 Hz, 1H, PyC*H*$_2$P), 4.01 (dd, $^2J_{HH}$ = 18.8 Hz, $^2J_{PH}$ = 10.2 Hz, 1H, PyC*H*$_2$P), 2.81–2.69 (m, 2H, PC*H*$_2$ + C*H*$_2$CH$_3$), 2.63–2.51 (m, 1H, C*H*$_2$CH$_3$), 2.38 (dd, $^2J_{HH}$ =14.8 Hz, $^2J_{PH}$ = 3.1 Hz, 1H, PC*H*$_2$), 2.32–2.18 (m, 3H, C*H*$_2$CH$_3$), 2.16–2.09 (m, 1H, C*H*$_2$CH$_3$), 2.07–2.00 (m, 1H, C*H*$_2$CH$_3$), 1.95 (d, $^2J_{HH}$ = 13.9 Hz, 2H, C*H*$_2$), 1.86 (d, $^2J_{HH}$ = 13.9 Hz, 1H, C*H*$_2$), 1.85 (d, $^2J_{HH}$ = 13.9 Hz, 1H, C*H*$_2$), 1.91–1.63 (m, 9H, C*H*$_2$CH$_3$), 1.51 (s, 3H, C*H*$_3$), 1.50 (s, 3H, C*H*$_3$), 1.42 (s, 9H, C(C*H*$_3$)$_3$), 1.36 (s, 9H, C(C*H*$_3$)$_3$), 0.95–0.76 (m, 24H, CH$_2$C*H*$_3$). ^{13}C{^{1}H} NMR (THF-d_8, 25 °C): δ 168.0 (d, J_{PC} = 7 Hz), 167.3 (dd, J_{PC} = 6 and 3 Hz), 160.4 (dd, J_{PC} = 14 and 5 Hz), 154.9 (d, J_{PC} = 2 Hz), 154.8 (d, J_{PC} = 10 Hz), 152.7 (d, J_{PC} = 2 Hz), 152.5 (s), 150.9 (d, J_{PC} = 7 Hz), 150.8 (d, J_{PC} = 10 Hz), 143.9 (d, $^1J_{PC}$ = 47 Hz, EindP=*C*H), 130.9 (s), 128.9 (dd, J_{PC} = 20 and 4 Hz), 126.9 (dd, 37 and 6 Hz), 124.0 (d, $^3J_{PC}$ = 9 Hz, Ar), 123.4 (d, $^4J_{PC}$ = 2 Hz, *p*-Eind), 121.6 (d, J_{PC} = 25 Hz), 119.6 (d, $^3J_{PC}$ = 9 Hz, Ar), 118.2 (dd, J_{PC} = 12 and 8 Hz), 54.8 (s), 54.7 (s), 51.1 (d, $^1J_{PC}$ = 26 Hz, Py*C*H$_2$P), 49.0 (s), 48.9 (s), 44.5 (vt, J_{app} = 4 Hz), 43.7 (s, *C*H$_2$), 43.6 (s, *C*H$_2$), 40.8 (d, $^1J_{PC}$ = 34 Hz, P*C*H$_2$), 38.1 (s), 36.0 (s), 34.8 (s, *C*H$_2$CH$_3$), 34.6 (s, *C*H$_2$CH$_3$), 34.52 (s, *C*H$_2$CH$_3$), 34.47 (s, *C*H$_2$CH$_3$), 34.4 (s, *C*H$_2$CH$_3$), 34.1 (s, *C*H$_2$CH$_3$), 33.7 (s, *C*H$_3$), 33.6 (d, $^4J_{PC}$ = 2 Hz, C(*C*H$_3$)$_3$), 33.4 (s, *C*H$_2$CH$_3$), 33.3 (s, *C*H$_2$CH$_3$), 31.9 (s, *C*H$_3$), 31.8 (s, C(*C*H$_3$)$_3$), 10.90 (s, CH$_2$*C*H$_3$), 10.86 (s, CH$_2$*C*H$_3$), 10.6 (s, CH$_2$*C*H$_3$), 10.5 (s, CH$_2$*C*H$_3$), 9.8 (s, 2 × CH$_2$*C*H$_3$), 9.7 (s, 2 × CH$_2$*C*H$_3$). ^{31}P{^{1}H} NMR (THF-d_8, 25 °C): δ 232.7 (d, $^2J_{PP}$ = 480 Hz), 25.4 (d, $^2J_{PP}$ = 480 Hz). Anal. Calcd for $C_{53}H_{79}ClNP_2Ir$: C, 62.42; H, 7.81; N, 1.37. Found: C, 62.23; H, 7.86; N, 1.24.

Synthesis of Eind-PPEP* Complexes (12 and 13). A solution of ^{t}BuOK (6.7 mg, 0.060 mmol) and 18-crown-6 (16 mg, 0.060 mmol) in THF (1 mL) was added to a THF solution (1 mL) of **10** (56 mg, 0.060 mmol). The color of the solution instantly changed from dark red to dark greenish brown. After 20 min at room temperature, the complete conversion of **10** was confirmed by $^{31}P\{^1H\}$ NMR analysis. The solvent was removed under reduced pressure, and Et_2O (0.3 mL) was added to the residue, affording dark brown crystals of [K(18C6)][RhCl(Eind-PPEP*)] ([K(18C6)][**12**]). The supernatant was removed by decantation, and the crystalline soild was washed with Et_2O (0.3 mL × 5) and dried under vacuum (59 mg, 0.048 mmol, 80%). The complex [K(18C6)][IrCl(Eind-PPEP*)] ([K(18C6)][**13**]) was similarly prepared from **11** as dark green crystals (80%).

[K(18C6)][12]: ^{1}H NMR (THF-d_8, 25 °C): δ 7.52 (dd, $^2J_{PH}$ = 16.3 Hz, $^3J_{RhH}$ = 2.7 Hz, 1H, EindP=C*H*), 7.27 (dd, $^4J_{PH}$ = 3.8 Hz, $^4J_{HH}$ = 1.4 Hz, 1H, Ar), 7.08 (d, $^4J_{HH}$ = 1.4 Hz, 1H, Ar), 6.74 (s, 1H, *p*-Eind), 6.03 (m, 1H, Py), 5.92 (dd, $^3J_{HH}$ = 8.4 Hz, $^4J_{PH}$ = 2.8 Hz, 1H, Py), 5.49 (dd, $^3J_{HH}$ = 6.5 Hz, $^4J_{PH}$ = 3.9 Hz, 1H, Py), 3.56 (vt, 1H, Py=C*H*P), 3.53 (s, 24H, 18-crown-6), 3.11–3.03 (m, 1H, CH_2CH$_3$), 2.74–2.70 (m, 1H, CH_2CH$_3$), 2.46 (dd, $^2J_{HH}$ = 13.5 Hz, $^3J_{PH}$ = 4.0 Hz, 1H, PCH_2), 2.33–2.19 (m, 4H, CH_2CH$_3$), 2.10–1.94 (m, 2H, CH_2CH$_3$), 1.88 (d, $^2J_{HH}$ = 13.6 Hz, 2H, CH_2), 1.82 (d, $^2J_{HH}$ = 13.6 Hz, 1H, CH_2), 1.80 (d, $^2J_{HH}$ = 13.6 Hz, 1H, CH_2), 1.71 (s, 9H, C(CH_3)$_3$), 1.71–1.54 (m, 9H, 4 × CH_2CH$_3$ + PCH_2), 1.42 (s, 3H, CH_3), 1.38 (s, 3H, CH_3), 1.31 (s, 9H, C(CH_3)$_3$), 0.91 (t, $^3J_{HH}$ = 7.3 Hz, 6H, CH$_2$CH_3), 0.87–0.77 (m, 18H, CH$_2$CH_3). The coupling constant for the vinylic proton at δ 3.56 was obscure due to the overlap with a residual signal of THF-d_8. $^{13}C\{^1H\}$ NMR (THF-d_8, 25 °C): δ 173.5 (dd, J_{PC} = 25 Hz, J_{RhC} = 3 Hz), 163.6 (d, J_{PC} = 10 Hz), 158.6 (dd, J_{PC} = 10 and 5 Hz), 153.8 (d, J_{PC} = 10 Hz), 152.45 (s), 152.41 (s), 150.5 (d, J_{PC} = 2 Hz), 149.7 (d, $^1J_{PC}$ = 33 Hz, EindP=*C*H), 149.4 (d, J_{PC} = 4 Hz), 149.1 (d, J_{PC} = 5 Hz), 136.7–136.5 (br d, J_{PC} = 25 Hz), 132.8 (ddd, J_{PC} = 29 and 20 Hz, J_{RhC} = 7 Hz), 129.4 (vt, J_{app} = 3 Hz), 121.1 (d, $^3J_{PC}$ = 7 Hz, Ar), 120.8 (s, *p*-Eind), 117.6 (d, $^3J_{PC}$ = 7 Hz, Ar), 109.3 (dd, J_{PC} = 21 and 10 Hz), 100.4 (d, J_{PC} = 28 Hz), 74.7 (d, $^1J_{PC}$ = 51 Hz, Py=*C*HP), 71.0 (s, 18-crown-6), 54.4 (s), 54.2 (s), 48.34 (s), 48.30 (s), 43.7 (d, $^1J_{PC}$ = 27 Hz, P*C*H$_2$), 43.8–43.7 (m), 43.6 (s, *C*H$_2$), 43.5 (s, *C*H$_2$), 38.6 (s), 35.3 (s), 34.7 (s, *C*H$_2$CH$_3$), 34.6 (s, *C*H$_2$CH$_3$), 34.5 (s, *C*H$_2$CH$_3$), 34.4 (s, *C*H$_2$CH$_3$), 34.03 (s, C(*C*H$_3$)$_3$), 34.00 (s, *C*H$_3$), 33.97 (s, *C*H$_2$CH$_3$), 33.7 (d, $^4J_{PC}$ = 3 Hz, *C*H$_2$CH$_3$), 32.9 (s, *C*H$_2$CH$_3$), 32.8 (s,

CH_2CH_3), 32.3 (d, $^3J_{PC}$ = 8 Hz, CH_3), 31.8 (s, C(CH_3)$_3$), 11.0 (s, CH_2CH_3), 10.9 (s, CH_2CH_3), 10.4 (s, CH_2CH_3), 10.3 (s, CH_2CH_3), 9.5 (s, 2 × CH_2CH_3), 9.4 (s, 2 × CH_2CH_3). $^{31}P\{^1H\}$ NMR (THF-d_8, 25 °C): δ 211.3 (dd, $^2J_{PP}$ = 433 Hz, $^1J_{RhP}$ = 182 Hz), 19.2 (dd, $^2J_{PP}$ = 433 Hz, $^1J_{RhP}$ = 169 Hz). Anal. Calcd for $C_{65}H_{102}ClKNO_6P_2Rh$: C, 63.32; H, 8.34; N, 1.14. Found: C, 63.04; H, 8.54; N, 1.08.

[K(18C6)][13]: ^{1}H NMR (THF-d_8, 25 °C): δ 8.90 (dd, $^2J_{PH}$ = 11.7 Hz, $^4J_{PH}$ = 3.6 Hz, 1H, EindP=C*H*), 7.27 (dd, $^4J_{PH}$ = 3.8 Hz, $^4J_{HH}$ = 1.7 Hz, 1H, Ar), 7.12 (d, $^4J_{HH}$ = 1.7 Hz, 1H, Ar), 6.76 (s, 1H, *p*-Eind), 6.13 (dd, $^3J_{HH}$ = 8.1 and 6.8 Hz, 1H, Py), 6.06–6.03 (m, 2H, Py), 3.89 (vt, J_{app} = 3.8 Hz, Py=C*H*P), 3.53 (s, 24H, 18-crown-6), 3.23–3.14 (m, 1H, CH_2CH$_3$), 2.90–2.81 (m, 1H, CH_2CH$_3$), 2.37 (br dd, $^1J_{HH}$ = 13.6 Hz, $^2J_{PH}$ = 7.2 Hz, 1H, PCH_2), 2.32–2.17 (m, 4H, CH_2CH$_3$), 2.03–1.93 (m, 2H, CH_2CH$_3$), 1.88 (d, $^2J_{HH}$ = 13.8 Hz, 2H, CH_2), 1.81 (d, $^2J_{HH}$ = 13.8 Hz, 1H, CH_2), 1.80 (d, $^2J_{HH}$ = 13.8 Hz, 1H, CH_2), 1.71–1.57 (m, 9H, 4 × CH_2CH$_3$ + PCH_2), 1.55 (s, 9H, C(CH_3)$_3$), 1.47 (s, 3H, CH_3), 1.37 (s, 3H, CH_3), 1.32 (s, 9H, C(CH_3)$_3$), 0.92–0.77 (m, 24H, CH_2CH_3). $^{13}C\{^1H\}$ NMR (THF-d_8, 25 °C): δ 177.4 (d, J_{PC} = 20 Hz), 167.4 (dd, J_{PC} = 8 and 3 Hz), 159.0 (dd, J_{PC} =13 and 5 Hz), 154.0 (d, J_{PC} = 9 Hz), 152.5 (s), 150.71 (s), 150.69 (s), 149.7 (d, J_{PC} = 5 Hz), 149.4 (d, J_{PC} = 6 Hz), 141.9 (d, $^1J_{PC}$ = 48 Hz, EindP=*C*H), 135.8 (dd, J_{PC} = 34 and 5 Hz), 133.8 (dd, J_{PC} = 22 and 17 Hz), 130.7 (s), 122.3 (d, $^3J_{PC}$ = 7 Hz, Ar), 121.2 (s, *p*-Eind), 117.8 (d, $^3J_{PC}$ = 8 Hz, Ar), 105.9 (dd, J_{PC} = 18 and 8 Hz), 98.6 (d, J_{PC} = 26 Hz), 73.1 (d, $^1J_{PC}$ = 64 Hz, Py=*C*HP), 71.1 (s, 18-crown-6), 54.5 (s), 54.3 (s), 48.3 (s), 48.2 (s), 43.9 (s, *C*H$_2$), 43.7 (s, *C*H$_2$), 43.3 (br s), 43.1 (d, $^1J_{PC}$ = 29 Hz, P*C*H$_2$), 38.5 (s), 35.4 (s), 34.44 (s, *C*H$_2$CH$_3$), 34.43 (s, *C*H$_2$CH$_3$), 34.35 (s, *C*H$_2$CH$_3$), 34.34 (s, *C*H$_2$CH$_3$), 34.2 (d, $^4J_{PC}$ = 2 Hz, C(*C*H$_3$)$_3$), 34.1 (s, *C*H$_3$), 33.9 (br s, *C*H$_2$CH$_3$), 33.2 (br s, *C*H$_2$CH$_3$), 33.1 (s, *C*H$_2$CH$_3$), 32.9 (s, *C*H$_2$CH$_3$), 32.4 (d, $^3J_{PC}$ = 9 Hz, *C*H$_3$), 31.8 (s, C(*C*H$_3$)$_3$), 11.02 (s, CH_2CH_3), 10.98 (s, CH_2CH_3), 10.5 (s, CH_2CH_3), 10.4 (s, CH_2CH_3), 9.6 (s, 2 × CH_2CH_3), 9.5 (s, 2 × CH_2CH_3). $^{31}P\{^1H\}$ NMR (THF-d_8, 25 °C): δ 218.8 (d, $^2J_{PP}$ = 458 Hz), 18.9 (d, $^2J_{PP}$ = 458 Hz). Anal. Calcd for $C_{65}H_{102}ClIrKNO_6P_2$: C, 59.04; H, 7.78; N, 1.06. Found: C, 58.64; H, 8.00; N, 1.22.

Reactions of Eind-PPEP* Complexes with Ammonia. A THF-d_8 solution (0.3 mL) of K[N(SiMe$_3$)$_2$] (2.0 mg, 0.010 mmol) was added to a THF-d_8 solution (0.3 mL) of **10** (9.3 mg, 0.010 mmol) at room temperature in an NMR sample tube. The color of the solution instantly

changed from dark red to dark greenish brown. After 30 min at room temperature, the complete conversion of **10** to K[**12**] was confirmed by ^{1}H and ^{31}P{^{1}H} NMR analysis. The resulting solution was degassed by freeze-pump-thaw cycles (3 times), and charged with an anhydrous NH_3 gas (1 atm). The solution color changed to reddish brown. Volatile materials were removed under reduced pressure, and the residue was dissolved in hexane (1 mL) and filtered through a glass fiber filter to remove KCl. The filtrate was concentrated to dryness under reduced pressure to give a reddish brown crystalline solid of [Rh(NH_3)(Eind-PPEP*)] (**14**) (9.0 mg, 98 %). Complex **14** was gradually degraded upon drying under reduced pressure, probably due to dissociation of the ammine ligand. Therefore, the complex did not give a satisfactory elemental analysis, and its composition was confirmed by HRMS analysis and NMR spectroscopy.

Complex K[**13**] was similarly prepared from **11** and K[N($SiMe_3$)$_2$] in THF-d_8, and treated with NH_3 (1 atm) at room temperature. The reaction was instantly completed, and [Ir(NH_2)(Eind-PPEP)] (**15**) was isolated a dark green crystalline solid (99 %).

[14]: ^{1}H NMR (THF-d_8, 25 °C): δ 7.64 (dd, $^{2}J_{PH}$ = 17.4 Hz, $^{3}J_{RhH}$ = 2.9 Hz, 1H, EindP=C*H*), 7.38 (dd, $^{4}J_{PH}$ = 4.1 Hz, $^{4}J_{HH}$ = 1.8 Hz, 1H, Ar), 7.18 (d, $^{4}J_{HH}$ = 1.8 Hz, 1H, Ar), 6.85 (s, 1H, *p*-Eind), 6.04 (m, 1H, Py), 5.91 (dd, $^{3}J_{HH}$ = 8.2 Hz, $^{4}J_{PH}$ = 4.7 Hz, 1H, Py), 5.49 (t, $^{3}J_{HH}$ = 5.7 Hz, $^{4}J_{PH}$ = 5.7 Hz, 1H, Py), 3.48 (br d, $^{2}J_{PH}$ = 3.9 Hz, 1H, Py=C*H*P), 2.89–2.80 (m, 1H, CH_2CH$_3$), 2.68–2.58 (m, 1H, CH_2CH$_3$), 2.34–2.23 (m, 4H, CH_2CH$_3$), 2.13 (br, 3H, NH_3), 2.09–2.01 (m, 3H, PCH_2 + CH_2CH$_3$), 1.89 (br s, 4H, CH_2), 1.79 (s, 9H, C(CH_3)$_3$), 1.78 (dd, $^{1}J_{HH}$ = 13.8 Hz, $^{2}J_{PH}$ = 4.6 Hz, 1H, PCH_2), 1.70–1.49 (m, 8H, CH_2CH$_3$), 1.42 (s, 3H, CH_3), 1.39 (s, 3H, CH_3), 1.32 (s, 9H, C(CH_3)$_3$), 0.91 (t, $^{3}J_{HH}$ = 7.2 Hz, 6H, CH$_2$CH_3), 0.85 (t, $^{3}J_{HH}$ = 7.2 Hz, 12H, CH$_2$CH_3), 0.81–0.75 (m, 6H, CH$_2$CH_3). ^{13}C{^{1}H} NMR (THF-d_8, 25 °C): δ 173.6 (dd, J_{PC} = 24 Hz, J_{RhC} = 3 Hz), 162.8 (br d, J_{PC} = 10 Hz), 159.5 (dd, J_{PC} = 12 and 4 Hz), 156.3 (d, $^{1}J_{PC}$ = 37 Hz, EindP=*C*H), 154.0 (d, J_{PC} = 10 Hz), 152.7 (s), 152.3 (d, J_{PC} = 1 Hz), 152.0 (s), 150.6 (d, J_{PC} = 5 Hz), 150.5 (d, J_{PC} = 5 Hz), 134.4 (br d, J_{PC} = 30 Hz), 130.9 (vt, J_{app} = 5 Hz), 130.2–129.8 (m), 123.0 (d, $^{3}J_{PC}$ = 7 Hz, Ar), 122.2 (s, *p*-Eind), 118.7 (d, $^{3}J_{PC}$ = 7 Hz, Ar), 113.4 (dd, J_{PC} = 21 and 12 Hz), 103.5 (d, J_{PC} = 33 Hz), 74.0 (d, $^{1}J_{PC}$ = 54 Hz, Py=*C*HP), 54.4 (s), 54.3 (s), 48.59 (s), 48.57 (s), 44.2–44.1 (m), 43.4 (s, *C*H$_2$), 43.3 (d, $^{1}J_{PC}$ = 28 Hz, P*C*H$_2$), 43.2 (s, *C*H$_2$), 38.5 (s), 35.5 (s), 35.0 (s, *C*H$_2$CH$_3$), 34.7 (s, *C*H$_2$CH$_3$), 34.1 (s, 2 × *C*H$_2$CH$_3$),

33.9 (d, $^4J_{PC}$ = 4 Hz, CH_2CH_3), 33.7 (d, $^4J_{PC}$ = 3 Hz, $C(CH_3)_3$), 33.5 (d, $^4J_{PC}$ = 4 Hz, CH_2CH_3), 33.4 (s, CH_3), 33.18 (s, CH_2CH_3), 33.15 (s, CH_2CH_3), 32.1 (d, $^3J_{PC}$ = 8 Hz, CH_3), 31.7 (s, $C(CH_3)_3$), 10.7 (s, CH_2CH_3), 10.31 (s, CH_2CH_3), 10.25 (s, CH_2CH_3), 10.2 (s, CH_2CH_3), 9.5 (s, 2 × CH_2CH_3), 9.4 (s, 2 × CH_2CH_3). $^{31}P\{^1H\}$ NMR (THF-d_8, 25 °C): δ 215.2 (dd, $^2J_{PP}$ = 368 Hz, $^1J_{RhP}$ = 177 Hz), 16.4 (dd, $^2J_{PP}$ = 368 Hz, $^1J_{RhP}$ = 167 Hz). HRMS (ESI): Calcd for $C_{53}H_{81}N_2P_2Rh$ 910.4925 ($[M]^+$); Found 910.4936.

[15]: ^1H NMR (THF-d_8, 25 ºC): δ 8.72 (dd, $^2J_{PH}$ = 7.5 Hz, $^4J_{PH}$ = 3.4 Hz, 1H, EindP=C*H*), 7.63 (ddd, $^3J_{HH}$ = 8.0 Hz, $^3J_{HH}$ = 6.8 Hz, $^5J_{PH}$ = 3.0 Hz, 1H, Py), 7.45 (dd, $^4J_{PH}$ = 4.5 Hz, $^4J_{HH}$ = 1.6 Hz, 1H, Ar), 7.30 (d, $^4J_{HH}$ = 1.6 Hz, 1H, Ar), 6.95 (s, 1H, *p*-Eind), 6.88 (br d, $^3J_{HH}$ = 8.0 Hz, 1H, Py), 6.69 (br d, $^3J_{HH}$ = 6.8 Hz, 1H, Py), 4.15 (dd, $^2J_{HH}$ = 20.3 Hz, $^2J_{PH}$ = 10.7 Hz, 1H, PyC*H*$_2$P), 4.14 (dd, $^2J_{HH}$ = 20.3 Hz, $^2J_{PH}$ = 10.2 Hz, 1H, PyC*H*$_2$P), 3.95 (br, 2H, N*H*$_2$), 2.98–2.89 (m, 1H, C*H*$_2$CH$_3$), 2.77–2.68 (m, 1H, C*H*$_2$CH$_3$), 2.63 (dd, $^2J_{HH}$ = 15.1 Hz, $^2J_{PH}$ = 4.0 Hz, 1H, PC*H*$_2$), 2.40 (dt, $^2J_{HH}$ = 15.1 Hz, $^2J_{PH}$ = 3.7 Hz, 1H, PC*H*$_2$), 2.24–1.93 (m, 6H, C*H*$_2$CH$_3$), 1.90–1.88 (m, 4H, C*H*$_2$), 1.86–1.60 (m, 8H, C*H*$_2$CH$_3$), 1.53 (s, 3H, C*H*$_3$), 1.52 (s, 3H, C*H*$_3$), 1.38 (s, 9H, C(C*H*$_3$)$_3$), 1.36 (s, 9H, C(C*H*$_3$)$_3$), 0.95–0.67 (m, 24H, CH$_2$C*H*$_3$). $^{13}C\{^1H\}$ NMR (THF-d_8, 25 ºC): δ 163.5 (dd, J_{PC} = 6 and 2 Hz), 161.0 (dd, J_{PC} = 7 and 3 Hz), 159.8 (dd, J_{PC} = 14 and 5 Hz), 155.2 (d, J_{PC} = 10 Hz), 154.3 (d, J_{PC} = 2 Hz), 151.0 (s), 150.9 (s), 150.3 (d, J_{PC} = 7 Hz), 150.1 (d, J_{PC} = 7 Hz), 135.1 (d, $^1J_{PC}$ = 43 Hz, EindP=*C*H), 131.1 (d, J_{PC} = 18 Hz), 125.5 (dd, J_{PC} = 32 and 5 Hz), 123.7 (d, $^3J_{PC}$ = 8 Hz, Ar), 123.2 (vt, J_{app} = 3 Hz), 122.8 (d, J_{PC} = 25 Hz), 122.6 (d, $^4J_{PC}$ = 2 Hz, *p*-Eind), 119.1 (d, $^3J_{PC}$ = 8 Hz, Ar), 113.3 (dd, J_{PC} = 13 and 4 Hz), 54.7 (s), 54.6 (s), 50.0 (d, $^1J_{PC}$ = 29 Hz, Py*C*H$_2$P), 48.35 (s), 48.34 (s), 44.0 (t, J_{PC} = 4 Hz), 43.6 (s, *C*H$_2$), 43.4 (s, *C*H$_2$), 43.2 (d, $^1J_{PC}$ = 34 Hz, P*C*H$_2$), 38.2 (s), 35.7 (s), 34.3 (s, *C*H$_2$CH$_3$), 34.23 (s, *C*H$_2$CH$_3$), 34.15 (s, *C*H$_2$CH$_3$), 34.07 (s, *C*H$_2$CH$_3$), 33.7 (s, *C*H$_3$), 33.2 (s, *C*H$_2$CH$_3$), 33.14 (s, *C*H$_2$CH$_3$), 33.06 (d, $^4J_{PC}$ = 2 Hz, C(*C*H$_3$)$_3$), 32.3 (s, *C*H$_2$CH$_3$), 32.2 (s, *C*H$_2$CH$_3$), 31.6 (s, C(*C*H$_3$)$_3$), 31.5 (s, *C*H$_3$), 10.5 (s, CH$_2$*C*H$_3$), 10.43 (s, CH$_2$*C*H$_3$), 10.37 (s, CH$_2$*C*H$_3$), 10.3 (s, CH$_2$*C*H$_3$), 9.52 (s, 2 × CH$_2$*C*H$_3$), 9.49 (s, 2 × CH$_2$*C*H$_3$). $^{31}P\{^1H\}$ NMR (THF-d_8, 25 ºC): δ 173.6 (d, $^2J_{PP}$ = 468 Hz), 26.4 (d, $^2J_{PP}$ = 468 Hz). Anal. Calcd for $C_{53}H_{81}N_2P_2Ir$: C, 63.63; H, 8.16; N, 2.80. Found: C, 63.35; H, 8.24; N, 2.55.

X-Ray Crystal Structure Determination. The intensity data were collected at 103 K on a Rigaku Saturn70 CCD diffractometer with the VariMax Optic, using Mo Ka radiation (*l* =

0.71075 Å). The intensity data were corrected for Lorentz and polarization effects and for absorption (multi-scan[12]). The structures were solved by direct methods (SHELXS-97)[13] and refined by least-squares calculations on F^2 for all reflections (SHELXL-97),[13] using Yadokari-XG 2009.[14] Non-hydrogen atoms were refined anisotropically. Hydrogen atoms were placed at calculated positions, and included in calculation without refinement of their parameters. The crystallographic data and the summary of solution and refinement are listed in Table 1 and 2.

Computational Details. DFT calculations were carried out by using the Gaussian 09 program.[15] The author adopted the B3LYP-D functional, which is the B3LYP hybrid functional[16] combined with an empirical dispersion correction developed by Grimme.[17] For optimization, the author chose the SDD for Ir and Rh and 6-31G(d) for the other atoms as basis sets, respectively.[18] Systematic vibrational analyses were carried out for all complexes to characterize stationary-point structures. To determine the energy differences, the author performed single-point calculations at the optimized geometries using the 6-311+G(d,p) basis set instead of the 6-31G(d) basis set. Solvation effects (THF) were taken into account by using the polarizable continuum model (PCM).[19] Thermal corrections at 298.15 K were applied for evaluating the free energy changes (ΔG_{298}). The optimized structures of **14** and **15** in Scheme 4 are given in Figure 3.

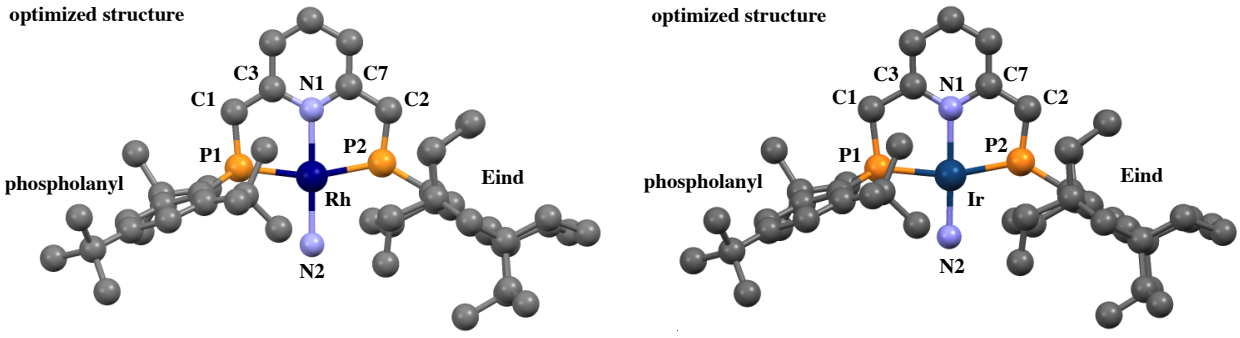

14 **15**

Figure 3. Optimized structures of [Rh(NH_3)(Eind-PPEP*)] (**14**) and [Ir(NH_2)(Eind-PPEP)] (**15**). Hydrogen atoms are omitted for clarity. Selected bond distances (Å) and angles (deg): [**14**] Rh−P1 2.302, Rh−P2 2.231, Rh−N1 2.101, Rh–N2 2.149, P1−C1 1.758, P2−C2 1.681, C1−C3 1.394, C2−C7 1.451, P1−Rh−P2 162.28, N1−Rh−N2 178.81; [**15**] Ir−P1 2.265, Ir−P2 2.237, Ir−N1 2.116, Ir–N2 1.970, P1−C1 1.870, P2−C2 1.697, C1−C3 1.512, C2−C7 1.422, P1−Ir−P2 162.75, N1−Ir−N2 177.15.

Table 1. Crystal Data and Details of Structure Determination for **8** and **9**

complex	**8**	**9**
empirical formula	$C_{53}H_{79}ClNP_2Rh$	$C_{53}H_{79}ClIrNP_2$
formula weight	930.47	1019.76
T (K)	103(2)	103(2)
crystal system	Orthorhombic	Orthorhombic
space group	$P2_12_12_1$	$P2_12_12_1$
a (Å)	14.904(4)	14.9689(18)
b (Å)	17.034(5)	16.995(2)
c (Å)	19.351(6)	19.372(2)
α (°)	90	90
β (°)	90	90
γ (°)	90	90
V (Å^3)	4913(3)	4928.4(10)
Z	4	4
d_{calc} (g/cm^3)	1.258	1.374
μ(Mo Ka) (mm^{-1})	0.502	2.863
F(000)	1984	2112
crystal size	0.10 × 0.01 × 0.01	0.14 × 0.10 × 0.06
θ range (°)	1.59 to 24.50	2.10 to 27.50
reflections collected	39728	50475
independent reflections (R_{int})	8182 (0.1482)	11301 (0.0183)
absorption correction	multi-scan	multi-scan
max. and min. transmission	0.9950 and 0.9515	1.0000 and 0.9386
data / restraints / parameters	8182 / 0 / 540	11301 / 0 / 540
GOF on F^2	1.072	1.074
$R1$, $wR2$ [$I > 2\sigma(I)$]	0.0796, 0.1918	0.0198, 0.0440
$R1$, $wR2$ (all data)	0.1108, 0.2333	0.0211, 0.0591
absolute structure parameter	0.04(6)	–0.017(4)
largest peak and hole (e Å^3)	2.043 and –0.984	1.506 and –0.437

Table 2. Crystal Data and Details of Structure Determination for [K(18C6)][**12**] and [K(18C6)][**13**]

complex	[K(18C6)][**12**]	[K(18C6)][**13**]
empirical formula	$C_{65}H_{102}ClKNO_6P_2Rh$	$C_{65}H_{102}ClIrKNO_6P_2$
formula weight	1232.88	1322.17
T (K)	103(2)	103(2)
crystal system	Monoclinic	Monoclinic
space group	$P2_1/c$	$P2_1/c$
a (Å)	12.1391(13)	12.222(3)
b (Å)	29.372(3)	29.346(8)
c (Å)	18.861(2)	18.875(5)
α (°)	90	90
β (°)	104.2756(14)	104.227(3)
γ (°)	90	90
V (Å^3)	6517.2(12)	6562(3)
Z	4	4
d_{calc} (g/cm^3)	1.257	1.338
μ(Mo Ka) (mm^{-1})	0.464	2.235
F(000)	2632	2760
crystal size	0.19 × 0.07 × 0.05	0.11 × 0.05 × 0.01
θ range (°)	1.73 to 27.50	1.72 to 25.00
reflections collected	78774	54836
independent reflections (R_{int})	14941 (0.0477)	11540 (0.0929)
absorption correction	multi-scan	multi-scan
max. and min. transmission	0.9772 and 0.9170	1.0000 and 0.7957
data / restraints / parameters	14941 / 0 / 710	11540 / 0 / 710
GOF on F^2	1.160	1.159
$R1$, $wR2$ [$I > 2\sigma(I)$]	0.0474, 0.1190	0.0511, 0.1183
$R1$, $wR2$ (all data)	0.0570, 0.1321	0.0692, 0.1404
largest peak and hole (e Å^3)	1.387 and –1.117	1.927 and –1.179

References and Notes

(1) (a) Dugal-Tessier, J.; Conrad, E. D.; Dake, G. R.; Gates, D. P. In *Phosphorus (III) Ligands in Homogeneous Catalysis: Design and Synthesis*; Kamer, P. C. J., van Leeuwen, P. W. N. M., Eds.; Wiley: Chichester, U.K., 2012; Chapter 10. (b) Ozawa, F.; Kawagishi, S.; Ishiyama, T.; Yoshifuji, M. *Organometallics* **2004**, *23*, 1325–1332. (c) Le Floch, P. *Coord. Chem. Rev.* **2006**, *250*, 627–681. (d) Müller, C.; Pidko, E. A.; Lutz, M.; Spek, A. L.; Vogt, D. *Chem. A Eur. J.* **2008**, *14*, 8803–8807.

(2) (a) Ozawa, F.; Yoshifuji, M. *Dalton Trans.* **2006**, 4987–4995. (b) Ozawa, F. *J. Synth. Org. Chem. Jpn.* **2009**, *67*, 529–539.

(3) For recent examples, see: (a) Nakajima, Y.; Nakao, Y.; Sakaki, S.; Tamada, Y.; Ono, T.; Ozawa, F. *J. Am. Chem. Soc.* **2010**, *132*, 9934–9936. (b) Nakajima, Y.; Shiraishi, Y.; Tsuchimoto, T.; Ozawa, F. *Chem. Commun.* **2011**, *47*, 6332–6334. (c) Chang, Y.-H.; Nakajima, Y.; Ozawa, F. *Organometallics* **2013**, *32*, 2210–2215. (d) Chang, Y.-H.; Nakajima, Y.; Tanaka, H.; Yoshizawa, K.; Ozawa, F. *J. Am. Chem. Soc.* **2013**, *135*, 11791–11794. (e) Chang, Y.-H.; Nakajima, Y.; Tanaka, H.; Yoshizawa, K.; Ozawa, F. *Organometallics* **2014**, *33*, 715–721. (f) Taguchi, H.; Chang, Y.-H.; Takeuchi, K.; Ozawa, F. *Organometallics* **2015**, *34*, 1589–1596. (g) Chang, Y.-H.; Takeuchi, K.; Wakioka, M.; Ozawa, F. *Organometallics* **2015**, *34*, 1957–1962. (h) Chang, Y.-H.; Tanigawa, I.; Taguchi, H.; Takeuchi, K.; Ozawa, F. *Eur. J. Inorg. Chem.* **2016**, 754–760.

(4) For related studies on phosphaalkene complexes, see: (a) Jouaiti, A.; Geoffroy, M.; Bernardinelli, G. *Tetrahedron Lett.* **1992**, *33*, 5071–5074. (b) Daugulis, O.; Brookhart, M.; White, P. S. *Organometallics* **2002**, *21*, 5935–5943. (c) Ionkin, A. S.; Marshall, W. J. *Heteroat. Chem.* **2002**, *13*, 662–666. (d) Dugal-Tessier, J.; Dake, G. R.; Gate, D. P. *Organometallics* **2007**, *26*, 6481–6486. (e) Orthaber, A.; Belaj, F.; Pietschnig, R. *Inorg. Chim. Acta* **2011**, *374*, 211–215. (f) Ito, S.; Nanko, M.; Mikami, K. *ChemCatChem*, **2014**, 6, 2292–2297.

(5) For recent reviews, see: (a) Gunanathan, C.; Milstein, D. In *Pincer and Pincer-Type Complexes: Application in Organic Synthesis and Catalysis*; Szabó, K. J., Wendt, O. F., Eds.; Wiley-VCH: Weineim, Germany, 2014, Chapter I. (b) Zell, T.; Milstein, D. *Acc. Chem. Res.* **2015**, *48*, 1979–1994. (c) Gunanathan, C.; Milstein, D. *Chem. Rev.* **2014**, *114*, 12024–12087.

(d) Khusnutdinova, J. R.; Milstein, D. *Angew. Chem., Int. Ed.* **2015**, *54*, 12236–12273.

(6) (a) Tsang, C.; Rohrick, C. A.; Saini, T. S.; Patrick, B. O.; Gates, D. P. *Organometallics* **2002**, *21*, 1008–1010. (b) Houdard, R.; Mézailles, N.; Le Goff, X.-F.; Le Floch, P. *Organometallics* **2009**, *28*, 5952–5959.

(7) (a) Matsuo, T.; Tamao, K. *C. R. Chimie* **2010**, *13*, 1104–1110. (b) Matsuo, T.; Tamao, K. *Bull. Chem. Soc. Jpn.* **2015**, *88*, 1201–1220. (c) Matsuo, T.; Suzuki, K.; Fukawa, T.; Li, B.; Ito, M.; Shoji, Y.; Otani, T.; Li, L.; Kobayashi, M.; Hachiya, M.; Tahara, Y.; Hashizume, D.; Fukunaga, T.; Fukazawa, A.; Li, Y.; Tsuji, H.; Tamao, K. *Bull. Chem. Soc. Jpn.* **2011**, *84*, 1178–1191.

(8) (a) Jouaiti, A.; Geoffroy, M.; Bernardinelli, G. *Tetrahedron Lett.* **1992**, *33*, 5071–5074. (b) Yam, M.; Chong, J. H.; Tsang, C.-W.; Patrick, B. O.; Lam, A. E.; Gates, D. P. *Inorg. Chem.* **2006**, *45*, 5225–5234.

(9) Shah, S.; Protasiewicz, J. D. *Chem. Commun.* **1998**, *3*, 1585–1586.

(10) Li, B.; Tsujimoto, S.; Li, Y.; Tsuji, H.; Tamao, K.; Hashizume, D.; Matsuo, T. *Heteroat. Chem.* **2014**, *25*, 612–618.

(11) Hayashi, A.; Okazaki, M.; Ozawa, F.; Tanaka, R. *Organometallics* **2007**, *26*, 5246–5249.

(12) Blessing, R. H. *Acta Crystallogr., Sect. A* **1995**, *51*, 33–38.

(13) Sheldrick, G. M. *SHELXL-97*, University of Göttingen, Germany, 1997.

(14) Kabuto, C.; Akine, S.; Kwon, E. *J. Crystallogr. Soc. Jpn.* **2009**, *51*, 218–224.

(15) Frisch, M. J.; Trucks, G. W.; Schlegel, H. B.; Scuseria, G. E.; Robb, M. A.; Cheeseman, J. R.; Scalmani, G.; Barone, V.; Mennucci, B.; Petersson, G. A.; Nakatsuji, H.; Caricato, M.; Li, X.; Hratchian, H. P.; Izmaylov, A. F.; Bloino, J.; Zheng, G.; Sonnenberg, J. L.; Hada, M.; Ehara, M.; Toyota, K.; Fukuda, R.; Hasegawa, J.; Ishida, M.; Nakajima, T.; Honda, Y.; Kitao, O.; Nakai, H.; Vreven, T.; Montgomery, J. A., Jr.; Peralta, J. E.; Ogliaro, F.; Bearpark, M.; Heyd, J. J.; Brothers, E.; Kudin, K. N.; Staroverov, V. N.; Kobayashi, R.; Normand, J.; Raghavachari, K.; Rendell, A.; Burant, J. C.; Iyengar, S. S.; Tomasi, J.; Cossi, M.; Rega, N.; Millam, J. M.; Klene, M.; Knox, J. E.; Cross, J. B.; Bakken, V.; Adamo, C.; Jaramillo, J.; Gomperts, R.; Stratmann, R. E.; Yazyev, O.; Austin, A. J.; Cammi, R.; Pomelli, C.; Ochterski, J. W.; Martin, R. L.; Morokuma, K.; Zakrzewski, V. G.; Voth, G. A.; Salvador,

P.; Dannenberg, J. J.; Dapprich, S.; Daniels, A. D.; Farkas, Ö.; Foresman, J. B.; Ortiz, J. V.; Cioslowski, J.; Fox, D. J. Gaussian 09, Revision C.01, Gaussian, Inc., Wallingford CT, 2009.

(16) (a) Becke, A. D. *Phys. Rev. A* **1988**, *38*, 3098–3100. (b) Becke, A. D. *J. Chem. Phys.* **1993**, *98*, 5648–5652. (c) Lee, C.; Yang, W.; Parr, R. G. *Phys. Rev. B* **1988**, *37*, 785–789. (d) Stephens, P. J.; Devlin, F. J.; Chabalowski, C. F.; Frisch, M. J. *J. Phys. Chem.* **1994**, *98*, 11623–11627.

(17) Grimme, S. *J. Comput. Chem.* **2006**, *27*, 1787–1799.

(18) (a) Ditchfield, R.; Hehre, W. J.; Pople, J. A. *J. Chem. Phys.* **1971**, *54*, 724–728. (b) Hehre, W. J.; Ditchfield, R.; Pople, J. A. *J. Chem. Phys.* **1972**, *56*, 2257–2261. (c) Hariharan, P. C.; Pople, J. A. *Theor. Chim. Acta* **1973**, *28*, 213–222. (d) Clark, T.; Chandrasekhar, J.; Spitznagel, G. W.; Schleyer, P. V. R. *J. Comput. Chem.* **1983**, *4*, 294–301. (e) Francl, M. M.; Petro, W. J.; Hehre, W. J.; Binkley, J. S.; Gordon, M. S.; DeFrees, D. J.; Pople, J. A. *J. Chem. Phys.* **1982**, *77*, 3654–3665. (f) Andrae, D.; Häußermann, U.; Dolg, M.; Stoll, H.; Preuß, H. *Theor. Chim. Acta* **1990**, *77*, 123–141.

(19) Tomasi, J. ; Mennucci, B.; Cammi, R. *Chem. Rev.* **2005**, *105*, 2999–3094.

Chapter 3

Unsymmetrical PNP-Pincer Type Phosphaalkene Complexes of Group 9 Metals: Catalytic Application to Hydrosilylation of Carbon Dioxide

Abstract

The complexes [K(18-crown-6)][IrCl(PPEP*)] (**1**) and [K(18-crown-6)][IrCl(Eind-PPEP*)] (**2**), and [K(18-crown-6)][RhCl(Eind-PPEP*)] (**3**) bearing noninnocent PNP-pincer type phosphaalkene ligands (PPEP* and Eind-PPEP*) efficiently catalyze hydrosilylation of CO_2 (1 atm) with $HSiMe_2Ph$ to give HCO_2SiMe_2Ph. The turnover number reaches 3100 at room temperature and 5100 at 40 °C in the presence of 0.01 mol% of **1**. This catalysis is applied to one-pot synthesis of formamides in high yields. A novel catalytic process involving non-innocent behavior of the PPEP* ligand is proposed based on experimental and theoretical observations.

Introduction

Metal–ligand cooperative activation of chemical bonds through noninnocent behavior of supporting ligands has proven to be a powerful approach to highly efficient catalysis.[1–4] Milstein *et al.* have demonstrated that pyridine-based pincer ligands act as a particularly useful component in such catalytic systems.[5–7] PNP- and PNN-pincer complexes of group 8 and 9 metals undergo deprotonation at the benzylic position to cause dearomatization of the pyridine ring. The dearomatized complex cleaves a range of H–Y bonds (Y = H, C, N, O, B, Si, etc.) in a heterolytic manner via metal–ligand cooperation accompanied by regeneration of the aromatized pyridine ring, where the metal center and the dearomatized ligand serve as a Lewis acid and a Brønsted base, respectively. This bond activation protocol has been applied to environmentally benign catalytic reactions via dehydrogenation and hydrogenation processes.[6–7]

Recently, Chang *et al.* have documented that the reactivity of a dearomatized PNP-pincer complex of Ir(I) toward metal–ligand cooperative activation of the N–H bond of NH_3 is dramatically enhanced by introducing a phosphaalkene unit into the pincer scaffold.[8] Phosphaalkenes with a P=C bond possess an extremely low-lying π* orbital, thus serving as a strong π-acceptor toward transition metals.[9] DFT calculations have revealed that this particular ligand property effectively stabilizes five-coordinated intermediates and transition states, leading to instant cleavage of the N–H bond at room temperature.

In this chapter, the author discloses that dearomatized Ir(I) and Rh(I) complexes **1**–**3** in Chart 1, having a PNP-pincer type phosphaalkene ligand with a dearomatized pyridine unit (PPEP* and Eind-PPEP*), serve as highly active catalysts for hydrosilylation of CO_2 (eq 1). Thus far, a variety of molecular catalysts including transition metal complexes have been documented to promote this transformation,[10] but reactions that proceed at ambient temperature under normal pressure of CO_2 have been limited.[11] Complexes **1**–**3** catalyze the conversion of CO_2 and $HSiMe_2Ph$ into HCO_2SiMe_2Ph under these very mild reaction conditions in high yields.

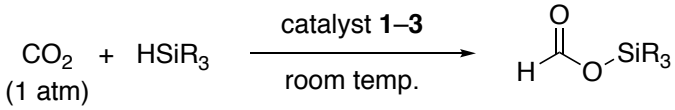

(1)

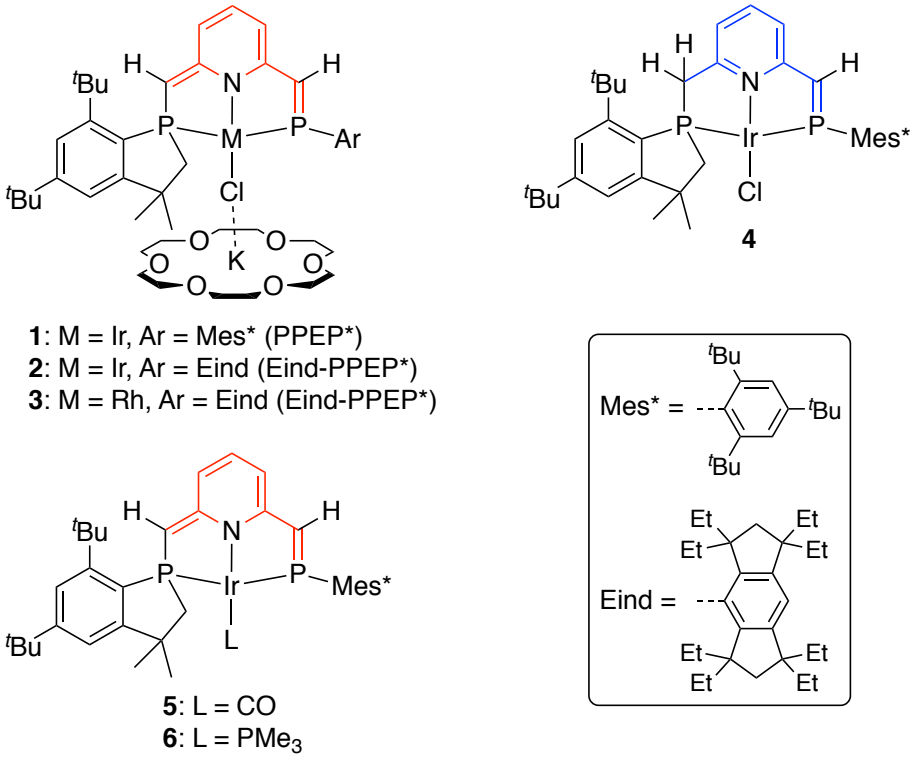

Chart 1. PNP-pincer type phosphaalkene complexes of group 9 metals.

Results and Discussion

First of all, several Ir(I) and Rh(I) complexes listed in Chart 1 were tested as catalysts. All reactions were run in THF at room temperature, using catalyst (1 mol%), hydrosilane ($HSiR_3$) (0.50 mmol), and CO_2 (1 atm). Table 1 summarizes the results. The dearomatized complexes of Ir(I) bearing PPEP* and Eind-PPEP* ligands (**1** and **2**) were highly catalytically active, and converted $HSiMe_2Ph$ into HCO_2SiMe_2Ph in 3 h in almost quantitative yields (entries 1 and 2). The reaction using the Eind-PPEP* complex of Rh(I) (**3**) was not completed in 3 h (62% conversion), but reached completion in 6 h to afford HCO_2SiMe_2Ph in 93% yield (entry 3). In this case, the remaining part of $HSiMe_2Ph$ was converted to $PhMe_2SiOSiMe_2Ph$. In contrast, the aromatized complex of Ir(I) (**4**) was totally inactive, even in the presence of $AgPF_6$ (1 equiv/**4**) (entries 4 and 5). Moreover, complexes **5** and **6** having CO and PMe_3 ligands in place of the Cl^- ligand in **1** were also inactive to the catalytic reaction. As for hydrosilanes, $HSiEt_3$ and $HSiMePh_2$ were less reactive than $HSiMe_2Ph$ (entries 8 and 9), and $HSi(OEt)_3$ and poly(dimethylsiloxane) (PDMS) did not form hydrosilylation products (entries 10 and 11).

Table 1. Catalytic Hydrosilylation of CO_2 in THF using Ir(I) and Rh(I) Complexes [a]

entry	catalyst	$HSiR_3$	time (h)	conv (%) [b]	yield (%) [b]
1	**1**	$HSiMe_2Ph$	3	100	100
2	**2**	$HSiMe_2Ph$	3	100	98
3	**3**	$HSiMe_2Ph$	6	100	93
4	**4**	$HSiMe_2Ph$	3	0	0
5	**4** + $AgPF_6$	$HSiMe_2Ph$	3	0	0
6	**5**	$HSiMe_2Ph$	3	0	0
7	**6**	$HSiMe_2Ph$	3	0	0
8	**1**	$HSiEt_3$	10	81	60
9	**1**	$HSiMePh_2$	10	68	52
10	**1**	$HSi(OEt)_3$	10	47	0
11	**1**	PMHS	10	—	0

[a] All reactions were run at room temperature in THF (0.5 mL), using catalyst (1 mol%), $HSiR_3$ (0.50 mmol), and CO_2 (1 atm). [b] The conversion of $HSiR_3$ and the yield of HCO_2SiR_3 were determined by ^1H NMR analysis using mesitylene as an internal standard.

Table 2. Catalytic Hydrosilylation of CO_2 with $HSiMe_2Ph$ under Neat Conditions [a]

entry	catalyst	amount (mol%)	time (h) [b]	yield (%) [b]
1	**1**	0.1	7	99
2	**2**	0.1	7	99
3	**3**	0.1	7	27
4	**1**	0.01	24	15
5	**1** + [K(18C6)]Cl	0.01 + 0.1	24	31
6 [c]	**1** + [K(18C6)]Cl	0.01 + 0.1	24	51

[a] Unless otherwise noted, the reactions were run at room temperature under neat conditions, using catalyst (0.1 or 0.01 mol%), $HSiMe_2Ph$ (5.0 mmol), and CO_2 (1 atm). [b] The yield of HCO_2SiMe_2Ph was determined by ^1H NMR analysis using mesitylene as an internal standard. [c] The reaction was run at 40 °C.

The catalytic hydrosilylation of CO_2 with $HSiMe_2Ph$ could be conducted with much lower catalyst loading under neat conditions (Table 2). The reactions using Ir(I) complexes **1** and **2** were completed in 7 h at room temperature using 0.1 mol% of catalyst, to afford the desired product in almost quantitative yields (entries 1 and 2), whereas Rh(I) complex **3** was less reactive (entry 3). The catalytic reaction proceeded even when the amount of **1** was reduced to 0.01 mol% (entry 4). In this case, the addition of [K(18-crown6)]Cl to the system clearly improved the product yield, and the reaction attained the TON of 3100 at room temperature and of 5100 at 40 °C (entries 5 and 6).

Since silyl formates are known to serve as formylating agents for alcohols and amines, the present catalytic hydrosilylation was tested on one-pot synthesis of formamides (Scheme 1). The silyl formate was prepared under the same conditions as entry 1 in Table 2 (step 1), and then reacted with amines (0.5 equiv/$HSiMe_2Ph$) at room temperature without isolation (step 2). For all cases, the full conversion of amines was observed, and the desired products were obtained in high yields. Cyclic and *N*-methyl secondary amines reacted within 3 h, whereas the reactions of dibenzylamine and *N*-methylaniline took 12 h for completion. Primary amines such as benzyl amine and aniline were also formylated smoothly.

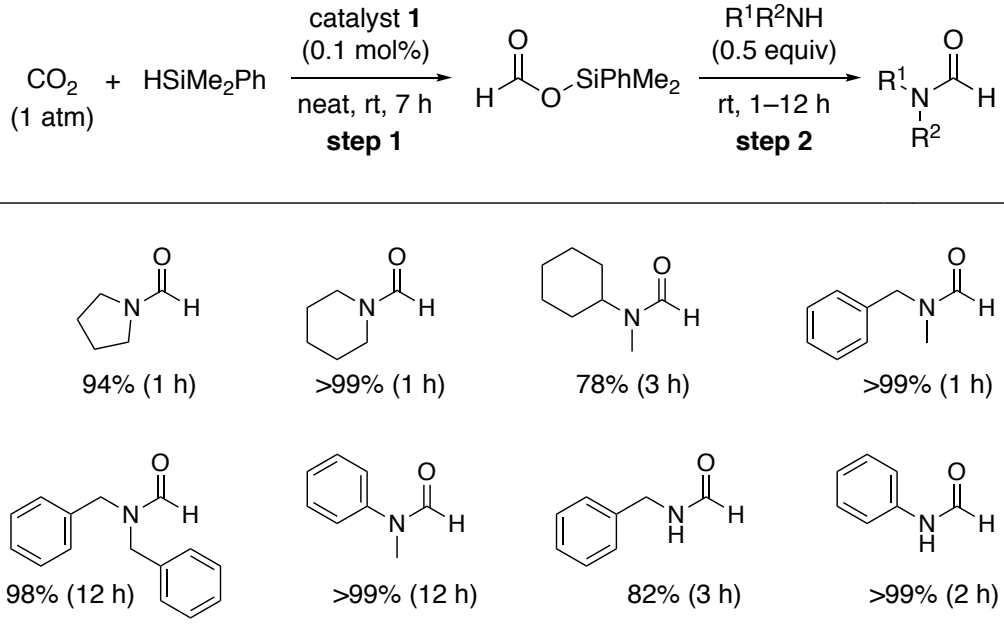

Scheme 1. One-pot synthesis of formamides using catalytic hydrosilylation of CO_2.

Scheme 2 shows a plausible catalytic cycle for hydrosilylation of CO_2 using Ir(I) precursors **1** and **2**, where the phospholanyl group and the aryl substituent at the low-coordinate phosphorus atom (Mes* or Eind) are shown as Ar and PR'$_2$, respectively. This cycle was supported by DFT calculations.

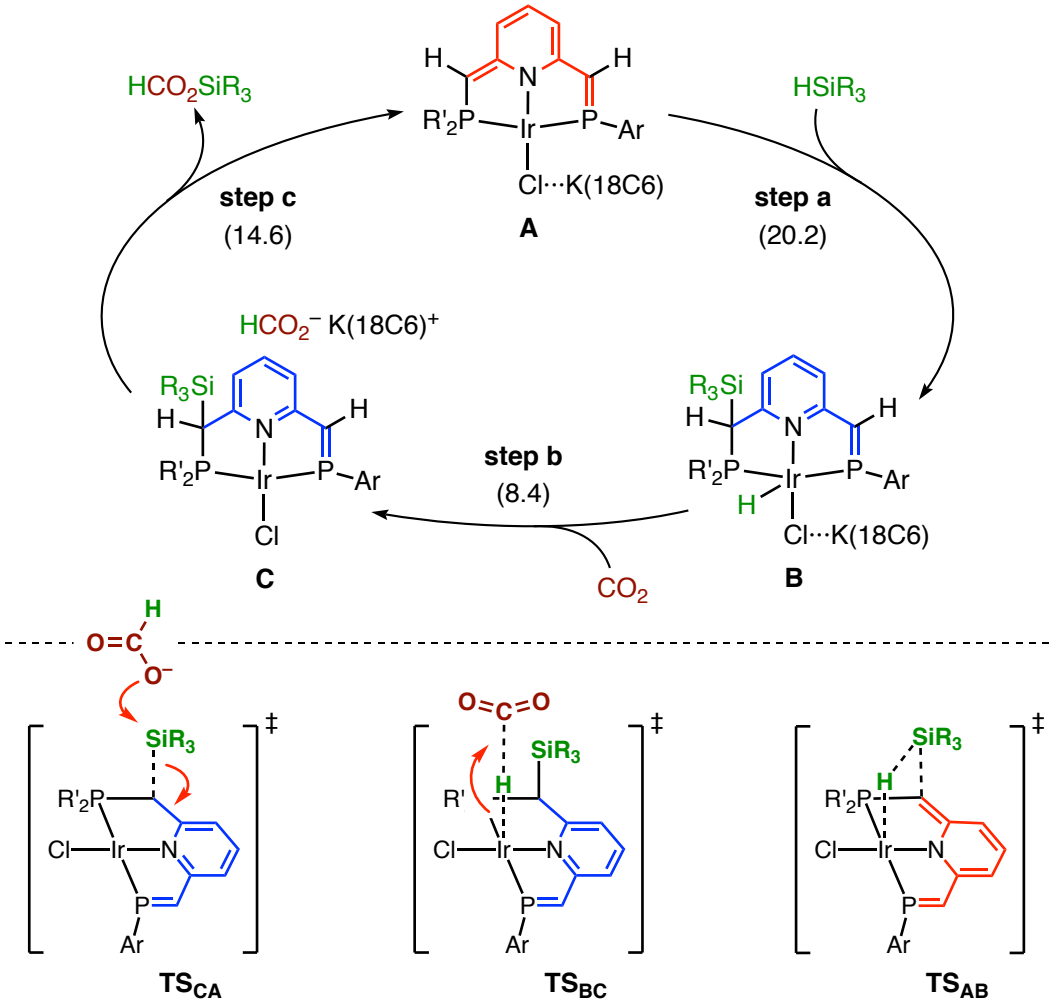

Scheme 2. Plausible catalytic cycle for hydrosilylation of CO_2 promoted by Ir(I) complexes. The values in parentheses are activation barriers ($\Delta G^{\ddagger}$, kcal/mol) for the reaction of CO_2 and $HSiMe_3$ in THF promoted by **1**, estimated by DFT calculations using the B3LYP-D method.

The first step is the metal–ligand cooperative activation of the H–Si bond across the Ir and vinylic carbon atoms in **A**, to form **B** (step a). Then, the hydrido ligand at the apical position of **B** nucleophilically migrates from iridium to the carbon atom of CO_2, to generate a formate

ion (HCO_2^-) and a neutral complex **C** bearing a silyl group at the benzylic position (step b). Finally, the silyl group of **C** undergoes nucleophilic substitution with the formate ion, leading to the elimination of silyl formate and regeneration of **A** (step c). The theoretical activation barriers ($\Delta G^{\ddagger}$), estimated for the reaction of CO_2 and $HSiMe_3$ promoted by **1**, are (a) 20.2, (b) 8.4, and (c) 14.6 kcal/mol, respectively. Thus, the H–Si bond activation (step a) can be identified as the turnover limit for the catalytic cycle, and the relatively small activation energy for this step (20.2 kcal/mol) is consistent with the rapid catalytic reaction at room temperature. Moreover, the small activation energy for step b (8.4 kcal/mol) rationalizes the facile capture of CO_2 under normal pressure.

DFT calculations have indicated that the metal–ligand cooperative activation of the H–Si bond (step a) starts from the coordination of hydrosilane to iridium at the apical position of **A**, to facilitate the subsequent interaction of the silyl group with the vinylic carbon atom. In this case, the coordination of the Cl^- ligand to the equatorial position is the essential requirement to ensure the apical orientation of hydrosilane. A similar situation has been observed for the N–H bond cleavage of ammonia with **1**.[8b] The subsequent attack of the hydrido ligand to CO_2 on **B** occurs at the apical position as well. Thus, the equatorial coordination of the Cl^- ligand is of particular importance for advancing the catalytic hydrosilylation, and we may consider that the catalytic reaction is therefore facilitated by added [K(18-crown6)]Cl when the catalyst concentration is low (entries 5 and 6 in Table 2).

Conclusion

The author found that catalytic hydrosilylation of CO_2 with $HSiMe_2Ph$ easily proceeded at room temperature under normal pressure of CO_2 in the presence of catalytic amounts of dearomatized PNP-pincer type phosphaalkene complexes of Ir(I) and Rh(I). The Ir(I) complex **1** was particularly active, and the TON reached 3100 at room temperature and 5100 at 40 °C. These values are clearly higher than those previously reported for iridium complexes.[10c–f] DFT calculations suggested a catalytic cycle initiated by metal–ligand cooperative activation of the H–Si bond through the noninnocent behavior of the PPEP* ligand. It would be reasonable that the enhanced Lewis acidity of metal centers caused by phosphaalkene units with strong π-accepting ability enhances the catalytic activity to a large extent.

Experimental Section

General Considerations. All manipulations were carried under a nitrogen atmosphere using standard Schlenk techniques and a glove box. Nitrogen gas was dried by passing through a P_2O_5 column (Merck, SICAPENT). THF was dried over sodium/benzophenone and calcium hydride, distilled, and stored over activated MS4A. [K(18-crown-6)][IrCl(PPEP*)] (**1**),[8a] [K(18-crown-6)][IrCl(Eind-PPEP*)] (**2**),[12] [K(18-crown-6)][RhCl(Eind-PPEP*)] (**3**),[12] [IrCl(PPEP)] (**4**),[8a] [Ir(CO)(PPEP*)] (**5**),[8a] [Ir(PMe_3)(PPEP*)] (**6**),[13] and [K(18-crown-6)]Cl[14] were prepared according to the literature. Other chemicals were purchased from commercial sources and used without purification. NMR spectra were recorded on a 400 MHz spectrometer. Chemical shifts are reported in δ (ppm), referenced to ^{1}H (residual) and ^{13}C signals of deuterated solvents as internal standards or to the ^{31}P signal of 85% H_3PO_4 as an external standard. The assignments of ^{13}C signals are based on HMQC experiments. Elemental analysis was performed by ICR Analytical Laboratory, Kyoto University.

General Procedure for Hydrosilylation of CO_2. A typical procedure (Table 1, entry 1) is as follows. Dimethylphenylsilane (77 μL, 0.5 mmol) and THF (0.5 mL) were added to a Schlenk tube containing **1** (5.9 mg, 0.005 mmol). The resulting solution was degassed by freeze-pump-thaw cycles. The Schlenk tube was equipped with CO_2 balloon, and the solution was stirred vigorously at room temperature. After 3 h, dehydrated mesitylene (69 μL, 0.5 mmol) was added as an internal standard, and a portion of the solution was diluted with C_6D_6 and analyzed by ^{1}H NMR to reveal the formation of silyl formate in quantitative yield.

General Procedure for One-Pot Synthesis of formamides. A typical procedure is as follows. Hydrosilylation of CO_2 with $HSiMe_2Ph$ (5.0 mmol) was conducted under the condition of entry 1 in Table 2. Piperidine (0.25 mL, 2.5 mmol) was added dropwise to the resulting solution, and the mixture was stirred at room temperature for 1 h. The yield of *N*-formylpiperidine was determined by ^{1}H NMR analysis using mesitylene as an internal standard.

DFT Calculations. Intermediates and transition structures on potential energy surfaces were searched by using the Gaussian 09 program.[15] The PPEP* ligand as well as [K(18-crown-8)] was treated without any simplification. As a result, the whole system is neutral and the electronic ground state is the closed-shell singlet throughout the reaction. We adopted the

B3LYP-D functional, which is the B3LYP hybrid functional[16a–d] combined with an empirical dispersion correction developed by Grimme.[16e] For optimization the SDD and 6-31G(d) basis sets were chosen for Ir and the other atoms, respectively.[17] Systematic vibrational analyses were carried out for all reaction species to characterize stationary-point structures. An appropriate connection between a reactant and a product for each reaction step was confirmed by intrinsic reaction coordinate (IRC) calculations.[18] Zero-point energy corrections were applied for energy changes (E) and activation energies (E_a) calculated for each reaction step.

References

(1) For reviews on metal–ligand cooperation, see: (a) van der Vlugt, J. I.; Reek, J. N. H. *Angew. Chem., Int. Ed.* **2009**, *48*, 8832–8846. (b) Schneider, S.; Meiners, J.; Askevold, B. *Eur. J. Inorg. Chem.* **2012**, 412–429. (c) van der Vlugt, J. I. *Eur. J. Inorg. Chem.* **2012**, 363–375. (d) Annibale, V. T.; Song, D. *RSC Adv.* **2013**, *3*, 11432–11449. (e) Gunanathan, C.; Milstein, D. *Chem. Rev.* **2014**, *114*, 12024–12087. (f) Khusnutdinova, J. R.; Milstein, D. *Angew. Chem., Int. Ed.* **2015**, *54*, 12236–12273. (g) Li, H.; Zheng, B.; Huang, K.-W. *Coord. Chem. Rev.* **2015**, *293–294*, 116–138.

(2) For related studies on Shvo's catalyst, see: (a) Blum, Y.; Czarkie, D.; Rahamim, Y.; Shvo, Y. *Organometallics* **1985**, *4*, 1459−1461. (b) Tanaka, R.; Yamashita, M.; Nozaki, K. *J. Am. Chem. Soc*. **2009**, *131*, 14168–14169. (c) Conley, B. L.; Pennington-Boggio, M. K.; Boz, E.; Williams, T. J. *Chem. Rev.* **2010**, *110*, 2294–2312. (c) Casey, C. P.; Guan, H. *J. Am. Chem. Soc*. **2007**, *129*, 5816–5817. (d) Casey, C. P.; Guan, H. *J. Am. Chem. Soc*. **2009**, *131*, 2499–2507. (e) Kusumoto, S.; Akiyama, M.; Nozaki, K. *J. Am. Chem. Soc.* **2013**, *135*, 18726–18729. (f) Kusumoto, S.; Nozaki, K. *Nat. Commun.* **2015**, *6*, 6296–6302. (g) Dou, X.; Hayashi, T. *Adv. Synth. Catal.* **2016**, *358*, 1054–1058.

(3) For reviews and papers on Noyori's catalyst, see: (a) Yamakawa, M.; Ito, H.; Noyori, R. *J. Am. Chem. Soc.* **2000**, *122*, 1466–1478. (b) Noyori, R.; Ohkuma, T. *Angew. Chem., Int. Ed.* **2001,** *40*, 40–73. (c) Noyori, R.; Yamakawa, M.; Hashiguchi, S. *J. Org. Chem.* **2001**, *66*, 7931–7944. (d) Ikariya, T.; Murata, K.; Noyori, R. *Org. Biomol. Chem.* **2006**, *4*, 393–406.

(4) For recent papers on non-pyridine-based pincer complexes, see: (a) Rodríguez-Lugo, R. E.; Trincado, M.; Vogt, M.; Tewes, F.; Santiso-Quinones, G.; Grützmacher, H. *Nat. Chem*. **2013**, *5*, 342–347. (b) Rivada-Wheelaghan, O.; Dauth, A.; Leitus, G.; Diskin-Posner, Y.; Milstein, D. *Inorg. Chem*. **2015**, *54*, 4526–4538. (c) Gellrich, U.; Khusnutdinova, J. R.; Leitus, G. M.; Milstein, D. J. *J. Am. Chem. Soc.* **2015**, *137*, 4851–4859. (d) Daw, P; Chakraborty, S; Garg, J.A; Ben-David,Y; Milstein, D. *Angew. Chem., Int. Ed*. **2016**, *55*, 14373–14377. (e) Chakraborty, S.; Gellrich, U.; Diskin-Posner, Y.; Leitus, G.; Avram, L.; Milstein. D. *Angew. Chem., Int. Ed.* **2017**, *56*, 4229–4233.

(5) For recent papers on metal–ligand cooperative cleavage of chemical bonds by pyridine-based pincer complexes, see: (a) Khaskin, E.; Iron, M. A.; Shimon, L. J. W.; Zhang, J.;

Milstein, D. *J. Am. Chem. Soc.* **2010**, *132*, 8542–8543. (b) Vogt, M.; Gargir, M.; Iron, M. A.; Diskin-Posner, Y.; Ben-David, Y.; Milstein, D. *Chem. Eur. J.* **2012**, *18*, 9194–9197. (c) Vogt, M.; Nerush, A.; Diskin-Posner, Y.; Ben-David, Y.; Milstein, D. *Chem. Sci*. **2014**, *5*, 2043–2051. (d) Anaby, A.; Butschke, B.; Ben-David, Y.; Shimon, L. J. W.; Leitus, G.; Feller, M.; Milstein, D. *Organometallics* **2014**, *33*, 3716–3726. (e) Feller, M.; Ben-Ari, E.; Diskin-Posner, Y.; Carmieli, R.; Weiner, L.; Milstein, D. *J. Am. Chem. Soc.* **2015**, *137*, 4634–4637.

(6) For reviews on dehydrogenative or hydrogenative coupling reactions, see: (a) Gunanathan, C.; Ben-David, Y.; Milstein, D. *Science* **2007**, *317*, 790–792. (b) Milstein, D. *Top. Catal.* **2010**, *53*, 915–923. (c) Gunanathan, C.; Milstein, D. *Top. Organomet. Chem.* **2011**, *37*, 55–84. (d) Gunanathan, C.; Milstein, D. *Acc. Chem. Res.* **2011**, *44*, 588–602. (e) Gunanathan, C.; Milstein, D. *Science* **2013**, *341*, 249–260. (f) Balaraman, E.; Milstein, D. *Top. Organomet. Chem.* **2014**, *48*, 19–44. (g) Zell, T.; Milstein, D. *Acc. Chem. Res.* **2015**, *48*, 1979–1994.

(7) For recent papers on dehydrogenative or hydrogenative coupling reactions, see: (a) Kumar, A.; Espinosa-Jalapa, N. A.; Leitus, G. ; Diskin-Posner, Y.; Avram. L. *Angew. Chem., Int. Ed* **2017**, *56*, 14992–14996. (b) Espinosa-Jalapa, N. A.; Kumar, A.; Milstein. D. *J. Am. Chem. Soc.* **2017**, *139*, 11722–11725. (c) Chakraborty, S.; Milstein. D. *ACS Catal*. **2017**, *7*, 3968–3972. (d) Hu, P.; Ben-David, Y.; Milstein, D. *J. Am. Chem. Soc.* **2016**, *138*, 6143−6146. (e) Nerush, A.; Vogt, M.; Gellrich, U.; Leitus, G.; Ben-David, Y.; Milstein, D. *J. Am. Chem. Soc.* **2016**, *138*, 6985–6997. (f) Mukherjee, A.; Nerush, A.; Leitus, G.; Shimon, L. J. W.; Ben David, Y.; Jalapa, N. A. E.; Milstein, D. *J. Am. Chem. Soc.* **2016**, *138*, 4298–4301. (g) Hu, P; Ben-David, Y; Milstein, D. *Angew. Chem., Int. Ed.* **2016**, *55*, 1061–1064.

(8) (a) Chang, Y.-H.; Nakajima, Y.; Tanaka, H.; Yoshizawa, K.; Ozawa, F. *J. Am. Chem. Soc.* **2013**, *135*, 11791−11794. (b) Chang, Y.-H.; Nakajima, Y.; Tanaka, H.; Yoshizawa, K.; Ozawa, F. *Organometallics* **2014**, *33*, 715−721.

(9) (a) Ozawa, F.; Kawagishi, S.; Ishiyama, T. *Organometallics* **2004**, *23*, 1325–1332. (b) Le Floch, P. *Coord. Chem. Rev.* **2006**, *250*, 627–681.

(10) For recent reviews and papers on catalytic hydrosilation of CO_2, see: (a) Fontaine, F.-G.; Stephan, D. W. *Current Opinion in Green and Sustainable Chemistry* **2017**, *3,* 28–32. (b) Fernández-Alvarez, F. J.; Aitani, A. M.; Oro, L. A. *Catal. Sci. Technol.* **2014**, *4*, 611–624. (c)

Lalrempuia, R.; Iglesias, M.; Polo, V.; Miguel, P. J. S.; Fernández-Alvarez, F. J.; Pérez-Torrente, J. J.; Oro, L. A. *Angew. Chem., Int. Ed.* **2012**, *51*, 12824–12827. (d) Oladipo, H. B.; Jaseer, E. A.; Julián, A.; Fernández-Alvarez, F. J.; Al-Khattaf, S.; Oro, L. A. *Journal of CO_2 Utilization* **2015**, *12*, 21–26. (e) Julián, A.; Polo, V.; Jaseer, E. A.; Fernández-Alvarez, F. J.; Oro, L. A. *ChemCatChem* **2015**, *7*, 3895–3902. (f) Julián, A.; Guzmán, J.; Jaseer, E. A.; Fernández-Alvarez, F. J.; Royo, R.; Polo, V.; García-Orduña, P.; Lahoz, F. J.; Oro, L. A. *Chem. Eur. J.* **2017**, *23*, 11898–11907. (g) González-Sebastiaán, L.; Flores-Alamo, M.; García, J. J. *Organometallics* **2013**, *32*, 7186–7194. (h) Motokura, K.; Kashiwame, D.; Takahashi, N.; Miyaji, A.; Baba, T. *Chem. Eur. J.* **2013**, *19*, 10030–10037. (i) Motokura, K.; Kashiwame, D.; Miyaji, A.; Baba, T. *Org. Lett.* **2012**, *14*, 2642–2645. (j) Sattler, W.; Parkin, G. *J. Am. Chem. Soc.* **2012**, *134*, 17462–17465. (k) Ríos, P.; Díez, J.; López-Serrano, J.; Rodríguez, A.; Conejero, S. *Chem. Eur. J.* **2016**, *22*, 16791–16795. (l) Itagaki, S.; Yamaguchi, K.; Mizuno, N. *J. Mol. Catal. A: Chem.* **2013**, *366*, 347–352. (m) Mukherjee, D.; Sauer, D. F.; Zanardi, A.; Okuda, J. *Chem. Eur. J.* **2016**, *22*, 7730–7733. (n) Motokura, K.; Naijo, M; Yamaguchi, S.; Miyaji, A.; Baba, T. *Chem. Lett.* **2015**, *44*, 1217–1219.

(11) For examples of CO_2 hydrosilylation at ambient temperature under normal pressure of CO_2, see: (a) Riduan, S. N.; Zhang, Y.; Ying, J. Y. *Angew. Chem., Int. Ed.* **2009**, *48*, 3322–3325. (b) Zhou, Q.; Li, Y. *J. Am. Chem. Soc*. **2015**, *137*, 10182–10189. (c) Zhang, L.; Cheng, J.; Hou, Z. *Chem. Commun.* **2013**, *49*, 4782–4784. (d) Scheuermann, M. L.; Semproni, S. P.; Pappas, I.; Chirik, P. J. *Inorg. Chem.* **2014**, *53*, 9463–9465. (e) Taori, V. P.; Bandari, R.; and Buchmeiser. M. R. *Chem. Eur. J.* **2014**, *20*, 3292–3296. (f) Takaya, J.; Iwasawa, N. *J. Am. Chem. Soc.* **2017**, *139*, 6074–6077.

(12) Taguchi, H.; Sasaki, D.; Takeuchi, K.; Tsujimoto, S.; Matsuo, T.; Tanaka, H.; Yoshizawa, K.; Ozawa, F. *Organometallics* **2016**, *35*, 1526–1533

(13) Chang, Y.-H.; Tanigawa, I.; Taguchi, H.; Takeuchi, K.; Ozawa, F. *Eur. J. Inorg. Chem.* **2016**, 754–760.

(14) Wilson, D. C.; Liu, S.; Chen, X.; Meyers, E. A.; Bao, X.; Prosvirin, A. V.; Dunbar, K. R.; Hadad, C. M.; Shore, S. G. *Inorg. Chem*. **2009**, *48*, 5725–5735.

(15) Frisch, M. J.; Trucks, G. W.; Schlegel, H. B.; Scuseria, G. E.; Robb, M. A.; Cheeseman, J. R.; Scalmani, G.; Barone, V.; Mennucci, B.; Petersson, G. A.; Nakatsuji, H.;

Caricato, M.; Li, X.; Hratchian, H. P.; Izmaylov, A. F.; Bloino, J.; Zheng, G.; Sonnenberg, J. L.; Hada, M.; Ehara, M.; Toyota, K.; Fukuda, R.; Hasegawa, J.; Ishida, M.; Nakajima, T.; Honda, Y.; Kitao, O.; Nakai, H.; Vreven, T.; Montgomery, J. A., Jr.; Peralta, J. E.; Ogliaro, F.; Bearpark, M.; Heyd, J. J.; Brothers, E.; Kudin, K. N.; Staroverov, V. N.; Keith, T.; Kobayashi, R.; Normand, J.; Raghavachari, K.; Rendell, A.; Burant, J. C.; Iyengar, S. S.; Tomasi, J.; Cossi, M.; Rega, N.; Millam, J. M.; Klene, M.; Knox, J. E.; Cross, J. B.; Bakken, C. Adamo, J. Jaramillo, V.; Gomperts, R.; Stratmann, R. E.; Yazyev, O.; Austin, A. J.; Cammi, R.; Pomelli, C.; Ochterski, J. W.; Martin, R. L.; Morokuma, K.; Zakrzewski, V. G.; Voth, G. A.; Salvador, P.; Dannenberg, J. J.; Dapprich, S.; Daniels, A. D.; Farkas, O.; Foresman, J. B.; Ortiz, J. V.; Cioslowski, J.; Fox, D. J. *Gaussian 09*, Revision C.01, Gaussian, Inc., Wallingford CT, 2010.

(16) (a) Becke, A. D. *Phys. Rev. A* **1988**, *38*, 3098–3100. (b) Becke, A. D. *J. Chem. Phys.* **1993**, *98*, 5648–5652. (c) Lee, C.; Yang, W.; Parr, R. G. *Phys. Rev. B* **1988**, *37*, 785–789. (d) Stephens, P. J.; Devlin, F. J.; Chabalowski, C. F.; Frisch, M. J. *J. Phys. Chem.* **1994**, *98*, 11623–11627. (e) Grimme, S. *J. Comput. Chem.* **2006**, *27*, 1787–1799.

(17) (a) Ditchfield, R.; Hehre, W. J.; Pople, J. A. *J. Chem. Phys.* **1971**, *54*, 724–728. (b) Hehre, W. J.; Ditchfield, R.; Pople, J. A. *J. Chem. Phys.* **1972**, *56*, 2257–2261. (c) Hariharan, P. C.; Pople, J. A. *Theor. Chim. Acta* **1973**, *28*, 213–222. (d) Clark, T.; Chandrasekhar, J.; Spitznagel, G. W.; Schleyer, P. V. R. *J. Comput. Chem.* **1983**, *4*, 294–301. (e) Francl, M. M.; Petro, W. J.; Hehre, W. J.; Binkley, J. S.; Gordon, M. S.; DeFrees, D. J.; Pople, J. A. *J. Chem. Phys.* **1982**, *77*, 3654–3665. (f) Andrae, D.; Häußermann, U.; Dolg, M.; Stoll, H.; Preuß, H. *Theor. Chim. Acta* **1990**, *77*, 123–141.

(18) (a) Fukui, K. *J. Phys. Chem.* **1970**, *74*, 4161–4163. (b) Fukui, K. *Acc. Chem. Res.* **1981**, *14*, 363–368. (c) Gonzalez, C.; Schlegel, H. B. *J. Phys. Chem.* **1990**, *94*, 5523–5527.

Chapter 4

A Square Planar Complex of Platinum(0)

Abstract

The Pt(0) complex [Pt(PPh_3)($Eind_2$-BPEP)] coordinated with a pyridine-based PNP-pincer type phosphaalkene ligand ($Eind_2$-BPEP) has a highly planar geometry around Pt: Σ(Pt) = 358.6°, τ_4 = 0.11. This coordination geometry is very uncommon for formal d^{10} complexes, and its Pd and Ni homologues with the same ligands adopt distorted tetrahedral geometries. Theoretical treatments on Pt and Pd complexes by DFT calculations reveal that both complexes are M(0) species with nearly ten valence electrons on the metals, whereas their atomic orbital occupancies are evidently different from one another. The Pt complex has a higher occupancy of the atomic 6s orbital because of strong s-d hybridization caused by relativistic effects, thereby adopting a highly planar geometry reflecting the shape and orientation of partially unoccupied d_{x2-y2} orbital.

Introduction

Four-coordinate complexes with a formal d^{10} metal center adopt a tetrahedral geometry in most cases. This is due to the lack of stereochemical preference arising from d^{10} configuration, and the coordination geometry settles in a tetrahedral form to relieve steric repulsion among ligands.[1] On the other hand, except for the cases where crystal packing forces cause a planar arrangement of ligands,[2] there are a few precedents of formal d^{10} complexes that adopt a square planar or distorted square planar geometry even in solution.[3] Most of them are dianionic species with low-coordinate phosphorus ligands such as phosphaalkenes and phosphinines, which possess extremely low-lying π^* orbitals.[4] A Ru(–2) complex of the formula Li_2[Ru(2,2'-biphosphinine)$_2$] is representative, having almost perfect planarity around Ru: Σ(Ru) = 360.5°.[3a] Nevertheless, the Ru center interacts with Li^+ ions at the apical positions, and DFT calculations have revealed that these electrostatic interactions clearly stabilize the planar geometry of [Ru(2,2'-biphosphinine)$_2$]$^{2-}$ unit.[5] Accordingly, the complex may be regarded as a six-coordinate species.

This chapter presents a more distinct example of a square planar complex with formal d^{10} configuration (Scheme 1). The author found that complex **1** bearing a 2,6-bis(phospha-ethenyl)pyridine ligand (Eind$_2$-BPEP) adopts a significantly planar geometry around Pt without ionic interactions at the apical positions. In contrast, the Pd and Ni homologues with the same ligands (**2** and **3**) have distorted tetrahedral structures. The remarkable change in coordination geometry depending on metals was examined by DFT calculations, which revealed a tight connection of the planar structure of **1** with strong hybridization of the atomic 5d and 6s orbitals of Pt due to relativistic effects.

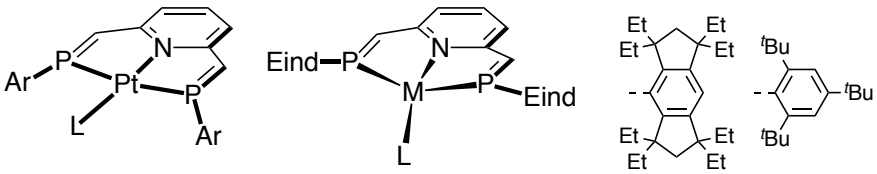

1: Ar = Eind, L = PPh_3 **2**: M = Pd, L = PPh_3
4: Ar = Mes*, L = PCy_3 **3**: M = Ni, L = PPh_3

Eind Mes*

Scheme 1. Eind$_2$-BPEP and BPEP complexes of group 10 metals.

Results and Discussion

Synthesis and Characterization of Complexes 1–3. This study is based on the observations on [Pt(PCy_3)(BPEP)] (**4**, Scheme 1) in Chapter 1;[6] its ^{31}P NMR signal was shifted unexpectedly upfield (δ_P 113.7) compared with other PNP-pincer type phosphaalkene complexes that have been examined in this research group (δ_P 180–260).[7] Although the formation of an unusual structure was indicated, complex **4** having 2,4,6-tri-*tert*-butylphenyl groups (Mes*) as steric protections of the P=C bonds could not be isolated owing to the reactivity of the Mes*-P=CH groups towards C–H addition/cyclization.[6] Thus, the author prepared complex **1** stabilized by fused-ring bulky 1,1,3,3,5,5,7,7-octaethyl-1,2,3,5,6,7-hexahydro-*s*-indacen-4-yl groups (Eind)[8] instead of Mes* groups.

Scheme 2 shows the synthetic route to **1**. $Eind_2$-BPEP was prepared from 2,6-pyridinedicarbaldehyde and Eind-P=PMe_3[9] by a two-step procedure (step a). Treatment of [$Pt(cod)_2$] with $Eind_2$-BPEP and PPh_3 at room temperature afforded the desired complex **1** (step b), which was isolated as green crystals and identified by NMR spectroscopy and elemental analysis. Similarly, the Pd and Ni complexes **2** and **3** were prepared from [Pd(η^5-C_5H_5)(η^3-C_3H_5)] and [$Ni(cod)_2$], respectively.

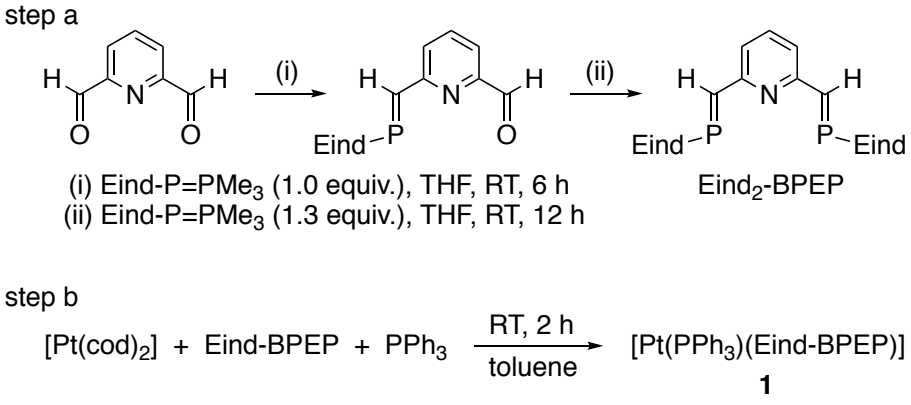

Scheme 2. Synthetic route to complex **1**.

The $^{31}P\{^1H\}$ NMR spectrum of **1** showed two sets of signals at δ_P 105.6 (d, $^2J_{PP}$ = 39 Hz, $^1J_{PtP}$ = 1594 Hz) and 7.0 (t, $^2J_{PP}$ = 39 Hz, $^1J_{PtP}$ = 4249 Hz), assignable to $Eind_2$-BPEP and PPh_3 ligands, respectively. Hence, the remarkable upfield shift of the phosphaalkene signal of

4 was reproduced with **1**. In contrast, the $Eind_2$-BPEP signals of **2** (Pd) and **3** (Ni) were observed in a typical region of phosphaalkene complexes: δ_P 231.4 (**2**) and 224.7 (**3**).

Figure 1 shows the X-ray structures of **1**–**3**.[10] Single crystals of **1** contain two crystallographically independent molecules in the unit cell, and one of them (**1A**) is depicted for simplicity. The most interesting finding about **1** is the significantly planar coordination geometry around Pt: Σ(Pt) = 358.6°, τ_4 = 0.11. On the other hand, **2** (Pd) and **3** (Ni) have distorted tetrahedral geometries: Σ(Pd) = 369.8°, τ_4 = 0.44; Σ(Ni) = 369.6°, τ_4 = 0.40.

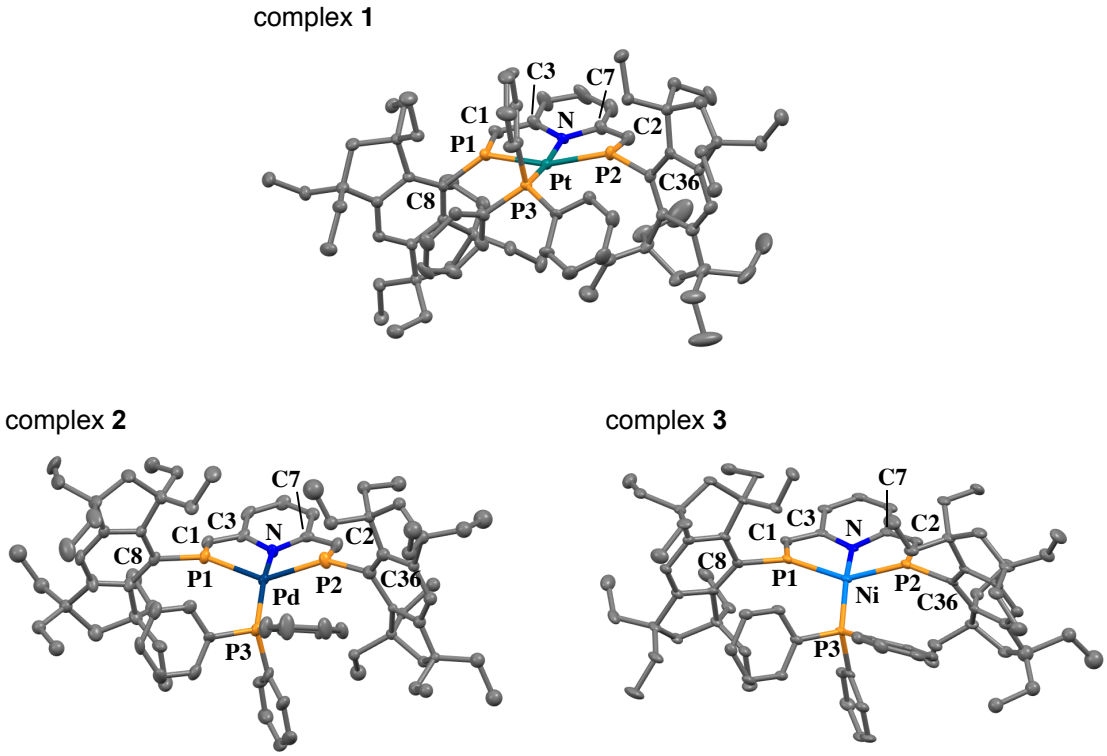

Figure 1. Molecular structures of [M(PPh_3)($Eind_2$-BPEP)] (**1**: M = Pt; **2**: M = Pd; **3**: M = Ni) with 50% probability ellipsoids. Hydrogen atoms, solvent molecules (CH_2Cl_2 for **1**; THF for **2**; Et_2O for **3**), and distorted atoms around Eind groups are omitted for clarity.

Table 1 compares selected bond distances and angles. The difference in coordination geometry is reflected in the N–M–P3 angles, which are bent in **2** (Pd) and **3** (Ni) but linear in **1** (Pt). The P1–C1 and P2–C2 bonds (1.703(6)–1.725(8) Å) are clearly elongated relative to normal P=C bonds (1.66–1.68 Å).[7] As a result, the phosphaalkene units are twisted as can be seen from reduced torsion angles of C8–P1–C1–C3 and C36–P2–C2–C7. This tendency is

Table 1. Selected Bond Distances (Å) and Angles (°) for [M(PPh_3)($Eind_2$-BPEP)] Complexes (**1**: M = Pt; **2**: M = Pd; **3**: M = Ni) [a]

complex	M−P1	M–P2	M–N	M–P3	P1–C1	P2–C2	P1–M–P2	N–M–P3	C8–P1–C1–C3	C36–P2–C2–C7
1A (Pt)	2.324(2)	2.301(2)	2.082(6)	2.270(2)	1.721(8)	1.717(8)	158.70(7)	173.0(2)	148.6(7)	166.8(6)
1B (Pt)	2.325(2)	2.318(2)	2.103(6)	2.274(2)	1.725(8)	1.713(8)	157.62(7)	174.1(2)	152.5(6)	165.6(7)
average	**2.317**		**2.092**	**2.272**	**1.719**		**158.2**	**173.6**		**158.4**
2 (Pd)	2.349(2)	2.341(2)	2.229(5)	2.306(2)	1.703(6)	1.705(6)	141.09(7)	156.1(1)	175.3(5)	175.1(5)
average	**2.345**		**2.229**	**2.306**	**1.704**		**141.1**	**156.1**		**175.2**
3 (Ni)	2.2552(9)	2.2594(9)	2.056(2)	2.232(1)	1.706(3)	1.713(3)	148.26(3)	154.97(6)	175.4(2)	166.1(2)
average	**2.257**		**2.056**	**2.232**	**1.710**		**148.3**	**155.0**		**170.8**

[a] See Figure 1 for the numbering of atoms.

more remarkable for **1** (Pt) than for **2** (Pd) and **3** (Ni), and the P1 and P2 atoms of **1** are significantly pyramidalized: Σ(P) = 341.9–349.9°. It is known that such pyramidalization enhances the s character of lone-pair orbitals and the p character of bonding orbitals, leading to an upfield shift of the ^{31}P NMR signal and a reduction of the $^{1}J_{PtP}$ coupling.[4a]

DFT Calculations. The coordination geometries of **1** (Pt) and **2** (Pd) were successfully reproduced by DFT calculations at the B3LYP-D3 level of theory (Figure 2). The geometry optimization was performed with whole molecules of **1** and **2** (**1**^{sp} and **2**^{dt}). The sums of the four angles around Pt and Pd are 358.0° and 369.2°, respectively, the values of which are almost identical to those observed for the X-ray structures. The P1–M–P2 and N–M–P3 angles also correspond closely with X-ray data: P1–Pt–P2: 154.3° (DFT) and 158.2° (X-ray); N–Pt–P3: 173.6° (DFT) and 173.6° (X-ray); P1–Pd–P2: 141.2° (DFT) and 141.1° (X-ray); N–Pd–P3: 156.1° (DFT) and 156.1° (X-ray). Furthermore, the calculated model of a distorted tetrahedral complex of Pt (**1**^{dt}) was found to be 8.6 kcal/mol less stable than **1**^{sp} with the

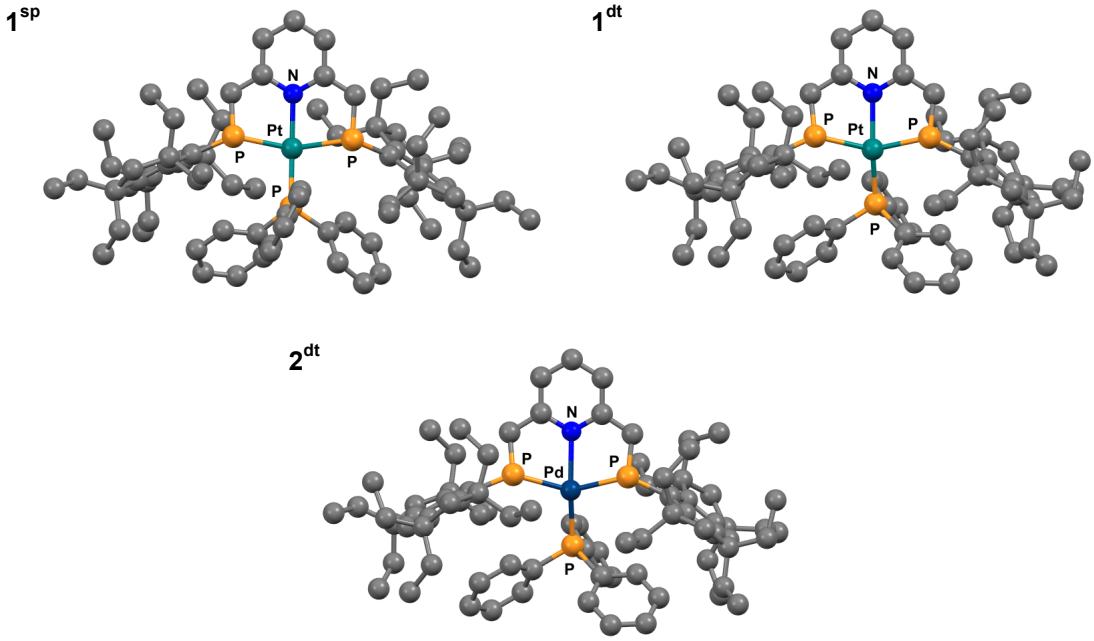

Figure 2. Theoretical structures of **1**^{sp} (square planar), **1**^{dt} (distorted tetrahedral), and **2**^{dt} (distorted tetrahedral). **1**^{sp} and **2**^{dt} are the structures optimized by DFT calculations for full models of **1** and **2**, respectively, whereas **1**^{dt} is an unstable form (+8.6 kcal/mol relative to **1**^{sp}) generated based on the geometry of **2**^{dt}.

square planar geometry. However, since it is difficult to exclude the possibility that steric interactions between bulky substituents affect the coordination geometry, the author next performed DFT calculations for simple models of **1** and **2** (**1**^{sm} and **2**^{sm}), in which Eind groups and PPh_3 ligand were replaced with H atoms and PH_3 ligand, respectively.

Figure 3 shows energy changes of **1**^{sm} and **2**^{sm} as a function of N–M–PH_3 angles, where the molecular geometry at each data point is optimized with a fixed N–M–PH_3 angle. Pt complex **1**^{sm} (●) is effectively stabilized by expanding the N–M–PH_3 angle and attains the minimum at 166.1°. Then the complex becomes somewhat unstable, but the rise in energy remains less than 1.1 kcal/mol even at 180°. Thus, it is reasonable that the Pt complex prefers a planar geometry by nature, and steric requirements arising from bulky substituents further facilitate the planarity. In contrast, the potential energy of Pd complex **2**^{sm} (×) is nearly unchanged up to 165° and thereafter increases to a large extent. This tendency accords with the distorted tetrahedral geometry of **2** (Pd).

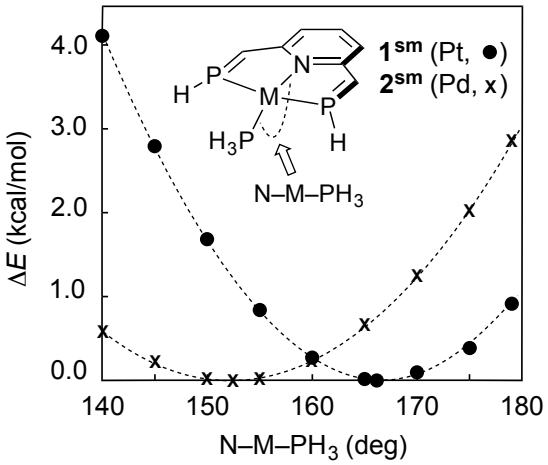

Figure 3. Plots of potential energies (Δ*E* kcal/mol) versus N–M–PH_3 angles (deg) for **1**^{sm} (Pt) and **2**^{sm} (Pd).

Figure 4 compares molecular orbitals (MOs) of **1**^{sp} and **2**^{dt}, which closely resemble each other. The LUMO(+1) corresponds to the σ* orbital generated by an antibonding interaction between M(d_{x2-y2}) and $Eind_2$-BPEP. On the other hand, the LUMO and HOMO are roughly assigned to the out-of-phase and in-phase π* orbitals of $Eind_2$-BPEP ligand, although the HOMO contains orbital components of metals to a certain extent. These MOs are followed by

π orbitals of $Eind_2$-BPEP and the other d orbitals at lower energy levels. A notable feature is a major contribution of the in-phase π* orbital of $Eind_2$-BPEP to the HOMO. A similar situation was previously reported for Li_2[Ru(2,2'-biphosphinine)$_2$] by Le Floch *et al.*[3a] They considered that since two of the ten electrons in formal d^{10} configuration are incorporated into a ligand-centered MO (HOMO), the complex is a d^8 species in reality and therefore adopts a square planar configuration.

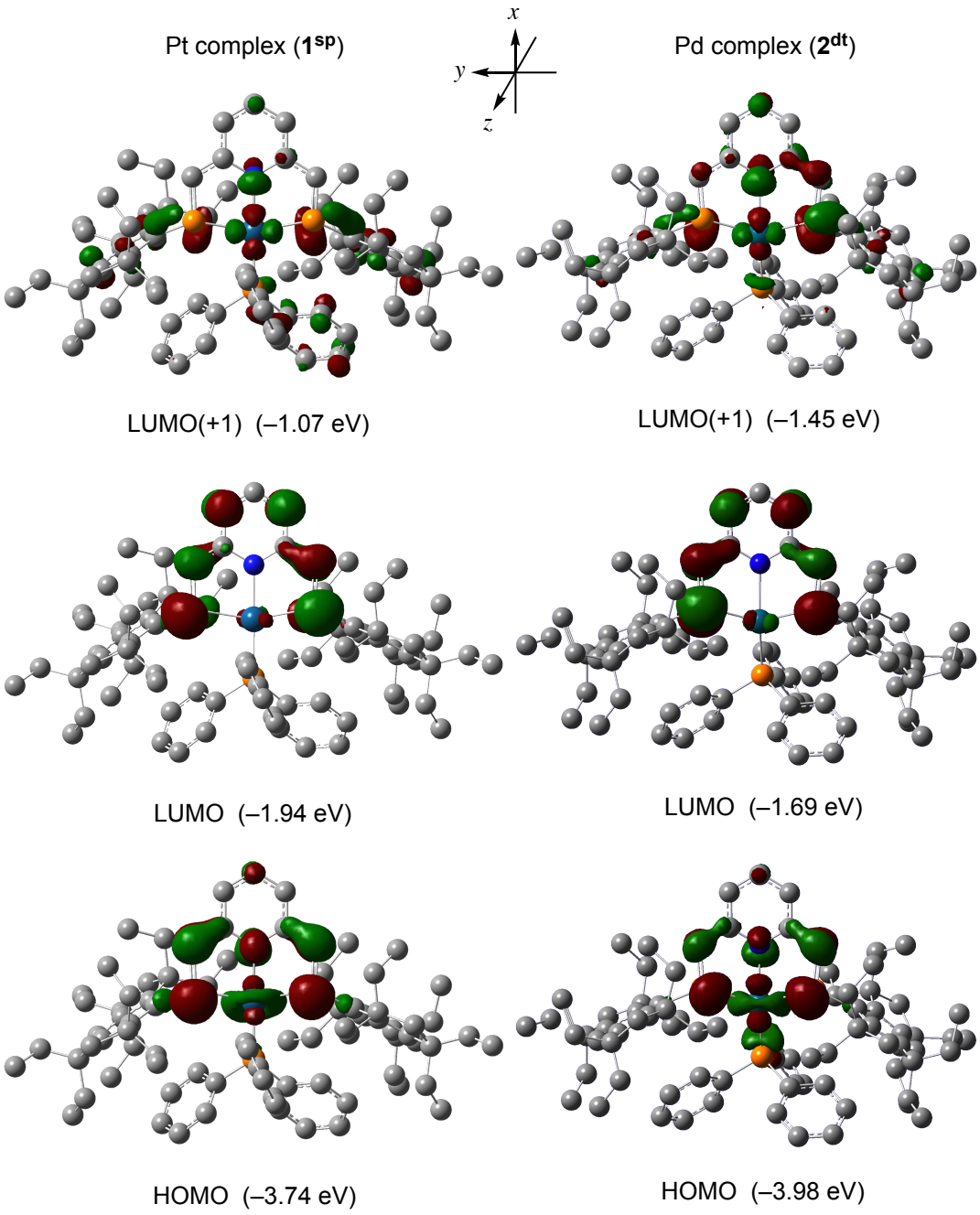

Figure 4. Frontier molecular orbitals of **1**^{sp} (left) and **2**^{dt} (right).

In contrast, the author found that complexes **1** and **2** have nearly ten valence electrons on the metals and both complexes can be identified as M(0) species. The natural atomic charges of Pt and Pd in $\mathbf{1}^{sp}$ and $\mathbf{2}^{dt}$ are 0.18 and 0.20, respectively, and the values are comparable to each other. Thus, although the HOMO with a large contribution of the in-phase π* orbital of $Eind_2$-BPEP should be responsible for elongation of P=C bonds, it is hard to rationalize the difference in coordination geometry between **1** and **2** based on this orbital situation.

Instead, the author found a notable difference in atomic orbital occupancies between Pt ($\mathbf{1}^{sp}$) and Pd ($\mathbf{2}^{dt}$) centers. The electron configurations were estimated to be [6s(0.62) + 5d(9.15)] for Pt and [5s(0.39) + 4d(9.37)] for Pd, respectively. Because the calculated model of a distorted tetrahedral Pt complex ($\mathbf{1}^{dt}$) has the electron configuration [6s(0.59) + 5d(9.18)] close to $\mathbf{1}^{sp}$, it is convincing that the higher occupancy of the atomic 6s orbital is not due to the coordination geometry but rather to the nature of the Pt atom. Although the formal d^{10} configuration is regarded as consisting of occupied d orbitals and empty s and p orbitals, some of the electrons are accommodated in an s orbital by s-d hybridization in reality. It is known that relativistic effects that remarkably appear in heavier elements including Pt enhance the s-d hybridization to a great extent.[11,12] Relativistic effects also cause a contraction of the s orbitals, thereby reducing electronic repulsion between the metal and ligating atoms. As a result, ligands tightly combine with metals via dative bonding, where the coordination geometry will be controlled by the shape and orientation of d_{x2-y2} orbital, which is partially unoccupied due to s-d hybridization. This situation is clearly reflected in shorter M–L bonds of **1** than those of **2** (see Table 1).

Conclusion

In summary, the author has found a rare example of Pt(0) complex that adopts a highly planar coordination geometry. Although the HOMO has a large orbital contribution of the low-coordinate phosphorus ligand ($Eind_2$-BPEP), complex **1** preserves nearly ten valence electrons on the Pt center. Instead, strong s-d hybridization due to relativistic effects facilitates the planar arrangement of ligands, which reflects the shape and orientation of partially unoccupied atomic d_{x2-y2} orbital. In contrast, complex **2** adopts ordinary distorted tetrahedral geometry because relativistic effects are less significant for Pd.[11]

Experimental Section

General Considerations. All manipulations were performed under a nitrogen atmosphere using a glove box and Schlenk techniques. Eind-PCl_2 (Eind = 1,1,3,3,5,5,7,7-octaethyl-1,2,3,5,6,7-hexahydro-*s*-indacen-4-yl),[9b] [$Pt(cod)_2$],[13] and [CpPd(π-allyl)][14] were prepared according to the literature. The other chemicals were obtained from commercial sources. NMR spectra were recorded on a 400 MHz spectrometer. Chemical shifts are reported in δ (ppm), referenced to ^1H (residual) and ^{13}C signals of deuterated solvents as internal standards or to the ^{31}P signal of 85% H_3PO_4 and the ^{195}Pt signal of K_2PtCl_4 as external standards. The assignments of ^{13}C signals were based on HMQC and HMBC experiments. Elemental analysis was performed by ICR Analytical Laboratory, Kyoto University. High resolution mass spectra (HRMS) were recorded on a Bruker MicroTOF ESI mass spectrometer.

Synthesis of Eind$_2$-BPEP. The title compound was prepared by a two-step procedure given in Scheme 2(a). (i) To a mixture of zinc dust (348 mg, 5.3 mmol) and Eind-PCl_2 (300 mg, 0.62 mmol) in THF (4 mL), was added a 1.0 M THF solution of PMe_3 (1.5 mL, 1.5 mmol) at room temperature. After stirring for 1 h, the reaction mixture was added dropwise to a THF solution (6 mL) of 2,6-pyridinedicarbaldehyde (86 mg, 0.64 mmol) by a cannula at 0 °C over 10 min. The mixture was stirred at room temperature for 6 h. Volatiles were removed under reduced pressure, and the residue was suspended in hexane (600 mL), and filtrated through a Celite pad to remove zinc dust, $ZnCl_2$, and Me_3PO. The filtrate was concentrated to half in volume, and purified by gel filtration using a 1,2-dihydroxy-3-propoxypropyl-modified silica gel and hexane as the eluent to afford 6-(2-Eind-2-phosphaethenyl)-2-pyridinecarboaldehyde as a pale-yellow powder (241 mg, 0.45 mmol, 74%).

^1H NMR (C_6D_6, 25 °C): δ 10.05 (s, 1H, C*H*O), 9.21 (d, $^2J_{PH}$ = 25.5 Hz, 1H, P=C*H*), 7.48 (d, $^3J_{HH}$ = 7.7 Hz, 1H, 4-Py), 7.31 (d, $^3J_{HH}$ = 7.7 Hz, 1H, 5-Py), 6.88 (t, $^3J_{HH}$ = 7.7 Hz, 1H, 3-Py), 6.86 (s, 1H, *p*-Eind), 2.07 (dq, $^2J_{HH}$ = 14.2 Hz, $^3J_{HH}$ = 7.4 Hz, 4H, CH*H*), 1.94 (dq, $^2J_{HH}$ = 14.2 Hz, $^3J_{HH}$ = 7.4 Hz, 4H, CH*H*), 1.78 (s, 4H, ind-CH_2), 1.73 (dq, $^2J_{HH}$ = 14.2 Hz, $^3J_{HH}$ = 7.4 Hz, 4H, CH*H*), 1.62 (dq, $^2J_{HH}$ = 14.2 Hz, $^3J_{HH}$ = 7.4 Hz, 4H, CH*H*), 0.90 (t, $^3J_{HH}$ = 7.4 Hz, 12H, CH_3), 0.86 (t, $^3J_{HH}$ = 7.4 Hz, 12H, CH_3). $^{13}C\{^1H\}$ NMR (C_6D_6, 25 °C): δ 193.3 (s, *C*HO), 180.3 (d, $^1J_{PC}$ = 36 Hz, P=*C*H), 158.8 (d, J_{PC} = 15 Hz), 153.9 (s), 150.7 (d, J_{PC} = 3 Hz), 150.2 (s), 137.8 (s), 136.3 (d, $^1J_{PC}$ = 48 Hz, *ipso*-Eind), 124.3 (d, J_{PC} = 18 Hz), 121.5 (s, *p*-Eind),

120.1 (d, J_{PC} = 6 Hz), 53.7 (s), 49.0 (s), 42.9 (s, *C*H_2), 34.4 (br s, *C*H_2CH_3), 33.7 (br s, *C*H_2CH_3), 10.1 (s, CH_2*C*H_3), 9.8 (s, CH_2*C*H_3). $^{31}P\{^1H\}$ NMR (C_6D_6, 25 °C): δ 284.2 (s). Anal. Calcd for $C_{35}H_{50}NOP$: C, 79.05; H, 9.48; N, 2.63. Found: C, 79.10; H, 9.62; N, 2.65.

(ii) To a mixture of zinc dust (650 mg, 9.9 mmol) and Eind-PCl_2 (630 mg, 1.3 mmol) in THF (8 mL), was added a 1.0 M THF solution of PMe_3 (4.0 mL, 4.0 mmol) at room temperature. After stirring for 1 h, the reaction mixture was added dropwise to a THF solution (10 mL) of 6-(2-Eind-2-phosphaethenyl)-2-pyridinecarboaldehyde (554 mg, 1.0 mmol) by a cannula at 0 °C. The mixture was stirred at room temperature for 12 h. Volatiles were removed under reduced pressure, and the residue was suspended in hexane (30 mL), and filtrated through a Celite pad to remove zinc dust, $ZnCl_2$, and Me_3PO. The filtrate was concentrated to dryness and washed with hexamethyldisiloxane (5 mL) to afford $Eind_2$-BPEP as an off-white solid (629 mg, 0.68 mmol, 65%).

^1H NMR (CD_2Cl_2, 25 °C): δ 8.89 (d, $^3J_{PH}$ = 25.6 Hz, 2H, P=C*H*), 7.60 (t, $^3J_{HH}$ = 7.6 Hz, 1H, 4-Py), 7.49 (d, $^3J_{HH}$ = 7.6 Hz, 2H, 3,5-Py), 6.73 (s, 2H, *p*-Eind), 1.86 (dq, $^2J_{HH}$ = 12.4 Hz, $^3J_{HH}$ = 7.4 Hz, 8H, CH*H*), 1.83 (dq, $^2J_{HH}$ = 12.4 Hz, $^3J_{HH}$ = 7.4 Hz, 8H, CH*H*), 1.81 (s, 8H, ind-CH_2), 1.70 (dq, $^2J_{HH}$ = 14.4 Hz, $^3J_{HH}$ = 7.4 Hz, 8H, CH*H*), 1.59 (dq, $^2J_{HH}$ = 14.4 Hz, $^3J_{HH}$ = 7.4 Hz, 8H, CH*H*), 0.84 (t, $^3J_{HH}$ = 7.4 Hz, 24H, CH_3), 0.77 (t, $^3J_{HH}$ = 7.4 Hz, 24H, CH_3). $^{13}C\{^1H\}$ NMR (CD_2Cl_2, 25 °C): δ 182.0 (d, $^1J_{PC}$ = 34 Hz, P=*C*H), 158.6 (d, $^2J_{PC}$ = 16 Hz, 2,6-Py), 150.4 (s), 149.4 (s), 137.3 (s, 4-Py), 136.2 (d, $^1J_{PC}$ = 48 Hz, *ipso*-Eind), 121.3 (s, *p*-Eind), 119.8 (d, $^3J_{PC}$ = 25 Hz, 3,5-Py), 48.8 (s), 42.7 (s), 34.1 (s), 33.5 (s), 9.9 (s), 9.6 (s). $^{31}P\{^1H\}$ NMR (CD_2Cl_2, 25 °C): δ 276.5 (s). HRMS (APCI): calcd for $C_{63}H_{95}NP_2$ ($[M+H]^+$) 928.7013; found 928.7013. Anal. Calcd for $C_{63}H_{95}NP_2$: C, 81.50; H, 10.31; N, 1.51. Found: C, 81.16; H, 10.24; N, 1.51.

Synthesis of [Pt(PPh_3)($Eind_2$-BPEP)] (1). $Eind_2$-BPEP (65 mg, 0.070 mmol), [$Pt(cod)_2$] (27 mg, 0.066 mmol), and PPh_3 (19 mg, 0.072 mmol) were placed in a Schlenk tube, and toluene (2 mL) was added at –78 °C. The mixture was gradually warmed to room temperature with stirring over 2 h. Volatiles were removed under reduced pressure, and the residue was dissolved in pentane (2 mL) and filtrated through a glass wool. The filtrate was concentrated and dissolved again in pentane (ca. 0.5 mL), and then allowed to stand at –35 °C to afford a green crystalline solid of **1** (22 mg, 0.016 mmol, 24%).

^{1}H NMR (THF-d_8, 25 °C): δ 8.12 (br, 2H, P=C*H*), 7.97 (br, 2H, 3,5-Py), 7.66 (t, $^{3}J_{HH}$ = 7.6 Hz, 1H, 4-Py), 7.41 (br, 6H, PPh_3), 7.10 (t, $^{3}J_{HH}$ = 7.4 Hz, 3H, PPh_3), 6.91 (br, 6H, PPh_3), 6.88 (s, 2H, *p*-Eind), 2.57 (dq, $^{2}J_{HH}$ = 13.6 Hz, $^{3}J_{HH}$ = 7.2 Hz, 4H, CH*H*), 1.91 (br, 4H, CH*H*), 1.79 (dq, $^{2}J_{HH}$ = 13.6 Hz, $^{3}J_{HH}$ = 7.2 Hz, 4H, CH*H*), 1.68 (s, 8H, ind-CH_2), 1.56 (dq, $^{2}J_{HH}$ = 13.6 Hz, $^{3}J_{HH}$ = 7.2 Hz, 8H, CH*H*), 1.50 (dq, $^{2}J_{HH}$ = 13.6 Hz, $^{3}J_{HH}$ = 7.2 Hz, 4H, CH*H*), 1.22 (dq, $^{2}J_{HH}$ = 13.6 Hz, $^{3}J_{HH}$ = 7.2 Hz, 4H, CH*H*), 0.97 (t, $^{3}J_{HH}$ = 7.2 Hz, 12H, CH_3), 0.84 (t, $^{3}J_{HH}$ = 7.2 Hz, 12H, CH_3), 0.75 (t, $^{3}J_{HH}$ = 7.2 Hz, 12H, CH_3), 0.62 (dq, $^{2}J_{HH}$ = 13.6 Hz, $^{3}J_{HH}$ = 7.2 Hz, 4H, CH*H*), 0.34 (t, $^{3}J_{HH}$ = 7.2 Hz, 12H, CH_3). ^{13}C{^{1}H} NMR (THF-d_8, 25 °C): δ 152.4 (s), 150.4 (s), 148.5 (s), 136.2 (s), 135.5 (br), 134.3 (br), 132.4 (br), 127.9 (d, J = 10 Hz), 122.9 (s), 120.0 (br), 54.3 (s), 47.6 (s), 43.6 (s), 35.5 (s), 34.6 (s), 32.3 (s), 31.3 (s), 10.9 (s), 9.8 (s), 9.4 (s), 9.3 (s). ^{31}P{^{1}H} NMR (THF-d_8, 25 °C): δ 105.6 (d, $^{2}J_{PP}$ = 39 Hz, $^{1}J_{PtP}$ = 1594 Hz, *P*=CH), 7.0 (t, $^{2}J_{PP}$ = 39 Hz, $^{1}J_{PtP}$ = 4249 Hz, *P*Ph_3). ^{195}Pt NMR (THF-d_8, 25 °C): δ –4451.1 (dt, $^{1}J_{PtP}$ = 4249 and 1594 Hz). HRMS (ESI): calcd for $C_{81}H_{110}NP_3Pt$ ($[M]^+$) 1384.7499; found 1384.7497. Anal. Calcd for $C_{81}H_{110}NP_3Pt$: C, 70.21; H, 8.00; N, 1.01. Found: C, 70.15; H, 8.29; N, 1.05.

Synthesis of [Pd(PPh_3)(Eind$_2$-BPEP)] (2). To a solution of Eind$_2$-BPEP (50 mg, 0.054 mmol) and PPh_3 (15 mg, 0.057 mmol) in toluene (2 mL), was added [CpPd(π-allyl)] (11 mg, 0.051 mmol) at –78 °C. The mixture was gradually warmed to room temperature with stirring over 2 h. Volatiles were removed under reduced pressure, and the residue was dissolved in Et_2O (2 mL) and filtrated through a glass wool. The filtrate was concentrated to ca. 0.5 mL, and allowed to stand at –35 °C to afford a green crystalline solid of **2** (23 mg, 0.018 mmol, 33%).

^{1}H NMR (THF-d_8, 25 °C): δ 8.54 (br, 2H, P=C*H*), 7.76 (m, 3H, Py), 7.24 (dd, $^{3}J_{PH}$ = 9.6 Hz, $^{3}J_{HH}$ = 7.2 Hz, 6H, PPh_3), 7.06 (t, $^{3}J_{HH}$ = 7.2 Hz, 3H, PPh_3), 6.88 (s, 2H, *p*-Eind), 6.87 (t, $^{3}J_{HH}$ = 7.2 Hz, 6H, PPh_3), 2.44 (br, 4H, CH*H*), 1.92 (br, 4H, CH*H*), 1.79 (dq, $^{2}J_{HH}$ = 14.0, $^{3}J_{HH}$ = 7.0 Hz, 4H, CH*H*), 1.73 (s, 8H, ind-CH_2), 1.70 (4H, CH*H*, the coupling pattern was obscure due to overlapping peaks), 1.60 (m, 12H, CH*H*), 1.36 (dq, $^{2}J_{HH}$ = 13.6, $^{3}J_{HH}$ = 7.0 Hz, 4H, C*H*H), 0.95 (t, $^{3}J_{HH}$ = 7.0 Hz, 12H, CH_3), 0.86 (t, $^{3}J_{HH}$ = 7.0 Hz, 12H, CH_3), 0.75 (t, $^{3}J_{HH}$ = 7.0 Hz, 12H, CH_3), 0.40 (br, 12H, CH_3). ^{13}C{^{1}H} NMR (THF-d_8, 25 °C): δ 158.9 (s), 150.5 (s), 145.6 (br, P=*C*H), 138.4 (s), 138.1 (s), 136.8 (br d, J_{PC} = 89 Hz), 134.7 (d, J_{PC} = 13 Hz,

PPh_3), 129.6 (s), 128.4 (d, J_{PC} = 9 Hz), 126.2 (s, Py), 122.4 (s, *p*-Eind), 120.4 (br, Py), 54.5 (s), 47.9 (s), 43.9 (br), 35.4 (s), 34.3 (br), 34.0 (br), 31.8 (s), 10.6 (br), 9.9 (s), 9.5 (s), 9.4 (s). $^{31}P\{^1H\}$ NMR (THF-d_8, 25 °C): δ 231.4 (d, $^2J_{PP}$ = 47 Hz, *P*=CH), 36.9 (t, $^2J_{PP}$ = 47 Hz, *P*PPh_3). HRMS (ESI): calcd for $C_{81}H_{110}NP_3Pd$ ($[M]^+$) 1295.6906; found 1295.6908. Anal. Calcd for $C_{81}H_{110}NP_3Pd$: C, 75.00 H, 8.55; N, 1.08. Found: C, 74.76; H, 8.44; N, 0.85.

Synthesis of [Ni(PPh_3)(Eind$_2$-BPEP)] (3). To a solution of Eind$_2$-BPEP (100 mg, 0.11 mmol) and PPh_3 (35 mg, 0.13 mmol) in toluene (3 mL), was added [Ni(cod)$_2$] (29 mg, 0.11 mmol) at –78 °C. The reaction solution was warmed to room temperature over 2 h. Volatiles were removed under reduced pressure, and the residue was dissolved in pentane (5 mL) and filtrated through a glass wool. The filtrate was concentrated to dryness. The residue was dissolved in Et_2O (0.5 mL), and allowed to stand at –35 °C to afford dark brown crystals of **3** (47 mg, 0.038 mmol, 35%), which were suitable for X-ray diffraction analysis, but did not give satisfactory elemental analysis. Moreover, because the isolated complex was unstable in solution in the absence of free PPh_3, the NMR spectra were recorded in THF-d_8 containing a small amount of added PPh_3 (ca. 4%: δ_H = 7.35, δ_P = –4.5) at low temperature (–40 °C). The ^1H NMR spectrum observed under these conditions exhibited two sets of Ph group signals of the PPh_3 ligand in a 2:1 ratio, showing freeze-rotation of PPh_3 around the Ni–P bond in an NMR time scale. Accordingly, the eight Et groups in each Eind group displayed chemically nonequivalent signals.

^1H NMR (THF-d_8, –40 °C): δ 8.45 (br, 2H, P=C*H*), 7.80 (t, $^3J_{HH}$ = 7.2 Hz, 1H, 4-Py), 7.74 (d, $^3J_{HH}$ = 7.2 Hz, 2H, 3,5-Py), 7.51 (br, 2H, PPh_3), 7.30 (m, 3H, PPh_3), 7.08 (t, $^3J_{HH}$ = 7.2 Hz, 4H, PPh_3), 6.93 (t, $^3J_{HH}$ = 7.2 Hz, 2H, PPh_3), 6.90 (s, 2H, *p*-Eind), 6.34 (d, $^3J_{HH}$ = 7.2 Hz, 4H, PPh_3), 3.10 (dq, $^2J_{HH}$ = 13.2 Hz, $^3J_{HH}$ = 6.8 Hz, 2H, CH*H*), 2.31 (dq, $^2J_{HH}$ = 13.6 Hz, $^3J_{HH}$ = 6.8 Hz, 2H, CH*H*), 1.91–1.16 (m, 36H, CH_2), 1.07 (t, $^3J_{HH}$ = 7.0 Hz, 6H, CH_3), 0.90, (t, $^3J_{HH}$ = 7.2 Hz, 6H, CH_3) 0.87 (t, $^3J_{HH}$ = 7.2 Hz, 6H, CH_3), 0.83 (t, $^3J_{HH}$ = 7.2 Hz, 6H, CH_3), 0.81 (t, $^3J_{HH}$ = 7.2 Hz, 6H, CH_3), 0.77 (t, $^3J_{HH}$ = 7.2 Hz, 6H, CH_3) 0.57 (t, $^3J_{HH}$ = 7.2 Hz, 6H, CH_3), 0.09 (br, 6H, CH_3). $^{13}C\{^1H\}$ NMR (THF-d_8, –40 °C): δ 153.8 (s), 152.0 (s), 150.0 (s), 149.6 (s), 148.4 (s), 141.3 (br, P=*C*H), 137.8 (d, J_{PC} = 37 Hz), 137.2 (br s), 135.8 (br d, J_{PC} = 31 Hz), 135.6 (d, J_{PC} = 32 Hz), 133.4 (d, J_{PC} = 11 Hz), 130.5 (s), 129.2 (s), 127.6 (d, J_{PC} = 12 Hz), 123.4 (s, Py), 123.0 (s, *p*-Eind), 121.0 (s, Py), 54.4 (s), 54.2 (s), 47.8 (s), 47.1 (s) 43.0 (s),

35.8 (s), 35.7 (s), 35.1 (s), 33.0 (s), 31.3 (s), 30.9 (s), 11.7 (br), 10.5 (s), 10.2 (s), 10.0 (s), 9.7 (br), 9.64 (s), 9.7 (s), 9.56 (s). $^{31}P\{^{1}H\}$ NMR (THF-d_8, –40 °C): δ 224.7 (br, *P*=CH), 47.1 (br, *P*Ph_3). HRMS (ESI): calcd for $C_{81}H_{110}NNiP_3$ ($[M]^+$) 1248.7277; found 1248.7278.

X-ray Crystal Structure Determination. Single crystals of **1**–**3** suitable for X-ray diffraction analysis were grown at –35 °C from CH_2Cl_2 (**1**), Et_2O/THF (ca. 10:1) (**2**), and Et_2O (**3**), respectively. The intensity data were collected at 103 K on a Rigaku Saturn70 CCD diffractometer with the VariMax Optic, using Mo Kα radiation (λ = 0.71075 Å). The intensity data were corrected for Lorentz and polarization effects and for absorption (multi-scan[15]). The structures were solved by direct methods (SHELXS-97)[16] and refined by least-squares calculations on F^2 (SHELXL-97),[16] using Yadokari-XG 2009.[17] Non-hydrogen atoms, except for solvent molecules and disordered atoms, were refined anisotropically. Hydrogen atoms were placed at calculated positions and included in calculations without refinement of their parameters. The crystallographic data and the summary of solution and refinement are given in Table 2.[10]

Computational Details. DFT calculations were carried out by using the Gaussian 09 program.[18] For calculations of full models (**1**^{sp}, **2**^{dt}, and **2**^{sp}), we adopted the B3LYP-D3 functional, which is the B3LYP hybrid functional[19] combined with an empirical dispersion correction developed by Grimme *et al.*[20] Geometry optimization was performed with the LANL2DZ (Pt and Pd) and 3-21G(d) (other atoms) basis sets. The energy differences were evaluated by single-point calculations at the optimized geometries using the SDD and 6-31G(d) basis sets. Systematic vibrational analyses were carried out for all models to characterize stationary-point structures. The optimized structures are shown in Figure 2. Selected structure parameters are listed in Table 3. Angular dependence of potential energies of simple models (**1**^{sm} and **2**^{sm}) in Figure 3 was examined by using the B3LYP functional and the SDD (Pt and Pd) and 6-31G(d) (other atoms) basis sets. It was confirmed for the stable form of **1**^{sm} (N–M–PH_3 ≈ 166°) that the B3LYP-D3 and B3LYP functional provided almost identical structures.

Table 2. Crystal Data and Details of Structure Determination for **1**–**3**

complex	**1**	**2**	**3**
empirical formula	$C_{81}H_{110}NP_3Pt\cdot(CH_2Cl_2)_2$	$C_{81}H_{110}NP_3Pd\cdot C_4H_8O$	$C_{81}H_{110}NNiP_3\cdot(C_4H_{10}O)_{0.5}$
formula weight	1555.55	1369.11	1286.37
T (K)	103(2)	103(2)	103(2)
crystal system	triclinic	triclinic	triclinic
space group	P–1	P–1	P–1
a (Å)	13.341(2)	11.0919(3)	11.537(4)
b (Å)	18.981(4)	17.5397(5)	17.264(6)
c (Å)	30.668(6)	21.00910(10)	19.333(7)
α (°)	93.859(3)	70.488(8)	81.885(9)
β (°)	90.885(3)	75.266(10)	83.562(12)
γ (°)	98.025(2)	84.033(10)	79.865(8)
V (Å^3)	7670(2)	3725.1(3)	3738(2)
Z	4	2	2
d_{calcd} (g/cm^3)	1.347	1.221	1.143
μ(Mo Kα) (mm^{-1})	2.075	0.359	0.367
F(000)	3240	1468	1394
crystal size	0.20 x 0.19 x 0.08	0.12 x 0.08 x 0.02	0.29 x 0.12 x 0.03
θ range (°)	1.776 to 25.000	1.863 to 24.250	1.510 to 24.250
reflections collected	61526	28640	38653
independent reflections (R_{int})	26729 (0.0518)	11982 (0.0925)	11605
absorption correction	multi-scan	multi-scan	multi-scan
max. and min. transmission	0.847 and 0.667	1.000 and 0.772	1.000 and 0.637
data / restraints / parameters	26729 / 12 / 1651	11982 / 15 / 784	11605 / 4 / 807
GOF on F^2	1.131	1.000	1.058
$R1$, $wR2$ [$I > 2\sigma(I)$]	0.0651, 0.1606	0.0679, 0.1601	0.0553, 0.1434
$R1$, $wR2$ (all data)	0.0749, 0.1713	0.1074, 0.2192	0.0635, 0.1544
largest peak and hole (e Å^3)	4.919 and –2.061	1.684 and –1.772	0.989 and –0.804

Table 3. Structural Parameters for [M(PPh_3)($Eind_2$-BPEP)] Complexes (M = Pt and Pd) [a]

Complex	M−P(=CH) (average)	M–N	M–PPh_3	P=CH (average)	P1–M–P2	N–M–P3	C8–P1–C1–C3 C36–P2–C2–C7
1 (X-ray)	2.317	2.092	2.272	1.719	158.2	173.6	158.4
$\mathbf{1}^{sp}$ (DFT)	2.382	2.120	2.295	1.722	154.3	173.6	154.4
$\mathbf{1}^{dt}$ (DFT)	2.346	2.192	2.271	1.708	144.0	158.3	168.3
2 (X-ray)	2.345	2.229	2.306	1.704	141.1	156.1	175.2
$\mathbf{2}^{dt}$ (DFT)	2.377	2.292	2.230	1.701	141.2	156.1	171.4

[a] Bond distances (Å) and angles (°) determined by X-ray diffraction analysis and DFT calculations.

Reference and Notes

(1) Albright, T. A.; Burdett, J. K.; Whangbo, M.-H. *Orbital Interactions in Chemistry, 2nd Ed.*; Wiley: Hoboken, USA, 2013.

(2) Young, A. G.; Hanton, L. R. *Coord. Chem. Rev.* **2008**, *252*, 1346–1386.

(3) (a) Rosa, P.; Mézailles, N.; Ricard, L.; Mathey, F.; Le Floch, P.; Jean, Y. *Angew. Chem., Int. Ed.* **2001**, *40*, 1251–1253. (b) Tirla, C.; Mézailles, N.; Ricard, L.; Mathey, F.; Le Floch, P. *Inorg. Chem.* **2002**, *41*, 6032–6037. (c) Moores, A.; Mézailles, N.; Ricard, L.; Mathey, F.; Le Floch, P. *Chem. Commun.* **2003**, 1914–1915.

(4) (a) Le Floch, P. *Coord. Chem. Rev.* **2006**, *250*, 627–681. (b) Dugal-Tessier, J.; Conrad, E. D.; Dake, G. R.; Gates, D. P. In *Phosphorus(III) Ligands in Homogeneous Catalysis: Design and Synthesis*; Kamer, P. C. J., van Leeuwen, P. W. N. M., Eds.; Wiley: Chichester, U.K., 2012; Chapter 10. (c) Müller, C.; Pidko, E. A.; Lutz, M.; Spek, A. L.; Vogt, D. *Chem. Eur. J.* **2008**, *14*, 8803–8807.

(5) Perron, H.; Moores, A.; Demachy, I.; Lledos, A.; Jean, Y.; Le Floch, P. *New J. Chem.* **2004**, *28*, 838–842.

(6) Taguchi, H.; Chang, Y. H.; Takeuchi, K.; Ozawa, F. *Organometallics* **2015**, *34*, 1589–1596.

(7) Ozawa, F.; Nakajima, Y. *Chem. Rec.* **2016**, *16*, 2314–2323.

(8) Matsuo, T.; Tamao, K. *Bull. Chem. Soc. Jpn.* **2015**, *88*, 1201–1220.

(9) (a) Shah, S.; Protasiewicz, J. D. *Chem. Commun.* **1998**, *3*, 1585–1586. (b) Li, B.; Tsujimoto, S.; Li, Y.; Tsuji, H.; Tamao, K.; Hashizume, D.; Matsuo, T. *Heteroat. Chem.* **2014**, *25*, 612–618.

(10) Crystallographic data have been deposited with the Cambridge Crystallographic Data Centre as supplementary publication: CCDC 1505566 (**1**), 1505567 (**2**), and 1505568 (**3**).

(11) (a) Ziegler, T.; Autschbach, J. *Chem. Rev.* **2005**, *105*, 2695–2722. (b) Autschbach, J.; Siekierski, S.; Seth, M.; Schwerdtfeger, P.; Schwarz, W. H. E. *J. Comput. Chem.* **2002**, *23*, 804–813. (c) Dedieu, A. *Chem. Rev.* **2000**, *100*, 543–600. (d) Frenking, G.; Fröhlich, N. *Chem. Rev.* **2000**, *100*, 717–774.

(12) For related coordination chemistry of Au featuring relativistic effects, see: Pyykkö, P. *Angew. Chem., Int. Ed.* **2004**, *43*, 4412–4456.

(13) Dell'Amico, D. B.; Labella, L.; Marchetti, F.; Samaritani, S. *J. Organomet. Chem.* **2011**, *696*, 1349–1354.

(14) Tatsuno, Y.; Yoshida, T.; Otsuka, S. *Inorg. Synth.* **1979**, *19*, 220–221.

(15) Blessing, R. H. *Acta Crystallogr., Sect. A* **1995**, *51*, 33–38.

(16) Sheldrick, G. M. *SHELXL-97*, University of Göttingen, Germany, 1997.

(17) Kabuto, C.; Akine, S.; Kwon, E. *J. Crystallogr. Soc. Jpn.* **2009**, *51*, 218–224.

(18) Frisch, M. J.; Trucks, G. W.; Schlegel, H. B.; Scuseria, G. E.; Robb, M. A.; Cheeseman, J. R.; Scalmani, G.; Barone, V.; Mennucci, B.; Petersson, G. A.; Nakatsuji, H.; Caricato, M.; Li, X.; Hratchian, H. P.; Izmaylov, A. F.; Bloino, J.; Zheng, G.; Sonnenberg, J. L.; Hada, M.; Ehara, M.; Toyota, K.; Fukuda, R.; Hasegawa, J.; Ishida, M.; Nakajima, T.; Honda, Y.; Kitao, O.; Nakai, H.; Vreven, T.; Montgomery, J. A., Jr.; Peralta, J. E.; Ogliaro, F.; Bearpark, M.; Heyd, J. J.; Brothers, E.; Kudin, K. N.; Staroverov, V. N.; Kobayashi, R.; Normand, J.; Raghavachari, K.; Rendell, A.; Burant, J. C.; Iyengar, S. S.; Tomasi, J.; Cossi, M.; Rega, N.; Millam, J. M.; Klene, M.; Knox, J. E.; Cross, J. B.; Bakken, V.; Adamo, C.; Jaramillo, J.; Gomperts, R.; Stratmann, R. E.; Yazyev, O.; Austin, A. J.; Cammi, R.; Pomelli, C.; Ochterski, J. W.; Martin, R. L.; Morokuma, K.; Zakrzewski, V. G.; Voth, G. A.; Salvador, P.; Dannenberg, J. J.; Dapprich, S.; Daniels, A. D.; Farkas, Ö.; Foresman, J. B.; Ortiz, J. V.; Cioslowski, J.; Fox, D. J. Gaussian 09, Revision C.01, Gaussian, Inc., Wallingford CT, 2009.

(19) (a) Becke, A. D. *Phys. Rev. A* **1988**, *38*, 3098–3100. (b) Becke, A. D. *J. Chem. Phys.* **1993**, *98*, 5648–5652. (c) Lee, C.; Yang, W.; Parr, R. G. *Phys. Rev. B* **1988**, *37*, 785–789. (d) Stephens, P. J.; Devlin, F. J.; Chabalowski, C. F.; Frisch, M. J. *J. Phys. Chem.* **1994**, *98*, 11623–11627.

(20) Grimme, S. *J. Comput. Chem.* **2006**, *27*, 1787–1799.

Chapter 5

On Geometrical Stability of Square Planar Platinum(0) Complexes Bearing a PNP-Pincer Type Phosphaalkene Ligand ($Eind_2$-BPEP)

Abstract

The author has described in Chapter 4 that the Pt(0) complex [Pt(L)($Eind_2$-BPEP)] (L = PPh_3) bearing a PNP-pincer type phosphaalkene ligand ($Eind_2$-BPEP) adopts a highly planar configuration around Pt (τ_4 = 0.11), and this coordination geometry is very uncommon for formal d^{10} complexes. In this chapter, a series of L with different electronic properties (DMAP, 2,6-lutidine, PMe_3, ^{t}BuNC, and CO) are introduced in place of PPh_3, and their effects on coordination geometries are examined. The X-ray structures have displayed planar configurations irrespective of L (τ_4 = 0.20–0.27); however, DFT calculations have revealed that the stability toward distortion around Pt significantly varies with L. The complexes with pyridine-based ligands as typical σ-donors have rigid planar structures, whereas those with π-accepting ligands such as CO are distorted in a wide range by small distortion energy. The electronic effects of L are also reflected in spectroscopic properties of complexes, showing a large color change in the near-infrared region.

Introduction

Four-coordinate complexes with a formal d^{10} metal center adopt a tetrahedral configuration around the metal due to the lack of stereochemical preference arising from the d^{10} configuration. This situation is commonly observed in coordination chemistry and basically unchanged even for PNP-pincer complexes with rigid meridional coordination (Scheme 1); they are significantly distorted (**A**),[1] otherwise change to a three-coordinate species to relieve the distortion (**B**).[2]

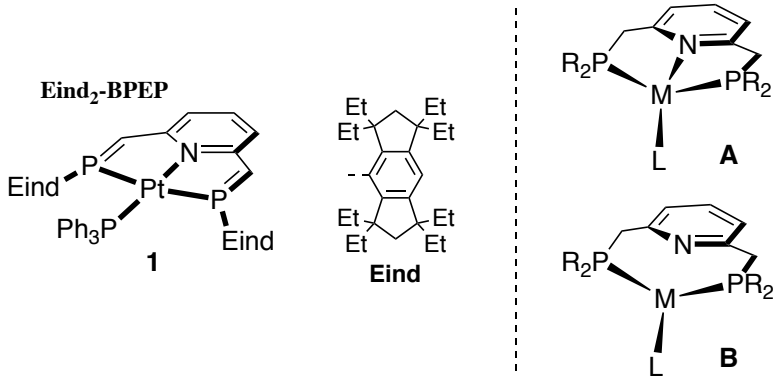

Scheme 1. Comparison between geometrical structures of $Eind_2$-BPEP complex of Pt(0) (**1**) and ordinary PNP-pincer complexes of formal d^{10} metals (**A** and **B**).

On the other hand, the author has recently found that the Pt(0) complex [$Pt(PPh_3)(Eind_2$-BPEP)] (**1**) bearing a PNP-pincer type phosphaalkene ligand ($Eind_2$-BPEP) adopts a highly planar configuration around Pt (τ_4 = 0.11).[3] Although there have been a few precedents of formal d^{10} complexes with a square planar or distorted square planar configuration, all of them are dianionic species of d^8 metals, which are stabilized by electrostatic interactions with Li^+ or Na^+ ions at apical positions.[4] In contrast, complex **1** is a neutral species without such interactions but stable in a square planar configuration.

Two crucial requirements have been found for the highly planar structure of **1**. One is the PNP-pincer type phosphaalkene ligand ($Eind_2$-BPEP) with P=C bonds, and DFT calculations have revealed that [$Pt(PMe_3)$(PNP)] (PNP = 2,6-bis(phosphanylmethyl)pyridine) without P=C bonds is stabilized as a three-coordinate species without coordination of the pyridine unit. On

the other hand, even if the $Eind_2$-BPEP ligand is coordinated, the Pd(0) and Ni(0) homologues are significantly distorted around the metals (τ_4 = 0.44 and 0.40).[3] Thus, the other requirement is the Pt atom, and the unique coordination geometry of **1** is largely due to the nature of this element. In fact, DFT calculations have indicated a tight connection between the planar structure and strong hybridization of the atomic 5d and 6s orbitals of Pt through relativistic effects, which often play a crucial role for heavier elements including Pt.[5]

In this study, the author introduced a series of L with different electronic properties in place of PPh_3 (Scheme 2), and examined their effects on coordination geometries of resulting complexes. As described below, all complexes adopt a planar configuration around Pt, but the coordination geometry gains flexibility toward distortion when L is a π-accepting ligand such as CO. Moreover, the electronic effects of L are clearly reflected in the spectroscopic properties observed by NMR and UV-vis-NIR spectroscopy.

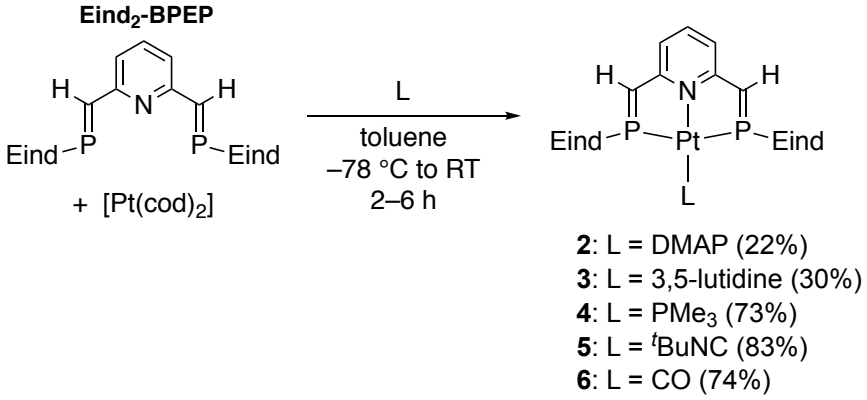

Scheme 2. Synthesis of Pt(0) $Eind_2$-BPEP complexes **2**–**6**.

Results and Discussion

Synthesis and X-Ray Structures of [Pt(L)($Eind_2$-BPEP)]. Complexes **2**–**6** listed in Scheme 2 were prepared by the reactions of $[Pt(cod)_2]$ with $Eind_2$-BPEP and L in toluene. In this case, there was a tendency that $[Pt(cod)_2]$ reacts with $Eind_2$-BPEP without participation of L, leading to a low product yield. The author therefore mixed the three components at a low temperature of –78 °C and gradually warmed to room temperature to complete the reaction. Complexes **4**–**6** attained the isolated yields of 73–83% with this protocol, whereas **2** and **3**

with pyridine derivatives remained in low yields (22 and 30%). Nonetheless, all complexes were isolated as crystalline solids and identified by NMR spectroscopy and elemental analysis. Moreover, the crystal structures of **3**–**6** were examined by X-ray diffraction analysis.

Figure 1 presents the X-ray structures. Selected bond lengths and angles are given in Table 1, together with the ^{31}P NMR data for **1**–**6**. It is seen that complexes **3**–**6** adopt a slightly distorted square planar configuration around Pt; the τ_4 values derived from P1–Pt–P2 and N–Pt–L angles are 0.21 (**3**), 0.20 (**4**), 0.20 (**5**), and 0.27 (**6**), respectively. The slightly large τ_4 value of CO complex **6** is mainly due to the bent N–Pt–CO bond (168.2°) relative to the other N–Pt–L bonds (173.6–175.5°). The P1–C1 and P2–C2 bonds (1.699(10)–1.715(5) Å) are longer than normal P=C bonds (1.66–1.68 Å).[6,7] This elongation along with decreasing double bond character causes pyramidalization at the phosphorus atoms; the sum of the three angles around P1 and P2 atoms of each complex is as follows: 353.4 and 352.7°(**3**); 351.6 and 347.6° (**4**); 353.4 and 354.4° (**5**); 352.0 and 348.3° (**6**).

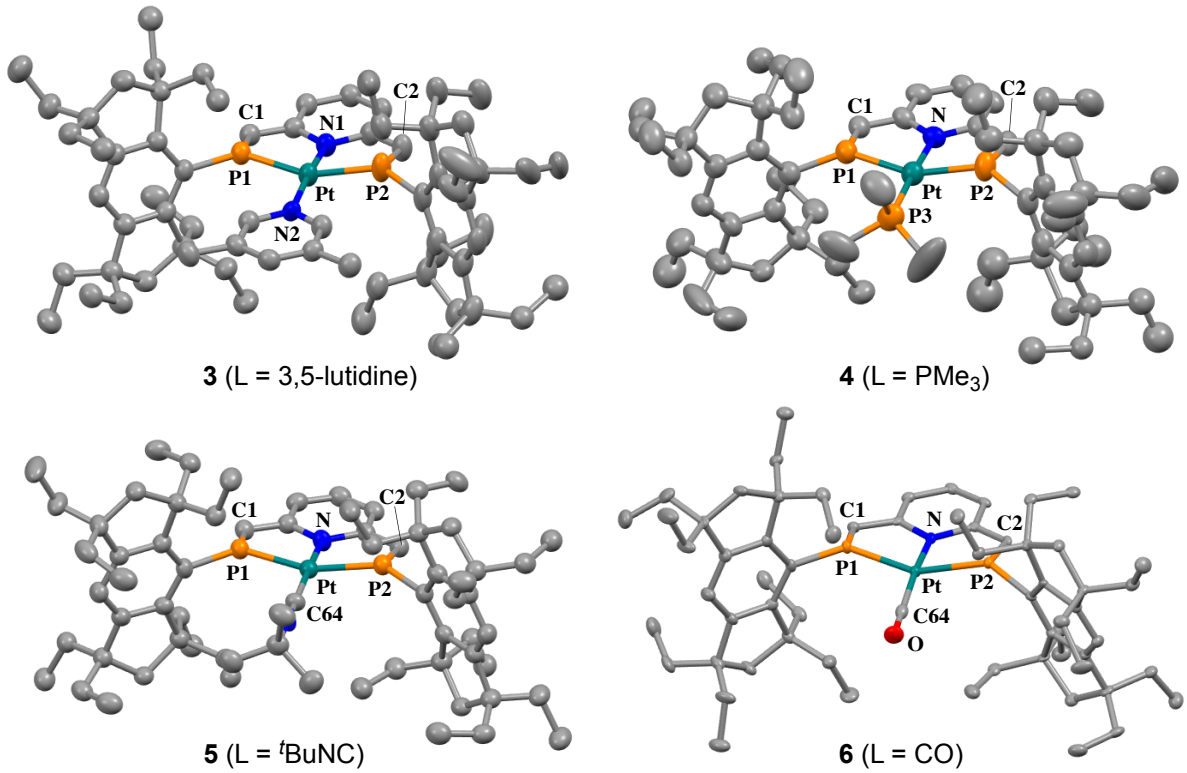

Figure 1. Molecular structures of **3**–**6** with 50% probability ellipsoids. Hydrogen atoms and disordered carbon atoms on Eind groups are omitted for clarity.

Table 1. ^{31}P NMR Data and Selected Bond Distances (Å) and Angles (°) for [Pt(L)(Eind$_2$-BPEP)] (**2**–**6**) [a]

complex (L)	δ_P ($^1J_{PtP}$, Hz)[b]	Pt–P1	Pt–P2	Pt–N	Pt–L	P1–C1	P2–C2	P1–M–P2	N–M–L	τ_4
3 (3,5-lutidine)	98.2 (1950)	2.271(1)	2.270(1)	2.045(4)	2.093(4)	1.707(5)	1.711(5)	155.80(5)	174.3(1)	0.21
4 (PMe_3)	101.2 (1883)	2.282(3)	2.280(3)	2.091(7)	2.242(3)	1.70(1)	1.71(1)	156.2(1)	175.5(2)	0.20
5 (^{t}BuNC)	110.5 (1977)	2.255(1)	2.258(1)	2.046(4)	1.919(6)	1.713(6)	1.715(6)	158.70(6)	173.6(2)	0.20
6 (CO)	127.3 (1745)	2.285(1)	2.288(1)	2.053(4)	1.854(5)	1.706(5)	1.715(5)	153.53(4)	168.2(2)	0.27

[a] See Figure 1 for the atom numbering. [b] ^{31}P NMR data for Eind$_2$-BPEP ligand in THF-d_8 at 25 °C. **1** (L = PPh_3): δ_p = 105.6 ($^1J_{PtP}$ = 1594 Hz). **2** (L = DMAP): δ_p = 95.1 ($^1J_{PtP}$ = 1817 Hz).

As the author pointed out for **1** (δ_P = 105.6) in Chapter 4,[3] such pyramidalization enhances the s character of lone-pair orbitals of phosphorus atoms, thereby causing a diamagnetic shift of the ^{31}P NMR signal.[8] Thus, the signals of **2**–**6** appeared remarkably upfield (δ_P = 95.1–127.3 ppm), compared with those of ordinary phosphaalkene complexes (δ_P = 220–260 ppm). The upfield shift tends to be reduced as the π-accepting ability of L increases. On the other hand, the $^1J_{PtP}$ coupling constants did not correlate with the electronic properties of L, but correlated linearly with the averaged Pt–P bond lengths (r = 0.96), where the bond lengths were extended with increasing steric congestion among the ligands.

DFT Calculations. The author has found a clear dependence of the ^{31}P NMR chemical shifts of **1**–**6** on the π-accepting ability of L. On the other hand, while CO complex **6** having the strongest π-acceptor among tested was more distorted than the others (τ_4 = 0.27), the coordination geometry of **3**–**5** was comparable to one another (τ_4 = 0.20–0.21). It is probable that the complex structures with bulky Eind groups are largely affected by steric demand of L. For example, although pyridine-based ligands generally adopt a vertical orientation against the coordination plane, the 3,5-lutidine ligand in **3** is oriented in parallel to fit the space between the two Eind groups. Accordingly, to evaluate the electronic effects of L under minimized steric conditions, the author next carried out DFT calculations for simple models of **3**, **4**, and **6** (**3**^{sm}, **4**^{sm}, and **6**^{sm}, respectively), in which the Eind groups were replaced with H atoms and the 3,5-lutidine ligand in **3** was replaced with pyridine. The author adopted the PBE1PBE functional and the SDD (Pt) and 6-311G(d,p) (other atoms) basis sets based on preliminary screening for **6**^{sm} (see the Experimental Section).

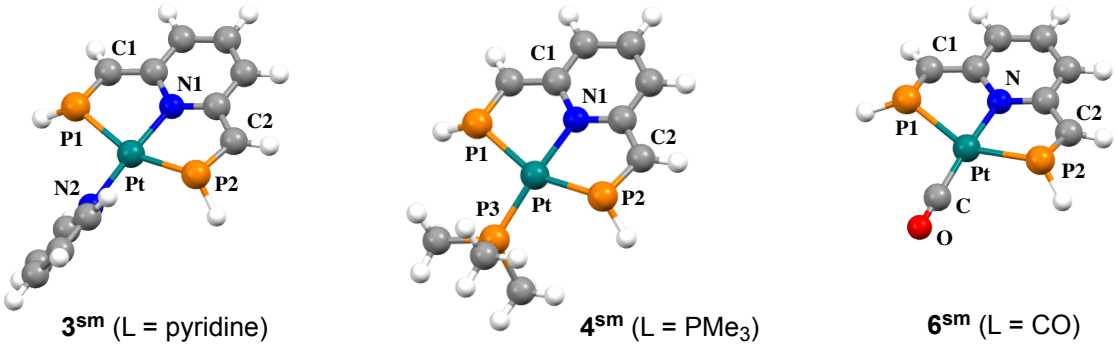

3^{sm} (L = pyridine) **4**^{sm} (L = PMe_3) **6**^{sm} (L = CO)

Figure 2. Optimized structures of **3**^{sm}, **4**^{sm}, and **6**^{sm}.

Table 2. Selected Bond Distances (Å) and Angles (°) for Optimized Structures of [Pt(L)(BPEP)] (**3**^{sm}, **4**^{sm}, **6**^{sm}) [a]

complex (L)	Pt−P1	Pt–P2	Pt–N	Pt–L	P1–C1	P2–C2	P1–Pt–P2	N–Pt–L	τ_4
3^{sm} (pyridine)	2.327	2.325	2.036	2.067	1.728	1.742	158.946	174.245	0.19
4^{sm} (PMe_3)	2.320	2.322	2.085	2.253	1.734	1.734	155.770	171.452	0.23
6^{sm} (CO)	2.345	2.345	2.074	1.860	1.728	1.729	152.558	167.661	0.28

[a] See Figure 2 for the atom numbering.

Figure 2 shows the optimized structures, and Table 2 lists the selected bond lengths and angles. Although the Pt–P and P=C bond lengths were somewhat longer than those of the X-ray structures, the coordination geometry of **6** (τ_4 = 0.27) was successfully reproduced for **6**^{sm} (τ_4 = 0.28). It is reasonable that the core structure of **6** bearing the compact CO ligand is little affected by bulky Eind groups and therefore reproducible with the simple model **6**^{sm}. On the other hand, although complexes **3** and **4** adopted nearly the same τ_4 values in the X-ray structures, their simple models **3**^{sm} (τ_4 = 0.19) and **4**^{sm} (τ_4 = 0.23) adopted clearly different τ_4 values from each other. As seen from the optimized structure in Figure 2, the pyridine ligand in **3**^{sm} is significantly twisted against the coordination plane, unlike the parallel orientation of the 3,5-lutidine ligand in **3**, and this change is very likely to be caused by release from the steric constraints of the Eind groups. Thus, the author may consider that the geometrical variations observed in the simple models mainly reflect the difference in electronic properties of L. In fact, the τ_4 values increase with increasing π-accepting ability of L [0.19 (**3**^{sm}) < 0.23 (**4**^{sm}) < 0.28 (**6**^{sm})], and this order is in accord with the decreasing order of the upfield shifts of ^{31}P NMR signals.

Figure 3 compares the energy changes for **3**^{sm} and **6**^{sm} as a function of the N–Pt–L angle, where the molecular geometry at each data point was optimized with a fixed N–Pt–L angle.

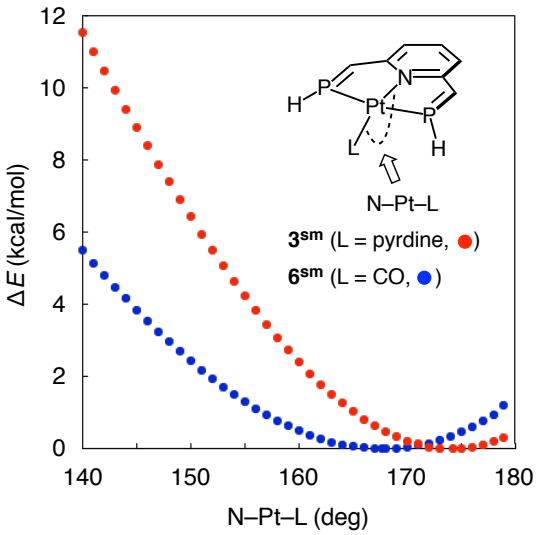

Figure 3. Dependence of potential energy on the N–Pt–L angle (deg) for **3**^{sm} and **6**^{sm}.

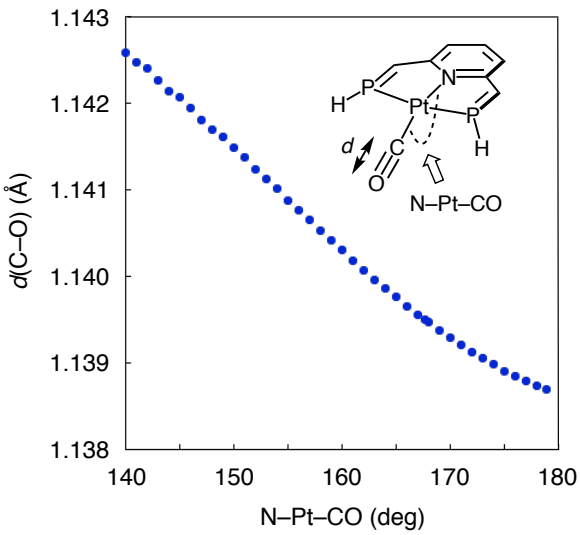

Figure 4. Dependence of CO bond length (Å) on the N–Pt–CO angle (deg) for **6**^{sm}.

The potential energy of pyridine complex **3**^{sm} significantly lowers with an increase in the N–Pt–pyridine angle, and becomes nearly constant above 170°. On the other hand, the potential energy of CO complex **6**^{sm} is clearly less sensitive to the change of N–Pt–CO angle, and remains lower than 1.3 kcal/mol over the range of 155–180°. Since the CO bond length is extended as the N–Pt–CO angle decreases as shown in Figure 4, the relatively flexible nature of **6**^{sm} toward geometrical distortion is due to the occurrence of π-back-donation to the CO ligand. In this case, since complex **6**^{sm} achieves the energy minimum at a relatively wide N–Pt–CO angle of 167.7° despite the continuous elongation of the CO bond, the potential energy is dictated by the balance between the instability arising from the geometrical distortion and the stability derived from the π-back-bonding. Thus, we may conclude that the $Eind_2$-BPEP complexes of Pt(0) possess a distinct tendency to adopt a highly planar coordination geometry by nature, but π-accepting ligands such as CO partially compensate for the instability derived from geometrical distortion.

The Origin of the Square Planar Configuration. Figure 5 compares the frontier orbitals of **3**^{sm} and **6**^{sm}. For both complexes, the HOMO and LUMO are roughly assigned to in-phase and out-of-phase π* orbitals of the BPEP ligand, respectively, although the HOMO contains orbital components of the metal (Pt) to a certain extent (ca. 15%). On the other hand, the LUMO(+3) of **3**^{sm} and LUMO(+1) of **6**^{sm} are assignable to σ* orbitals between Pt(d_{x2-y2}) and ligands. Moreover, the LUMO(+1) and LUMO(+2) of **3**^{sm} are mainly composed of π* orbitals of the pyridine ligand.

The most remarkable feature is the major contribution of the in-phase π* orbital of BPEP to the HOMO. As a result, the Mayer bond orders of P=C bonds were significantly reduced: 1.31 and 1.24 for **3**^{sm}; 1.31 and 1.31 for **6**^{sm}. Furthermore, the configurations around P1 and P2 atoms were pyramidalized as already pointed out for the X-ray structures in Figure 1. These structural variations in the BPEP ligand may be described with canonical structures **A**–**C** in Scheme 3, where **A** with two P=C bonds is assignable to an L_3 type ligand, whereas **B** and **C** with a dearomatized pyridine unit are ascribed to LX_2 type ligands. The BPEP ligand in **3**^{sm} and **6**^{sm} involve major contributions of **B** and **C**.

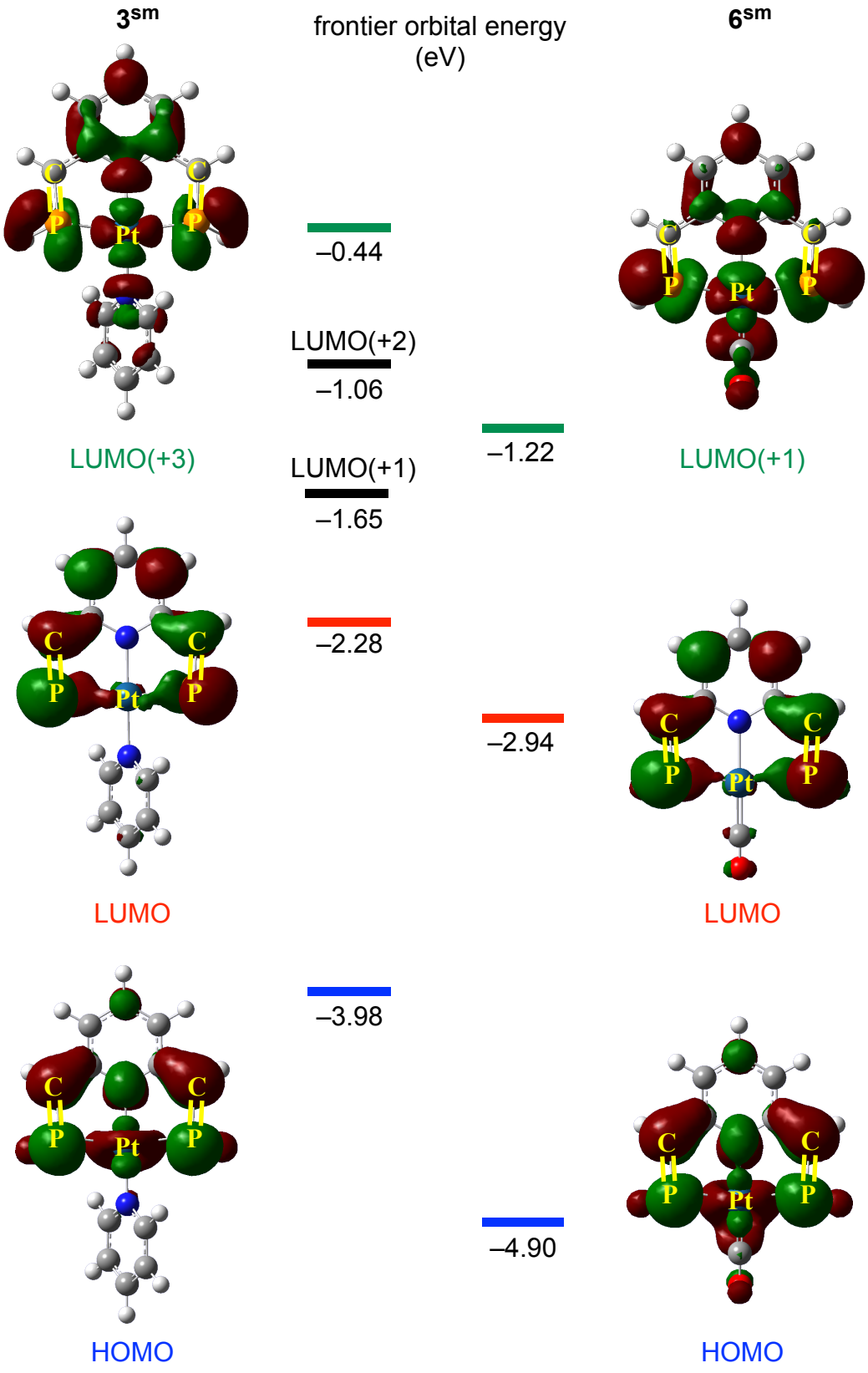

Figure 5. Comparison of frontier orbitals between **3**^{sm} and **6**^{sm}.

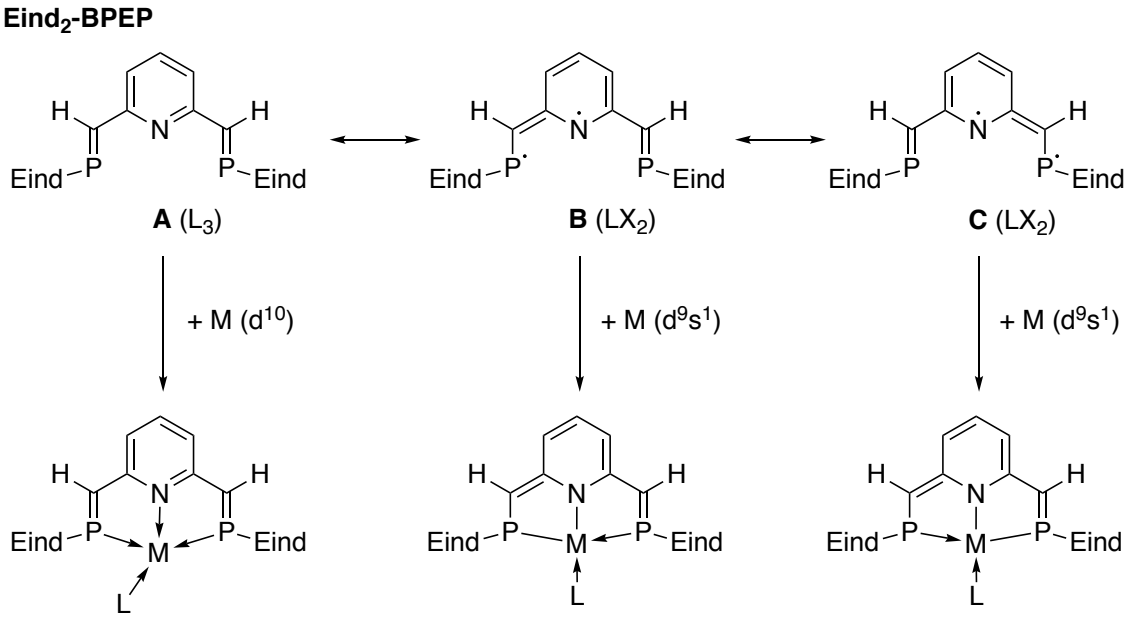

Scheme 3. A valence bond description for the bonding between $Eind_2$-BPEP and metals with d^{10} and d^9s^1 electron configurations.

On the other hand, similarly to [$Pt(PPh_3)$($Eind_2$-BPEP)] (**1**), the Pt centers of $\mathbf{3}^{sm}$ and $\mathbf{6}^{sm}$ undergo strong s-d hybridization through relativistic effects. The electron configurations estimated by NBO analysis are [6s(0.64) + 5d(8.99)] and [6s(0.69) + 5d(8.98)] for $\mathbf{3}^{sm}$ and $\mathbf{6}^{sm}$, respectively, and this situation was unchanged for the whole model of CO complex **6** [6s(0.65) + 5d(8.97)]. Thus, the BPEP complexes possess a d^9s^1 center instead of a d^{10} center, and this electron configuration is suitable for combining with the canonical structures **B** and **C** in Scheme 3, as illustrated with a valence bond description. It should be noted that, although the complexes have nearly 10 valence electrons on the Pt center, this bonding scheme resembles that of a d^8 complex rather than a d^{10} complex. In this case, the coordination geometry will be controlled by the shape and orientation of the d_{x2-y2} orbital, which is partially unoccupied due to s-d hybridization. The major contribution of the d_{x2-y2} orbital to metal–ligand σ bonds is reflected in the large distribution of this atomic orbital in the metal–ligand σ* orbitals (i.e., LUMO(+3) of $\mathbf{3}^{sm}$ and LUMO(+1) of $\mathbf{6}^{sm}$ in Figure 5).

UV-vis-NIR spectroscopy. The $Eind_2$-BPEP complexes displayed strong absorption in a near infrared region, exhibiting a very deep color in solution as well as in the solid (Figure 6).

The λ_{max} (nm) and ε (M^{-1} cm^{-1}) values of each complex in THF at room temperature are as follows: 924, 10023 (**2**); 907, 9739 (**3**); 845, 10493 (**4**); 825, 11744 (**5**); 776, 12329 (**6**). These absorption bands assignable to the HOMO–LUMO transitions were shifted to a shorter wavelength as the π-accepting ability of L increased. As seen from Figure 5, while the CO ligand lowers both of the HOMO and LUMO levels, the HOMO with a relatively large contribution of metal orbitals changes more remarkably than the LUMO. Thus, replacement of the pyridine ligand with CO results in a hypsochromic shift of the absorption.

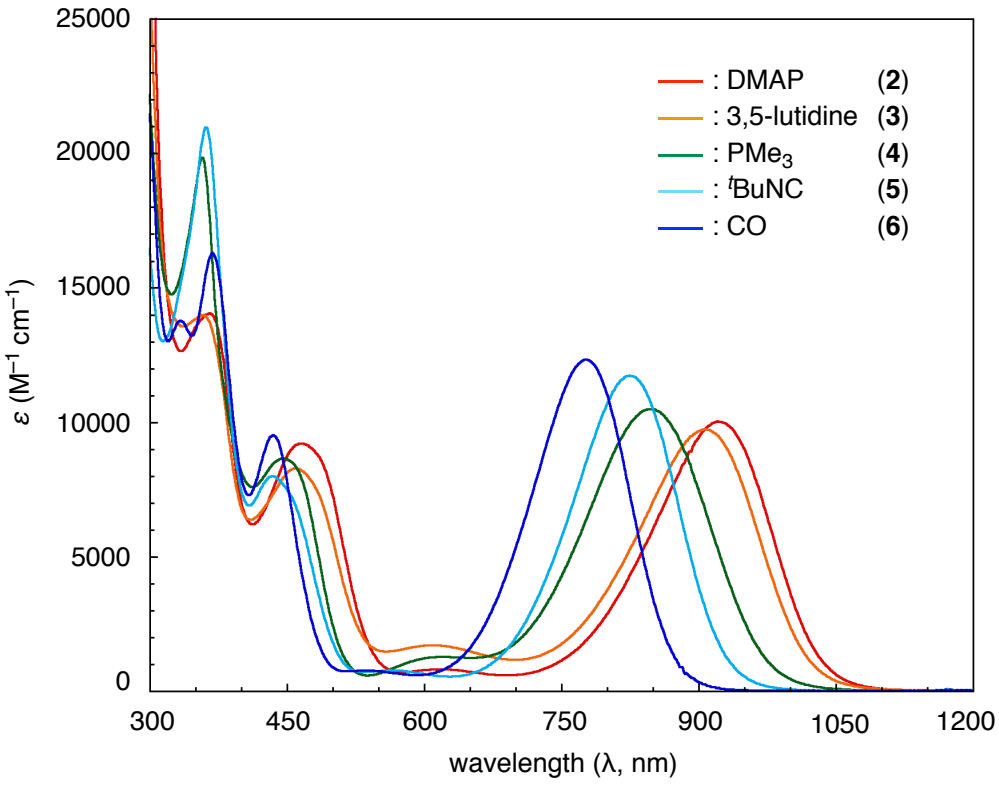

Figure 6. UV-vis-NIR spectra of [Pt(L)(Eind$_2$-BPEP)] (**2**–**6**) in THF at room temperature.

Conclusion

The author has confirmed that [Pt(L)(Eind$_2$-BPEP)] complexes (**2**–**6**) possess a distinct tendency to adopt a planar configuration around Pt irrespective of the electronic properties of L. While the CO ligand with a strong π-accepting ability makes the complex flexible toward distortion, the X-ray structure of **6** and the optimized structure of $\mathbf{6}^{sm}$ preserve the planarity around Pt. The highly adaptable electronic structure of the Eind$_2$-BPEP ligand and the strong

s-d hybridization on the Pt(0) center through relativistic effects have emerged as crucial reasons for the unusual coordination structures. On the other hand, π-accepting ligands significantly affect the HOMO levels of the complexes. Accordingly, complexes **2**–**6** display notable color variation in the near-infrared region depending on the electronic properties of L.

Experimental Section

General Considerations. All manipulations were performed under a nitrogen atmosphere using a glove box and Schlenk techniques. The compounds $Eind_2$-BPEP[3] and $[Pt(cod)_2]$[9] were prepared according to the literature. The other chemicals were obtained from commercial sources. NMR spectra were recorded on a 400 MHz spectrometer. Chemical shifts are reported in δ (ppm), referenced to ^{1}H (residual) and ^{13}C signals of deuterated solvents as internal standards or to the ^{31}P signal of 85% H_3PO_4 and the ^{135}Pt signal of K_2PtCl_4 as external standards. The assignments of ^{13}C signals were based on DEPT and HMQC experiments. Elemental analysis was performed by ICR Analytical Laboratory, Kyoto University.

Synthesis of Complexes 2–6. A typical procedure is reported for [Pt(DMAP)($Eind_2$-BPEP)] (**2**). A cold toluene (3.0 mL) was added to a Schlenk tube containing $Eind_2$-BPEP (37.1 mg, 0.040 mmol), $[Pt(cod)_2]$ (16.5 mg, 0.040 mmol), and 4-(*N*,*N*-dimethylamino)-pyridine (DMAP, 5.4 mg, 0.044 mmol) at –78 °C. The mixture was stirred at the same temperature for 5 min, and then gradually warmed to room temperature. The color of the reaction solution changed from dark-green to dark-brown within 30 min. After stirring for 4 h at room temperature, the solvent was removed under reduced pressure. The residue was dissolved in THF (1 mL) and filtrated through a Celite pad to remove an insoluble solid. The filtrate was concentrated to almost dryness under reduced pressure, and pentane (0.3 mL) was layered over the residue. This system was allowed to stand at –35 °C overnight to form a dark-brown solid, which was collected by filtration, washed with pentane (0.3 mL × 5), and dried in vacuo (17.4 mg, 0.014 mmol, 35%). The crude product was recrystallized from THF/pentane at room temperature to give **2** as a dark-brown crystalline solid (11.2 mg, 0.0088 mmol, 22%). Complexes **3**–**6** were similarly prepared and isolated as crystalline solids

in 30, 73, 83, and 74% yields, respectively.

[2]: ^{1}H NMR (THF-d_8, 25 °C): δ 8.27 (d, $^{3}J_{HH}$ = 7.2 Hz, 2H, 2,6-DMAP), 7.61 (br d, $^{3}J_{HH}$ = 6.8 Hz, 2H, 3,5-Py), 7.52 (br, 1H, 4-Py), 7.37 (br, 2H, P=C*H*), 6.80 (s, 2H, *p*-Eind), 6.06 (d, $^{3}J_{HH}$ = 7.2 Hz, 2H, 3,5-DMAP), 2.89 (s. 6H, N(CH_3)$_2$), 2.43 (dq, $^{2}J_{HH}$ = 13.7 Hz, $^{3}J_{HH}$ = 7.2 Hz, 4H, CH_2CH$_3$), 2.27 (dq, $^{2}J_{HH}$ = 13.9 Hz, $^{3}J_{HH}$ = 7.2 Hz, 4H, CH_2CH$_3$), 1.81 (d, $^{2}J_{HH}$ = 13.9 Hz, 4H, ind-CH_2), 1.75 (d, $^{2}J_{HH}$ = 13.9 Hz, 4H, ind-CH_2), 1.68–1.47 (m, 20H, CH_2CH$_3$), 0.88 (t, $^{3}J_{HH}$ = 7.2 Hz, 12H, CH$_2$CH_3), 0.83 (t, $^{3}J_{HH}$ = 7.2 Hz, 12H, CH$_2$CH_3), 0.77 (t, $^{3}J_{HH}$ = 7.2 Hz, 12H, CH$_2$CH_3), 0.53 (t, $^{3}J_{HH}$ = 7.2 Hz, 12H, CH$_2$CH_3). ^{1}H–^{1}H COSY experiments showed the overlap of four methylene protons of CH_2CH$_3$ with the ^{1}H NMR signals of ind-CH_2. ^{13}C{^{1}H} NMR (THF-d_8, 25 °C): δ 156.1, (s, 2,6-DMAP), 153.7 (s), 152.7 (s), 150.3 (s), 147.8 (s), 134.3 (br), 125.8 (br, P=*C*H), 121.6 (s, *p*-Eind), 121.3 (br, 3,5-Py), 117.5 (br, 4-Py), 107.8 (s, 3,5-DMAP), 54.3 (s), 47.9 (s), 43.4 (s, ind-*C*H$_2$), 38.7 (s, N(*C*H$_3$)$_2$), 34.5 (s, *C*H$_2$CH$_3$), 34.1 (s, *C*H$_2$CH$_3$), 33.6 (s, *C*H$_2$CH$_3$), 33.1 (s, *C*H$_2$CH$_3$), 10.6 (s, CH$_2$*C*H$_3$), 9.9 (s, CH$_2$*C*H$_3$), 9.5 (s, CH$_2$*C*H$_3$), 9.3 (s, CH$_2$*C*H$_3$). ^{31}P{^{1}H} NMR (THF-d_8, 25 °C): δ 95.1 (s, $^{1}J_{PtP}$ = 1814 Hz). ^{195}Pt NMR (THF-d_8, 25 °C): δ –3295.0 (t, $^{1}J_{PtP}$ = 1814 Hz). UV-vis-NIR spectra: λ_{max} (ε) = 365 (14043), 466 (9207), 614 (816), 924 (10023). Anal. Calcd for $C_{70}H_{105}N_3P_2Pt$: C, 67.50; H, 8.50; N, 3.37. Found: C, 67.44; H, 8.59; N, 3.38.

[3]: ^{1}H NMR (THF-d_8, 25 °C): δ 8.66 (br s, 2H, $^{3}J_{PtH}$ = 34.7 Hz, 2,6-lutidine), 7.70 (br d, 2H, $^{3}J_{HH}$ = 7.4 Hz, 3,5-Py), 7.57–7.54 (m, 3H, 4-Py + P=C*H*), 7.23 (br s, 1H, 4-lutidine), 6.87 (s, 2H, *p*-Eind), 2.65 (dq, $^{2}J_{HH}$ = 13.7 Hz, $^{3}J_{HH}$ = 7.1 Hz, 4H, CH_2CH$_3$), 2.24 (dq, $^{2}J_{HH}$ = 13.7 Hz, $^{3}J_{HH}$ = 7.1 Hz, 4H, CH_2CH$_3$), 1.91 (s, 6H, 3,5-(CH_3)$_2$ of lutidine), 1.85 (d, $^{2}J_{HH}$ = 14.0 Hz, 4H, ind-CH_2), 1.80–1.75 (m, 4H, CH_2CH$_3$), 1.77 (d, $^{2}J_{HH}$ = 14.0 Hz, 4H, ind-CH_2), 1.67–1.39 (m, 20H, CH_2CH$_3$), 0.88 (t, $^{3}J_{HH}$ = 7.3 Hz, 12H, CH$_2$CH_3), 0.85 (t, $^{3}J_{HH}$ = 7.5 Hz, 12H, CH$_2$CH_3), 0.82 (t, $^{3}J_{HH}$ = 7.2 Hz, 12H, CH$_2$CH_3), 0.53 (t, $^{3}J_{HH}$ = 7.3 Hz, 12H, CH$_2$CH_3). ^{13}C{^{1}H} NMR (THF-d_8, 25 °C): δ 155.3 (s, 2,6-lutidine), 153.3 (br), 150.7 (s), 147.7 (br), 137.8 (s, 4-lutidine), 135.8 (s), 133.1 (br), 125.3 (br, P=*C*H), 122.3 (s, *p*-Eind), 121.3 (br, 3,5-Py), 117.7 (s, 4-Py), 54.5 (s), 48.0 (s), 43.3 (s, ind-*C*H$_2$), 35.0 (s, *C*H$_2$CH$_3$), 34.5 (s, *C*H$_2$CH$_3$), 33.2 (s, *C*H$_2$CH$_3$), 32.7 (s, *C*H$_2$CH$_3$), 18.1 (s, 3,5-(*C*H$_3$)$_2$ of lutidine), 10.7 (s, CH$_2$*C*H$_3$), 9.7 (s, CH$_2$*C*H$_3$), 9.5 (s, CH$_2$*C*H$_3$), 9.4 (s, CH$_2$*C*H$_3$). ^{31}P{^{1}H} NMR (THF-d_8, 25 °C): δ 98.2 (s, $^{1}J_{PtP}$ = 1950 Hz). ^{195}Pt NMR (THF-d_8, 25 °C): δ –3263.0 (t, $^{1}J_{PtP}$ = 1950 Hz). UV-vis-NIR spectra:

λ_{max} (ε) = 358 (13979), 460 (8297), 610 (1707), 907 (9739). Anal. Calcd for $C_{70}H_{104}N_2P_2Pt$: C, 68.32; H, 8.52; N, 2.28. Found: C, 68.03; H, 8.55; N, 2.22.

[4]: ^{1}H NMR (THF-d_8, 25 °C): δ 8.03–8.01 (m, 4H, 3,5-Py + P=C*H*), 7.60 (br, 1H, 4-Py), 6.91 (s, 2H, *p*-Eind), 3.10 (dq, $^2J_{HH}$ = 13.3 Hz, $^3J_{HH}$ = 7.2 Hz, 4H, C*H*$_2$CH$_3$), 2.19 (dq, $^2J_{HH}$ = 13.9 Hz, $^3J_{HH}$ = 7.2 Hz, 4H, C*H*$_2$CH$_3$), 1.91 (d, $^2J_{HH}$ = 13.9 Hz, 4H, ind-C*H*$_2$), 1.82 (dq, $^2J_{HH}$ = 14.0 Hz, $^3J_{HH}$ = 7.2 Hz, 4H, C*H*$_2$CH$_3$), 1.79 (d, $^2J_{HH}$ = 13.9 Hz, 4H, ind-C*H*$_2$), 1.70–1.58 (m, 16H, C*H*$_2$CH$_3$), 1.39 (d, $^2J_{PH}$ = 10.3 Hz, 9H, P(C*H*$_3$)$_3$), 0.91 (t, $^3J_{HH}$ = 7.2 Hz, 12H, CH$_2$C*H*$_3$), 0.84 (t, $^3J_{HH}$ = 7.2 Hz, 12H, CH$_2$C*H*$_3$), 0.81 (t, $^3J_{HH}$ = 7.2 Hz, 12H, CH$_2$C*H*$_3$), 0.66 (t, $^3J_{HH}$ = 7.2 Hz, 12H, CH$_2$C*H*$_3$). ^{1}H–^{1}H COSY experiments showed the overlap of four methylene protons of C*H*$_2$CH$_3$ with the ^{1}H NMR signals of P(C*H*$_3$)$_3$. ^{13}C{^{1}H} NMR (THF-d_8, 25 °C): δ 153.1 (s), 150.7 (s), 148.6 (s), 132.9 (br), 124.7 (br, P=*C*H), 122.6 (s, *p*-Eind), 119.0 (br, 3,4- and 5-Py), 54.6 (s), 48.3 (s), 42.7 (s, ind-*C*H$_2$), 35.8 (s, *C*H$_2$CH$_3$), 35.4 (s, *C*H$_2$CH$_3$), 32.9 (s, *C*H$_2$CH$_3$), 32.5 (s, *C*H$_2$CH$_3$), 20.6 (d, $^1J_{PC}$ = 38 Hz, P(*C*H$_3$)$_3$), 10.5 (s, CH$_2$*C*H$_3$), 9.5 (s, CH$_2$*C*H$_3$), 9.4 (s, CH$_2$*C*H$_3$), 9.3 (s, CH$_2$*C*H$_3$). HMQC experiments showed the overlap of the 3,5-posidition carbon atoms of pyridine unit with the ^{13}C{^{1}H} NMR signal of 4-position carbon atom of pyridine unit at δ 119.0 ppm. ^{31}P{^{1}H} NMR (THF-d_8, 25 °C): δ 101.2 (d, $^2J_{PP}$ = 26 Hz, $^1J_{PtP}$ = 1883 Hz, *P*=CH), –44.5 (t, $^2J_{PP}$ = 26 Hz, $^1J_{PtP}$ = 3703 Hz, *P*Me$_3$). ^{195}Pt NMR (THF-d_8, 25 °C): δ –4532.0 (dt, $^1J_{PtP}$ = 1883 and 3703 Hz). UV-vis-NIR spectra: λ_{max} (ε) = 357 (19837), 446 (8656), 622 (1278), 845 (10493). Anal. Calcd for $C_{66}H_{104}NP_3Pt$: C, 66.08; H, 8.74; N, 1.17. Found: C, 66.03; H, 8.77; N, 1.23.

[5]: ^{1}H NMR (THF-d_8, 25 °C): δ 8.05–7.96 (m, 4H, 3,5-Py + P=C*H*), 7.56 (vt, J_{app} = 6.4 Hz, 1H, 4-Py), 6.93 (s, 2H, *p*-Eind), 2.58 (dq, $^2J_{HH}$ = 13.6 Hz, $^3J_{HH}$ = 7.3 Hz, 4H, C*H*$_2$CH$_3$), 1.98 (dq, $^2J_{HH}$ = 13.2 Hz, $^3J_{HH}$ = 7.3 Hz, 8H, C*H*$_2$CH$_3$), 1.91 (d, $^2J_{HH}$ = 14.0 Hz, 4H, ind-C*H*$_2$), 1.85 (d, $^2J_{HH}$ = 14.0 Hz, 4H, ind-C*H*$_2$), 1.81–1.57 (m, 20H, C*H*$_2$CH$_3$), 1.15 (s, 9H, (C*H*$_3$)$_3$NC), 0.92 (t, $^3J_{HH}$ = 7.3 Hz, 12H, CH$_2$C*H*$_3$), 0.87 (t, $^3J_{HH}$ = 7.4 Hz, 12H, CH$_2$C*H*$_3$), 0.83 (t, $^3J_{HH}$ = 7.3 Hz, 12H, CH$_2$C*H*$_3$), 0.76 (t, $^3J_{HH}$ = 7.3 Hz, 12H, CH$_2$C*H*$_3$). ^{13}C{^{1}H} NMR (THF-d$_8$, 25 °C): δ 153.9 (s), 150.3 (s), 148.7 (s), 130.8 (br), 125.1 (br, P=*C*H), 123.2 (s, *p*-Eind), 118.9 (br, 3,5-Py), 118.5 (br, 4-Py), 57.8 (s), 54.6 (s), 48.1 (s), 43.1 (s, ind-*C*H$_2$), 34.4 (s, *C*H$_2$CH$_3$), 34.2 (s, *C*H$_2$CH$_3$), 33.6 (s, *C*H$_2$CH$_3$), 30.4 (s, (*C*H$_3$)$_3$NC), 10.53 (s, CH$_2$*C*H$_3$), 10.52 (s, CH$_2$*C*H$_3$), 9.50 (s, CH$_2$*C*H$_3$), 9.46 (s, CH$_2$*C*H$_3$). The ^{13}C{^{1}H} NMR signal of *tert*-butyl

isocyanide (^{t}BuN*C*) was not observed. $^{31}P\{^1H\}$ NMR (THF-d_8, 25 °C): δ 110.5 (s, $^1J_{PtP}$ = 1977 Hz). ^{195}Pt NMR (THF-d_8, 25 °C): δ –4492.1 (t, $^1J_{PtP}$ = 1977 Hz). UV-vis-NIR spectra: λ_{max} (ε) = 362 (20958), 434 (7998), 825 (11744). IR (Nujol): ν(CN) 2165 cm^{-1}. Anal. Calcd for $C_{68}H_{104}N_2P_2Pt$: C, 67.69; H, 8.69; N, 2.32. Found: C, 67.64; H, 8.78; N, 2.29.

[6]: ^1H NMR (THF-d_8, 25 °C): δ 8.31 (s, 2H, P=C*H*), 8.26 (m, 2H, 3,5-Py), 7.72 (t, $^3J_{HH}$ = 7.6 Hz, 1H, 4-Py), 7.01 (s, 2H, *p*-Eind), 2.25 (dq, $^2J_{HH}$ = 13.9 Hz, $^3J_{HH}$ = 7.3 Hz, 4H, C*H*$_2$CH$_3$), 2.04 (dq, $^2J_{HH}$ = 13.9 Hz, $^3J_{HH}$ = 7.3 Hz, 4H, C*H*$_2$CH$_3$), 1.92 (d, $^2J_{HH}$ = 14.2 Hz, 4H, ind-C*H*$_2$), 1.88 (d, $^2J_{HH}$ = 14.2 Hz, 4H, ind-C*H*$_2$), 1.83–1.60 (m, 24H, C*H*$_2$CH$_3$), 0.94 (t, $^3J_{HH}$ = 7.3 Hz, 12H, CH$_2$C*H*$_3$), 0.89 (t, $^3J_{HH}$ = 7.3 Hz, 12H, CH$_2$C*H*$_3$), 0.81 (t, $^3J_{HH}$ = 7.3 Hz, 12H, CH$_2$C*H*$_3$), 0.76 (t, $^3J_{HH}$ = 7.3 Hz, 12H, CH$_2$C*H*$_3$). $^{13}C\{^1H\}$ NMR (THF-d_8, 25 °C): δ 181.8 (br, *C*O), 153.5 (s), 151.2 (s), 148.9 (br), 131.3 (t, J_{PC} = 13 Hz, P=*C*H), 130.1 (t, J_{PC} = 12 Hz), 124.0 (s, *p*-Eind), 120.9 (t, $^3J_{PC}$ = 15 Hz, 3,5-Py), 120.8 (s, 4-Py), 54.8 (s), 48.1 (s), 43.4 (s, ind-*C*H$_2$), 35.6 (s, *C*H$_2$CH$_3$), 34.3 (s, *C*H$_2$CH$_3$), 34.0 (s, *C*H$_2$CH$_3$), 33.5 (s, *C*H$_2$CH$_3$), 10.5 (s, CH$_2$*C*H$_3$), 10.4 (s, CH$_2$*C*H$_3$), 9.48 (s, CH$_2$*C*H$_3$), 9.45 (s, CH$_2$*C*H$_3$). $^{31}P\{^1H\}$ NMR (THF-d_8, 25 °C): δ 127.3 (s, $^1J_{PtP}$ = 1745 Hz). ^{195}Pt NMR (THF-d_8, 25 °C): δ –4624.8 (t, $^1J_{PtP}$ = 1745 Hz). UV-vis-NIR spectra: λ_{max} (ε) = 369 (16289), 435 (9518), 776 (12329). IR (Nujol): ν(CO) 2018 cm^{-1}. Anal. Calcd for $C_{64}H_{95}NOP_2Pt$: C, 66.72; H, 8.32; N, 1.22. Found: C, 66.75; H, 8.32; N, 1.30.

X-ray Crystal Structure Determination. Single crystals of **3**–**6** suitable for X-ray diffraction analysis were grown from a mixed solvent of THF and pentane (ca. 1:5) at room temperature. The intensity data were collected at 103 K on a Rigaku Saturn70 CCD diffractometer with the VariMax Optic, using Mo Kα radiation (λ = 0.71075 Å). The intensity data were corrected for Lorentz and polarization effects and for absorption (multiscan[10]). The structures were solved by direct methods (SHELXS-97)[11] and refined by least-squares calculations on F^2 (SHELXL-97)[11] using Yadokari-XG 2009.[12] Non-hydrogen atoms, except for solvent molecules and disordered atoms, were refined anisotropically. Hydrogen atoms were placed at calculated positions, and included in calculations without refinement of their parameters. The crystallographic data and the summary of solution and refinement are listed in Table 3.

Computational Details. DFT calculations were performed with the Gaussian 09 program.[13] First of all, the structure of $\mathbf{6}^{sm}$ as the simple model of CO complex **6** was examined using the B3LYP functional and the LANL2DZ (Pt) and 6-31G(d) (other atoms) basis sets; however, notable elongation of the Pt–P and P=C bonds in the optimized structure was observed. Thus, the author compared the structures optimized with several DFT methods as summarized in Table 4, and selected the PBE1PBE functional[14] and the SDD (Pt) and 6-311G(d,p) (other atoms) basis sets for further theoretical investigations.

Table 4. Comparison of Bond Distances (Å) and Angles (°) for [Pt(CO)(BPEP)] ($\mathbf{6}^{sm}$) Optimized by Several DFT Methods

functional	basis set [a]	Pt–P1	Pt–P2	P1–C1	P2–C2	P1–Pt–P2	N–Pt–CO
B3LYP	BS1	2.414	2.413	1.739	1.739	149.94	168.57
M06	BS1	2.423	2.422	1.731	1.730	147.05	167.45
B3PW91	BS1	2.375	2.374	1.735	1.735	151.68	168.49
mPW1PW91	BS1	2.367	2.367	1.731	1.731	151.77	168.47
PBE1PBE	BS1	2.363	2.362	1.731	1.732	152.02	168.46
B3PW91	BS2	2.356	2.356	1.732	1.732	152.32	167.75
mPW1PW91	BS2	2.349	2.349	1.728	1.729	152.39	167.71
PBE1PBE	BS2	2.345	2.345	1.728	1.729	152.56	167.66
X-ray structure (**6**)		2.285(1)	2.288(1)	1.706(5)	1.715(5)	153.53(4)	168.2(2)

[a] BS1: LANL2DZ for Pt; 6-31G(d) for other atoms. BS2: SDD for Pt; 6-311G(d,p) for other atoms.

Table 3. Crystal Data and Details of Structure Determination for **3**–**6**

complex	**3**	**4**	**5**	**6**
formula	$C_{70}H_{104}N_2P_2Pt$	$C_{66}H_{104}NP_3Pt$	$C_{68}H_{104}N_2P_2Pt$	$C_{64}H_{95}NOP_2Pt$
fw	1230.58	1199.50	1206.56	1151.43
crystal system	triclinic	monoclinic	triclinic	monoclinic
space group	*P*–1	*C*2/*c*	*P*–1	$P2_1/c$
a (Å)	9.84610(10)	43.115(10)	13.4947(3)	18.471(4)
b (Å)	10.9314(2)	10.5651(5)	15.0859(3)	16.117(3)
c (Å)	30.4883(4)	31.967(4)	17.8284(4)	21.248(4)
α (°)	93.0761(12)		69.476(2)	
β (°)	98.1872(11)	122.06(2)	85.4772(18)	113.3337(18)
γ (°)	106.9543(14)		64.360(2)	
V (Å^3)	3091.15(8)	12341(3)	3052.96(11)	5808(2)
Z	2	8	2	4
d_{calcd} (g cm^{-3})	1.322	1.291	1.313	1.317
μ (mm^{-1})	2.363	2.390	2.392	2.512
F(000)	1292	5040	1268	2408
crystal size (mm)	0.14 × 0.12 × 0.03	0.08 × 0.02 × 0.02	0.15 × 0.10 × 0.07	0.08 × 0.06 × 0.02
T (K)	103(2)	103(2)	103(2)	103(2)
absorption correction	multiscan	multiscan	multiscan	multiscan
transmission factors	0.7332–0.9325	0.8318–0.9538	0.8745–1.0000	0.8243– 0.9515
θ range (°)	1.96–25.00	2.01–24.50	1.60–25.00	1.64–25.00
no of reflns measured	40887	78119	40068	64552
no of unique reflns (R_{int})	10858 (0.0252)	10265 (0.1110)	10734 (0.0209)	10223 (0.0426)
no of reflns with $I > 2\sigma(I)$	10196	7326	10247	9225
no of variables (restrains)	691 (1)	653 (0)	677 (0)	661 (0)
GOF on F^2	1.170	1.068	1.240	1.275
*R*1, *wR*2 ($I > 2\sigma(I)$)	0.0563, 0.1396	0.0766, 0.1880	0.0559, 0.1445	0.0369, 0.0922
*R*1, *wR*2 (all data)	0.0593, 0.1449	0.1044, 0.2129	0.0596, 0.1516	0.0450, 0.1084
largest peak and hole (e Å^{-3})	2.974 and –0.924	2.039 and –1.249	3.327 and –1.056	1.104 and –1.004

References

(1) For representative examples, see: (a) Ekici, S.; Nieger, M.; Glaum, R.; Niecke, E. *Angew. Chem., Int. Ed*. **2003**, *42*, 435–438. (b) Hayashi, A.; Okazaki, M.; Ozawa, F.; Tanaka, R. *Organometallics* **2007**, *26*, 5246–5249. (c) Müller, C.; Pidko, E. A.; Lutz, M.; Spek, A. L.; Vogt, D. *Chem. Eur. J.* **2008**, *14*, 8803–8807. (d) Nakajima, Y.; Shiraishi, Y.; Tsuchimoto, T.; Ozawa, F. *Chem. Commun.* **2011**, *47*, 6332–6334.

(2) For representative examples, see: (a) van der Vlugt, J. I.; Pidko, E. A.; Vogt, D.; Lutz, M.; Spek, A. L.; Meetsma, A. *Inorg*. *Chem*. **2008**, *47*, 4442–4444. (b) Kumar, P.; Kashid, V. S.; Reddi, Y.; Mague, J. T.; Sunoj, R. B.; Balakrishna, M. S. *Dalton Trans*. **2015**, *44*, 4167–4179.

(3) Takeuchi, K.; Taguchi, H.; Tanigawa, I.; Tsujimoto, S.; Matsuo, T.; Tanaka, H.; Yoshizawa, K.; Ozawa, F. *Angew. Chem., Int. Ed.* **2016**, *55*, 15347–15350.

(4) (a) Rosa, P.; Mézailles, N.; Ricard, L.; Mathey, F.; Le Floch, P.; Jean, Y. *Angew. Chem., Int. Ed.* **2001**, *40*, 1251–1253. (b) Tirla, C.; Mézailles, N.; Ricard, L.; Mathey, F.; Le Floch, P. *Inorg. Chem.* **2002**, *41*, 6032–6037. (c) Moores, A.; Mézailles, N.; Ricard, L.; Mathey, F.; Le Floch, P. *Chem. Commun.* **2003**, 1914–1915. (d) Perron, H.; Moores, A.; Demachy, I.; Lledos, A.; Jean, Y.; Le Floch, P. *New J. Chem.* **2004**, *28*, 838–842.

(5) Li, J.; Schreckenbach, G.; Ziegler, T. *Inorg. Chem.* **1995**, *34*, 3245–3252.

(6) For uncoordinated phosphaalkenes, see: (a) Hopkinson, M. J.; Kroto, H. W.; Nixon, J. F.; Simmons, N. P. C. *J. Chem. Soc. Chem. Commun*. **1976**, 513–514. (b) Appel, R.; Knoll, F.; Ruppert, I. *Angew. Chem., Int. Ed. Engl.* **1981**, *20*, 731–744.

(7) For ordinary phosphaalkene complexes, see: (a) Hayashi, A.; Okazaki, M.; Ozawa, F.; Tanaka, R. *Organometallics* **2007**, *26*, 5246–5249. (b) Ozawa, F.; Nakajima, Y. *Chem. Rec.* **2016**, *16*, 2314–2323.

(8) Le Floch, P. *Coord. Chem. Rev.* **2006**, *250*, 627–681.

(9) Dell'Amico, D. B.; Labella, L.; Marchetti, F.; Samaritani, S. *J. Organomet. Chem.* **2011**, *696*, 1349–1354.

(10) Blessing, R. H. *Acta Crystallogr., Sect. A* **1995**, *51*, 33–38.

(11) Sheldrick, G. M. *SHELXL-97*, University of Göttingen, Germany, 1997.

(12) Kabuto, C.; Akine, S.; Kwon, E. *J. Crystallogr. Soc. Jpn.* **2009**, *51*, 218–224.

(13) Frisch, M. J.; Trucks, G. W.; Schlegel, H. B.; Scuseria, G. E.; Robb, M. A.; Cheeseman, J. R.; Scalmani, G.; Barone, V.; Mennucci, B.; Petersson, G. A.; Nakatsuji, H.; Caricato, M.; Li, X.; Hratchian, H. P.; Izmaylov, A. F.; Bloino, J.; Zheng, G.; Sonnenberg, J. L.; Hada, M.; Ehara, M.; Toyota, K.; Fukuda, R.; Hasegawa, J.; Ishida, M.; Nakajima, T.; Honda, Y.; Kitao, O.; Nakai, H.; Vreven, T.; Montgomery, J. A., Jr.; Peralta, J. E.; Ogliaro, F.; Bearpark, M.; Heyd, J. J.; Brothers, E.; Kudin, K. N.; Staroverov, V. N.; Kobayashi, R.; Normand, J.; Raghavachari, K.; Rendell, A.; Burant, J. C.; Iyengar, S. S.; Tomasi, J.; Cossi, M.; Rega, N.; Millam, J. M.; Klene, M.; Knox, J. E.; Cross, J. B.; Bakken, V.; Adamo, C.; Jaramillo, J.; Gomperts, R.; Stratmann, R. E.; Yazyev, O.; Austin, A. J.; Cammi, R.; Pomelli, C.; Ochterski, J. W.; Martin, R. L.; Morokuma, K.; Zakrzewski, V. G.; Voth, G. A.; Salvador, P.; Dannenberg, J. J.; Dapprich, S.; Daniels, A. D.; Farkas, Ö.; Foresman, J. B.; Ortiz, J. V.; Cioslowski, J.; Fox, D. J. Gaussian 09, Revision C.01, Gaussian, Inc., Wallingford CT, 2009.

(14) (a) Perdew, J.; Ernzerhof, M.; Burke, K. *J. Chem. Phys.* **1996**, *105*, 9982–9985. (b) Adamo, C.; Barone, V. *J. Chem. Phys.* **1999**, *110*, 6158–6170.

Conclusions

In the precedent studies, pyridine-based PNP-pincer type phosphaalkene ligands such as BPEP and PPEP have been found to form transition metal complexes with unique structures and reactivities. 2,6-Bis(phosphaethenyl)pyridine (BPEP) effectively stabilizes coordinatively unsaturated complexes, whereas PPEP bearing phosphoranylmethyl and phosphaethenyl groups at the 2,6-positions of the pyridine ring exhibits noninnocent behavior on Ir(I), leading to extremely high reactivity toward metal–ligand cooperative activation of chemical bonds. These particular ligand properties are ascribed to the strong π-accepting ability of phosphaalkene units. In this PhD study, the author has been interested in these unique ligand properties of BPEP and PPEP, and expanded their utility in organometallic chemistry by improving the ligand structures.

In Chapter 1, the author prepared free PPEP from BPEP using a Pt(0)/PCy_3 catalyst. The resulting ligand could be successfully applied to a Ru(II) complex, but was unstable on Rh(I), giving rise to intramolecular C–H addition/cyclization of the Mes*P=CH unit to lose the P=C double bond. Thus, the author investigated the stabilization of PPEP by steric protection of the phosphaalkene unit. On the other hand, an NMR observation of the catalytic solution for the conversion of BPEP to PPEP indicated the occurrence of a very unusual Pt(0) species. Thus, the author attempted its isolation.

In Chapter 2, a novel PPEP ligand stabilized by an Eind group instead of a Mes* group was prepared. The fused-ring bulky Eind group with an *s*-hydridancene skeleton was found to effectively stabilize the P=C double bond against intramolecular C–H addition/cyclization. Thus, the Eind-PPEP complexes of Rh(I) and Ir(I) were successfully prepared and converted to dearomatized Eind-PPEP* complexes in high yields. The Eind-PPEP* complexes displayed distinct difference in the reactivity toward ammonia; the Rh(I) complex formed an

ammine complex via simple ligand displacement, whereas the Ir(I) complex caused instant cleavage of the N–H bond at room temperature to form a parent amido complex. Moreover, the Eind-PPEP* complex of Ir(I) exhibited extremely high catalytic activity toward hydrosilylation of CO_2, leading to a high TON (up to 5100) under mild conditions (Chapter 3).

In Chapter 4, the isolation of a novel Pt(0) complex observed in Chapter 2 was examined. The author developed $Eind_2$-BPEP as a novel BPEP ligand stabilized by Eind groups, and succeeded in the isolation of [Pt(PPh_3)($Eind_2$-BPEP)] as the first example of a Pt(0) complex having a square planar configuration. This coordination geometry is very uncommon for formal d^{10} complexes, and the Pd and Ni homologues with the same ligands adopted distorted tetrahedral configurations. In Chapter 5, the $Eind_2$-BPEP ligand was introduced to Pt(0) complexes of the formula [Pt(L)($Eind_2$-BPEP)] bearing a variety of L with different electronic properties (i.e., DMAP, 2,6-lutidine, PMe_3, ^{t}BuNC, and CO). All complexes adopted highly planar configurations irrespective of L. DFT calculations revealed that this quite unique coordination structure is originated mainly from the low-lying π* orbitals of $Eind_2$-BPEP and the strong s-d hybridization of Pt due to relativistic effects. The electronic effects of L were reflected in spectroscopic properties of the Pt(0) complexes as well, showing a large color variation in the near-infrared region.

In summary, the author succeeded in developing novel PNP-pincer type phosphaalkene ligands protected by Eind groups (i.e., $Eind_2$-BPEP and Eind-PPEP). The fused-ring bulky Eind groups effectively prevented the undesirable side reaction resulting in the loss of P=C bonds. Accordingly, the author could expand the scope of application of BPEP and PPEP ligands, and discovered late transition metal complexes with thitherto-unknown structures, reactivities, and spectroscopic properties. These findings will demonstrate the new possibility of phosphaalkene ligands as strong π-acceptors in organometallic chemistry.

List of Publications

Chapter 1

"Catalytic Synthesis of an Unsymmetrical PNP-Pincer-Type Phosphaalkene Ligand"

Taguchi, H.; Chang, Y.-H.; Takeuchi, K.; Ozawa, F. *Organometallics* **2015**, *34*, 1589–1596.

(Chapter 1 is the unedited author's version of a submitted work that was subsequently accepted for publication in *Organometallics* (copyright © 2015 the American Chemical Society) after peer review. To access the final edited and published work see the following website: http://pubs.acs.org/doi/10.1021/acs.organomet.5b00195)

Chapter 2

"Unsymmetrical PNP-Pincer Type Phosphaalkene Ligands Protected by a Fused-Ring Bulky Eind Group: Synthesis and Applications to Rh(I) and Ir(I) Complexes"

Taguchi, H.; Sasaki, D.; Takeuchi, K.; Tsujimoto, S.; Matsuo, T.; Tanaka, H.; Yoshizawa, K.; Ozawa, F. *Organometallics* **2016**, *35*, 1526–1533.

(Chapter 2 is the unedited author's version of a submitted work that was subsequently accepted for publication in *Organometallics* (copyright © 2016 the American Chemical Society) after peer review. To access the final edited and published work see the following website: http://pubs.acs.org/doi/10.1021/acs.organomet. 6b00113)

Chapter 3

"Unsymmetrical PNP-Pincer Type Phosphaalkene Complexes of Group 9 Metals: Catalytic Application to Hydrosilylation of Carbon Dioxide"

Taguchi, H.; Chang, Y.-H.; Takeuchi, K.; Tanaka, H.; Yoshizawa, K.; Ozawa, F. *to be*

submitted.

(Chapter 3 is the author's version of an unsubmitted work that will be submitted for publication.)

Chapter 4

Takeuchi, K.; Taguchi, H.; Tanigawa, I.; Tsujimoto, S.; Matsuo, T.; Tanaka, H.; Yoshizawa,K.; Ozawa, F. *Angew. Chem., Int. Ed.* **2016**, *55*, 15347–15350.

(Chapter 4 is the unedited author's version of a submitted work that was subsequently accepted for publication in *Angew. Chem., Int. Ed.* (copyright © 2016 Wiley-VCH Verlag GmbH & Co. KGaA) after peer review. To access the final edited and published work see the following website: http://dx.doi.org/10.1002/anie.201609515)

Chapter 5

Taguchi, H.; Tanigawa, I.; Takeuchi, K.; Ozawa, F. *to be submitted*.

(Chapter 5 is the author's version of an unsubmitted work, which will be submitted for publication.)

Other Publication

Chang, Y.-H.; Tanigawa, I.; Taguchi, H.; Takeuchi, K.; Ozawa, F. *Eur. J. Inorg. Chem.* **2016**, 754–760.

Acknowledgements

The studies described in this thesis were carried out under the direction of Professor Fumiyuki Ozawa (April 2013 to March 2018) at the International Research Center for Elements Science, Instituted for Chemical Research and the Department of Energy and Hydrocarbon Chemistry, Graduate School of Engineering, Kyoto University.

Without the persistent help of many people, this thesis has not been possible. The author would like to express his sincerest to all of them.

To begin, the author would like to thank Professor Fumiyuki Ozawa for his kind guidance, helpful and insightful suggestions, and hearty encouragement during the course of this study.

The author deeply appreciates to Assistant Professor Katsuhiko Takeuchi for his daily guidance, helpful discussions and assistance with X-ray crystallographic analysis.

The author deeply appreciates to Assistant Professor Masayuki Wakioka for his hearty advice and assistance with X-ray crystallographic analysis.

The author strongly appreciates to Associate Professor Tsukasa Matsuo and Mr. Shota Tsujimoto in Kindai University for their useful advice, helpful guidance and suggestions on Eind derivatives.

The author would also like to thank Professor Katsunari Yoshizawa and Associate Professor Hiromasa Tanaka in Kyushu University for their continuous support for DFT calculations.

The author is thankful to Ms. Naoko Ikeda for kind and hearty support.

The author is thankful to Ms. Toshiko Hirano for elemental analysis.

The also thanks to other members of Professor Ozawa's group for their kind friendships: Dr. Yung-Hung Chang, Dr. Ya-Fan Lin, Ms. Nobuko Ichihara, Mr. Ataru Minami, Mr. Tomohiro Taketani, Ms. Yuki Nakamura (Ogata), Mr. Satoru Ishiki, Mr. Eisuke Iizuka, Mr. Ippei Tanigawa, Mr. Daichi Sasaki, Ms. Rina Takahashi, Mr. Yu-to Tanaka, Ms. Natsumi

Yamashita, Mr. Kai Xu, Mr. Naohiro Torii, Mr. Akito Yamasaki, Mr. Masahiro Suezaki, Mr. Takuya Nakagawa, Ms. Hazuki Morita and Mr. Rin Wakayama.

Financial support from the Japan Society for the Promotion of Science and the Research Fellowship for Young Scientists was indispensable. The author sincerely appreciates the support.

The thesis certainly would not have been possible without unwavering support and encouragement of his family. The author wants to give deepest thanks to his wife Kana. She has been his best friend for many years and, without her, making it through graduate school would have been tough for the author. The author would like to express his sincere appreciation to his father, Sadakazu Taguchi and his mother, Minako Taguchi and his sisters for their constant encouragement and affectionate assistance.

Hiro-omi Taguchi

Department of Energy and Hydrocarbon Chemistry
Graduate School of Engineering
Kyoto University
March 2018